NGU
Norges geologiske undersøkelse
Geological Survey of Norway

GEOLOGI FOR SAMFUNNET
GEOLOGY FOR SOCIETY

NGU Report 2011.073

Contour current driven sandwaves on the upper slope of the continental margin offshore northern Norway

NGU
Norges geologiske undersøkelse
Geological Survey of Norway

Geological Survey of Norway
Postboks 6315 Sluppen
NO-7491 Trondheim, Norway
Tel.: 47 73 90 40 00
Telefax 47 73 92 16 20

REPORT

Report no.: 2011.073	ISSN 0800-3416	Grading: Confidential until 31.12.2013

Title:
Contour current driven sandwaves on the upper slope of the continental margin offshore northern Norway - setting and morphometrics

Authors:
Edward L. King, Reidulv Bøe, Valérie K. Bellec, Leif Rise, Margaret Dolan

Client:
Norwegian Deep Water Programme (NDP)

County:

Commune:

Map-sheet name (M=1:250.000)

Map-sheet no. and -name (M=1:50.000)

Deposit name and grid-reference:

Number of pages: 93 Price (NOK): -
Map enclosures: 0

Fieldwork carried out:	Date of report:	Project no.:	Person responsible:
2008-2009	30.12 2011	342000	Jan Cramer

Summary: Sandwaves are common on many continental shelves and slopes around the world. Often their dynamic nature poses challenges for maritime installations such as pipelines and other constructions on the seafloor. Sandwaves and sandwave fields are indicative of strong currents causing erosion, sediment transport and deposition on the seabed. Several sandwave fields have recently been identified on the Norwegian continental slope in the Eggakanten mapping area, SW Barents Sea through the MAREANO programme (www.mareano.no). It is in this Eggakanten area that we investigate sandwaves further in the present project, with a view to raising the understanding of sandwave evolution and sand transport along the Norwegian continental slope.

In this report, based on existing MAREANO-data, a technique and results for morphometric description and cataloguing of the bedforms has been established. Robust statistical analyses present several indices which suggest a clustering or domains of bedforms which are somewhat tuned to the meso-morphology of the terrain in which they lie, a terrain inherited from glacial processes. This gives rise to the hypothesis that there is a much more complex hydrologic regime than a simple continuous northward contour current which drives the bedforms. Local steering, current acceleration and perhaps induced turbulence are suggested. An upward driving hydrologic component must be able to balance mid-term tendencies of down-slope grain migration. The complexity suggested provides some support for the initial hypothesis that relatively unique and poorly understood oceanic conditions are at play, possibly including tidal-wave driven internal waves channelled on the thermocline and tied to interaction with the slope near the shelf-break. All indications suggest active bedform mobility. The setting and morphometrics provide a good framework for future fieldwork by providing concepts and constraints for further sonar surveying, sampling and analysis of the samples.

Keywords:	Sandwaves	Sand transport
Sand ripples	Morphometrics	MAREANO
Multibeam bathymetry	Seabed video	Continental slope

CONTENTS

1. INTRODUCTION

Sand banks and sandwaves are common on many continental shelves around the world, e.g. in the Southern North Sea (Kenyon, 1970; Caston, 1972, 1981; Hulscher et al., 2001; Deleu et al., 2004; LeBot and Trentesaux, 2004; Bellec et al., 2010), the Gulf of Cadiz (Kenyon and Belderson, 1973; Baraza et al., 1999; Habgood et al., 2003), the Celtic Sea (Reynaud et al., 1999), on the SE African margin (Flemming, 1978, 1980; Ramsay, 1994), SE Brazilian margin (Viana et al., 1998b), offshore the southeastern Canadian margin (Amos and King 1984 and Li and King, 2007) and Newfoundland (Dalrymple et al., 1992), and offshore Norway (Rise et al., 1996; Bøe et al., 2009). Often their dynamic nature poses challenges for maritime installations such as pipelines and other constructions on the seafloor. In shallow areas, they can pose risks to navigation because of migration and changing bathymetry. Sandwaves and sandwave fields are indicative of strong currents causing erosion, sediment transport and deposition on the seabed.

Sandwaves also occur on the Norwegian continental shelf (e.g. Rise et al. 1996; Bøe et al. 2009) and slope (Bøe et al. 2010 in www.mareano.no) but so far no detailed studies on their nature and characteristics along the continental slope have been conducted. The principal factors controlling deposition of continental shelf bottom-current sands (by tidal, wave and geostrophic currents) are hydrodynamic regime, availability of coarse-grained sediments, physiographic context of the area swept by the currents, and global sea-level and climate changes (Viana et al., 1998a). Sediment waves in slope and canyon environments occur as ridges formed by downslope creep, contour currents, and turbidity currents (e.g., Faugères et al., 1999). Distinction between sediment ridges formed by different processes is often difficult because interaction between two or three ridge forming processes is common, and the original process of formation may be different from that which caused subsequent progradation and aggradation of the waves.

1.1 Study Area

Several sandwave fields have recently been identified in the Eggakanten mapping area, Norwegian continental slope, SW Barents Sea (Fig. 1) by the MAREANO programme (www.mareano.no). This report focuses on identification and characterization of the sedimentary bedforms and their geologic setting on the continental slope.

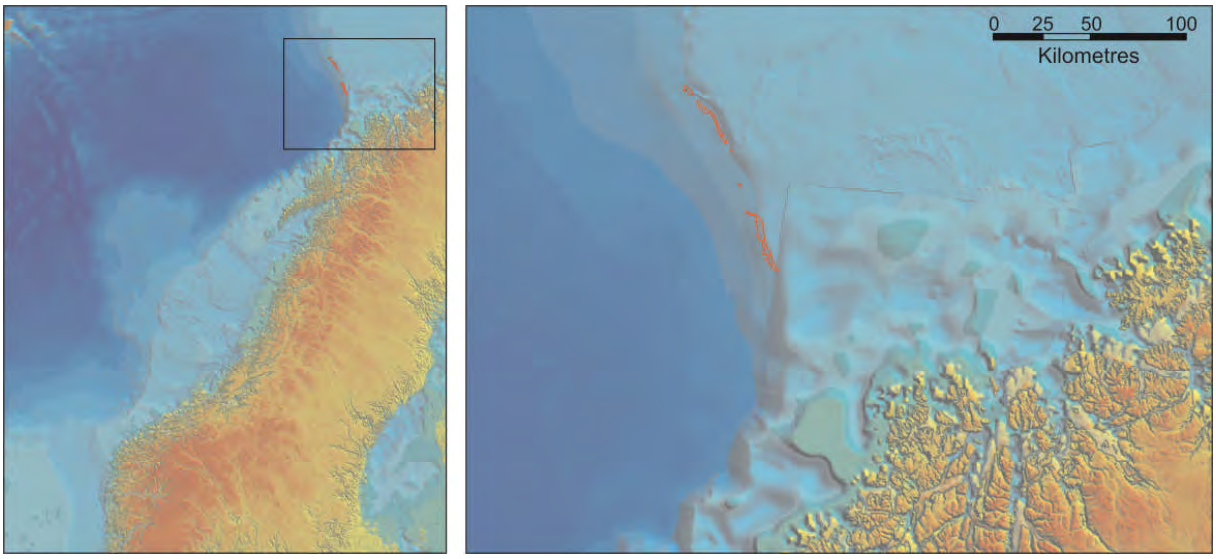

Figure 1. Location of the sandwave study area in the southwestern Barents Sea. The red outlines mark the sandwaves.

1.2 Bedform Terminology

Following the terminology of Belderson et al. (1982) we use the term sandwave to refer to the subaqueous, lower flow regime, transverse bedforms of sand that have larger wave lengths than sand ripples. Where two or more sizes of sandwaves occur together or superimposed it is convenient to refer to them as small sandwaves (same as dunes or megaripples; see discussions in Allen (1980), Amos and King (1984) and Ashley (1990)) and large sandwaves, without implying any genetic difference. This is because there appears to be a complete gradation in size, plan view and lee slope angle between sandwaves at various locations (Belderson et al., 1982).

2. OBJECTIVES AND SCOPE

The recognition of sandwaves on the upper continental slope of the SW Barents Sea from acoustic, video and sample data collected largely as part of the MAREANO project has identified the need to understand the nature and process of these features. Apart from academic drivers of this little-studied phenomenon, the main driver is an understanding of sandwaves on the shelf break and upper slope and the role that bottom currents and the sediments driven by them might have on potential seabed infrastructure. The infrastructure aspects are not considered here; this is an initial project report and considers only the bedform features, their setting and the process understanding that can be derived from existing data and site observations. The project will evolve further to collect new field data and address aspects as outlined in the proposal:

1. What are the sedimentary processes that have led to the formation of sandwave fields at particular locations along the continental slope of the Western Barents Sea? Examine sand origin and transport, erosion/deposition of sediments, geomorphology of the slope, sandwave formation processes, etc.
2. What is the mode of evolution of the sandwaves? Examine height, length, wavelength, volume, migration, shape, limiting factors (size, distribution), etc.
3. What is the role of ocean bottom (seabed) currents in the formation and maintenance of the sandwave fields on the continental slope? Model currents at scales relevant to sandwaves, examine currents/sediment interaction, direction, speed, variability, limiting factors, history of sandwave migration on the slope, etc.

This report introduces the bedforms based on existing acoustic survey, sample and video data, presents their geomorphologic and stratigraphic setting within the general continental slope setting, presents the techniques and results of a rigorous morphometric analysis, and addresses some of the implications of these findings toward inference of their processes of formation and for their further study.

3. GENERAL GEOLOGIC SETTING

The study area is located on the continental slope in the transition zone between the Norwegian Sea in the west and the Barents Sea in the east. In relation to the deeper geology, the sandwave area occurs east of the ocean-continent crustal boundary and west of the Senja Ridge (Gabrielsen et al. 1990), which comprises basement rocks overlain by thin sequences of Late Palaeozoic, Triassic and Jurassic rocks (Gabrielsen et al. 1990) and thick successions of Cretaceous and Tertiary rocks.

The southern Barents Sea continental shelf comprises alternating shallow banks and deeper troughs formed during the last glaciations, and massive diamictic sediments are found on the continental shelf, in the troughs and outer fjords of mainland Norway (Ottesen et al., 2005). This indicates that ice streams advanced through fjords, onto the continental shelf and to the shelf edge during the last (late Weichselian) glaciation, which reached a maximum slightly before 18 000 ^{14}C BP. Deglaciation along this margin took place from ~15 000 ^{14}C BP on the outer shelf, according to the dated onset of glaciomarine and then open-marine sedimentation, and at 13 600 ^{14}C BP, the ice margin was located along the present coastal area of Vesterålen (Knies et al., 2007).

The study area is situated on the southern flank of the Bear Island Trough Mouth Fan, which comprises thick deposits (up to 3000 m) of Quaternary sediments deposited during several glacial cycles (e.g., Ottesen et al. 2005, Andreassen et al. 2008, Laberg et al. 2010). The succession has not been properly dated due to lack of boreholes. Microfossil dating of outcropping, compacted sediments from the steep canyon margins near the bottom of Bleiksdjupet (Andøya Canyon) north of Andøya has given late Pliocene to early Pleistocene

ages (Oljedirektoratet 2010), and various evidences suggest that the canyons on the continental slope south of the study area started to form long before, possibly in the Miocene (Elliott et al. 2006, Rise et al. 2009, Rise et al. 2012).

During the middle-late Pleistocene, debris flow activity dominated the slope (Laberg and Vorren 1995, Vorren et al. 1998, Laberg et al. 2010). The northern part of the study area is characterized by numerous, shallow, braided and anatomising channels on the slope (both buried channels and surface channels, shown in Figs. 2 and 3.

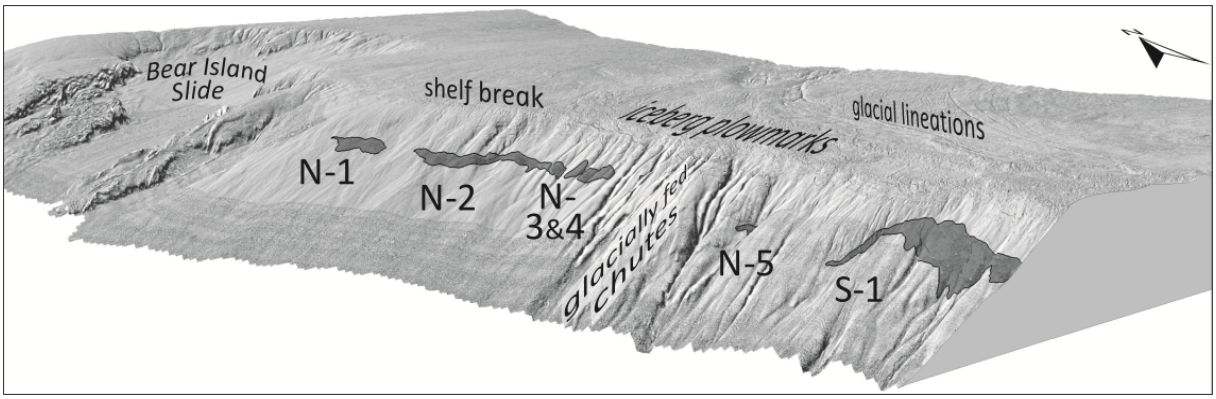

Figure 2. General setting of the sandwave fields along the SW margin of the Barents Sea. Field number designations shown (N: north, S: south). On this 3-D shaded relief image (vertical exaggeration X20) the shelf break is at about 400 m water depth and water depth on the lower slope is about 1000 m. The bedforms range from 480 to 750 m water depth. These are situated below a glaciated and (relict) iceberg scoured shelf, south of the large Bear Island Slide, and superimposed on multiple canyon-like chutes mainly formed by glacial processes.

We interpret these to be related to the debris flow activity and to density currents from the shelf. The new TOPAS™ sub-bottom profiler data (very high resolution parametric sub-bottom profiler) show that in the north, glacigenic debris flow (GDF) deposits occur directly below the seabed sand unit. In the south, layered glaciomarine deposits up to a few metres thick locally cover the debris flow deposits with sand on top. Deep gullies occur on the slope in the south (Figs. 2 and 3). In the sandwave areas they are typically 30-40 m deep, while they may be up to 150 m deep lower on the slope, where they merge (Vorren et al. 1998). We interpret the gullies to be formed by slide and debris flow activity and by downslope channelized meltwater discharge from stagnant ice on Tromsøflaket during the deglaciation and earlier. Formation by density currents/cold dense water formed on the shelf has also been suggested previously (Vorren et al. 1989, Vorren et al. 1998). The glacigenic debris flows (GDFs) and some cross-cutting mass transport deposits (MTDs) help provide insight into the timing and preservation of the sandwave sand deposits. They are considered in more detail in Section 5 where the stratigraphic relations to the sandwaves are established.

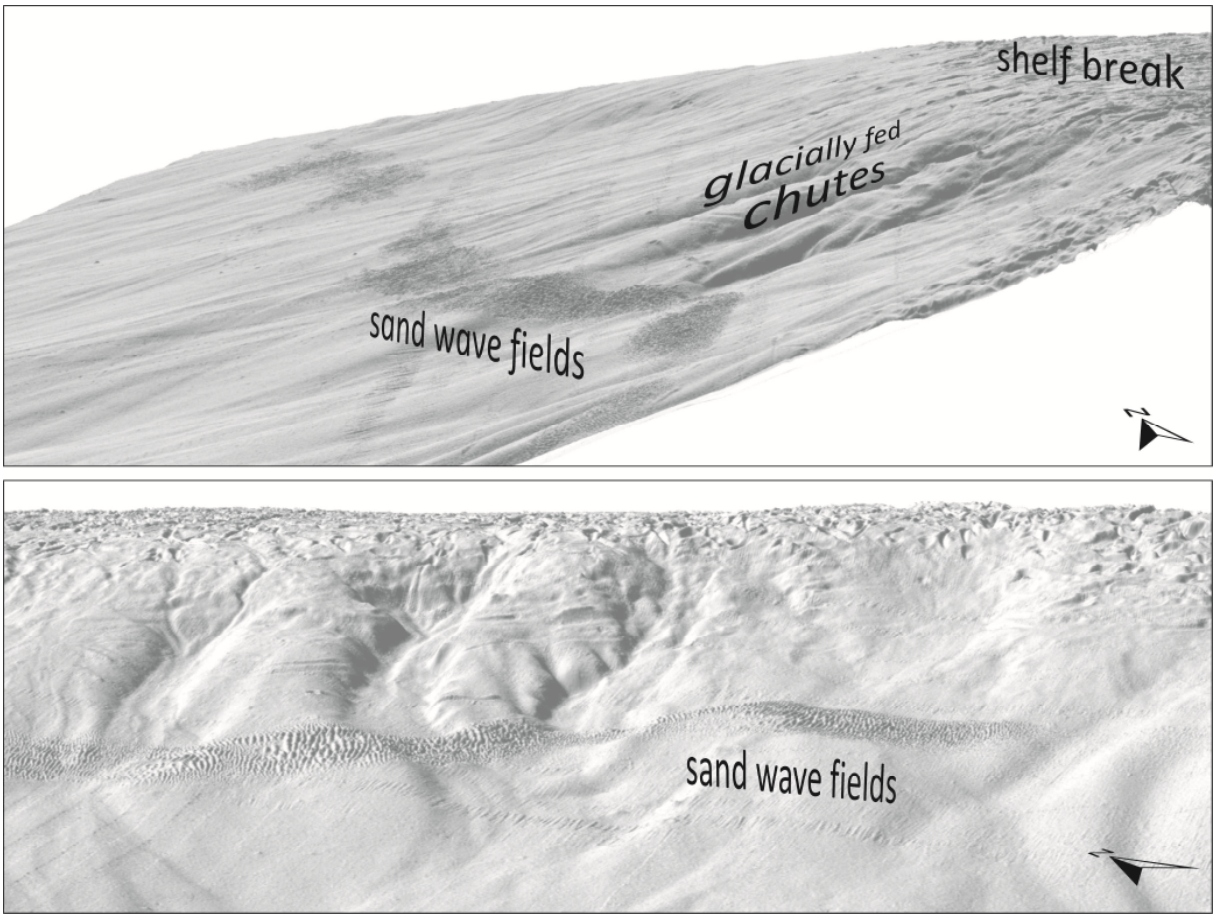

Figure 3. Alternate 3-D views of the sandwave fields at 10x vertical exaggeration. The upper image simulates the downstream view and the lower demonstrates the superposition of the bedforms on the topography

Several large slides have occurred in the glacigenic debris flow deposits in the central and southern parts of the study area (Fig. 2). These are to a large degree covered by younger debris flow deposits and glaciomarine sediments, and slide ages are uncertain. The gigantic Bear Island Slide on the Bear Island Trough Mouth Fan immediately north of the study area is 200 000-300 000 years old (Laberg and Vorren 1993).

MAREANO data and data from earlier studies show a sedimentation pattern on the continental shelf influenced by pre-existing glacial features and sediments, bathymetry and ocean currents (e.g., Hald and Vorren, 1984; Bellec et al., 2008; Bøe et al., 2009; Buhl-Mortensen et al., 2010; www.mareano.no). Lag deposits of cobbles and boulders occur on banks and locally on the continental slope, testifying to the influence of a high-energy environment eroding the glacial sediments. Deposition of fine-grained sediments and sand occurs in troughs and sheltered depressions and locally in channels and sandwave fields on the continental slope. Winnowing by along slope (contour) currents of the upper part of the Bear Island Trough Mouth Fan has occurred during interglacial periods (Laberg and Vorren 1993, 1995). Similar processes have been described below 1000 m depth on the continental margin off Lofoten (Laberg et al. 1999, Laberg and Vorren 2004).

4. DATA SETS AND METHODS

The study area (Fig. 1) was mapped by multibeam echosounder (EM710) by the Norwegian Hydrographic Service (NHS) in 2008 (northern and central area) and 2009 (southernmost area) as part of the MAREANO-programme (Buhl-Mortensen et al., 2010; www.mareano.no). The multibeam provides two datasets: bathymetry, which reveals detailed topography of the seabed, and backscatter intensity. The backscatter intensity (acoustic reflectance) is influenced mainly by sediment texture in the uppermost 0-30 cm of the seabed, and gives information on hardness and roughness. Details of data processing are given in Bellec et al. (2008). Hard/rough bottoms (bedrock, coarse or compacted sediments) generally show higher backscatter values than soft/flat bottom (mud, uncompacted sediments). The data density was sufficient for gridding at 5 m without the need for interpolation, allowing detailed analysis of seabed features. Secondary derivatives of this dataset include slope and curvature. Data sub-sets were the basis for further derivatives including 3-D rendering, crestline tracing, statistically robust bedform metrics, and bedform symmetry, steepness and lee-stoss slope ratio indices. Methods of bedform metrics extraction are discussed in Section 6.1.

Sub-bottom profiler data are from a TOPAS hull-mounted parametric source centered on about 3.7 kHz, heave compensated, and viewed and interpreted as envelope format, jpeg 2000 data with embedded scale and horizon picks utilizing custom software (Courtney 2007).

Seabed sediment samples, video transects and shallow seismic data were acquired during MAREANO cruises with the research vessels G.O. Sars in 2009-2010 to calibrate the multibeam backscatter data, and for biological, geological, and geochemical sampling and analysis. The video surveys were performed using the Institute of Marine Research (IMR) towed video platform CAMPOD, which is a metal-framed tripod equipped with low light CCD overview camera and a high definition (HD) video camera for detailed seabed observations. The CAMPOD is also equipped with current meter and ADCP (acoustic doppler current profiler). Further details on the CAMPOD and its operation are given in Bellec et al. (2008), Dolan et al. (2009) and Buhl-Mortensen et al. (2009). A topographic parametric sonar (TOPAS) from Kongsberg Maritime was used for acquiring shallow seismic data to study subbottom stratigraphy and internal structures of sandwaves. Sampling for biological and sedimentological studies was performed by grab, boxcorer, epibenthic sledge and beam trawl (www.mareano.no). Sub-bottom profiler data within the sandwave fields is limited in extent but sufficient to provide the latest glacial and post-glacial sedimentation history. Figure 4 shows the range of sampling equipment utilized.

Ocean current data include ship-borne ADCP and results from a moored current meter that was deployed on the seabed within one of the sandwave areas by the NDP-Metocean project (www.ndwp.org). The intention was to leave this for one year to give long term measurements of current conditions (current strength, current direction, current variability) at the seabed, but the instrument was removed by trawling and the current meter closest to seabed was damaged. Thus, only a three months time series of current data in depth interval 80-250 m above seabed

are available so far in the project. Figure 5 shows the locations of the various data sets as well as location of some of the illustrations in this report.

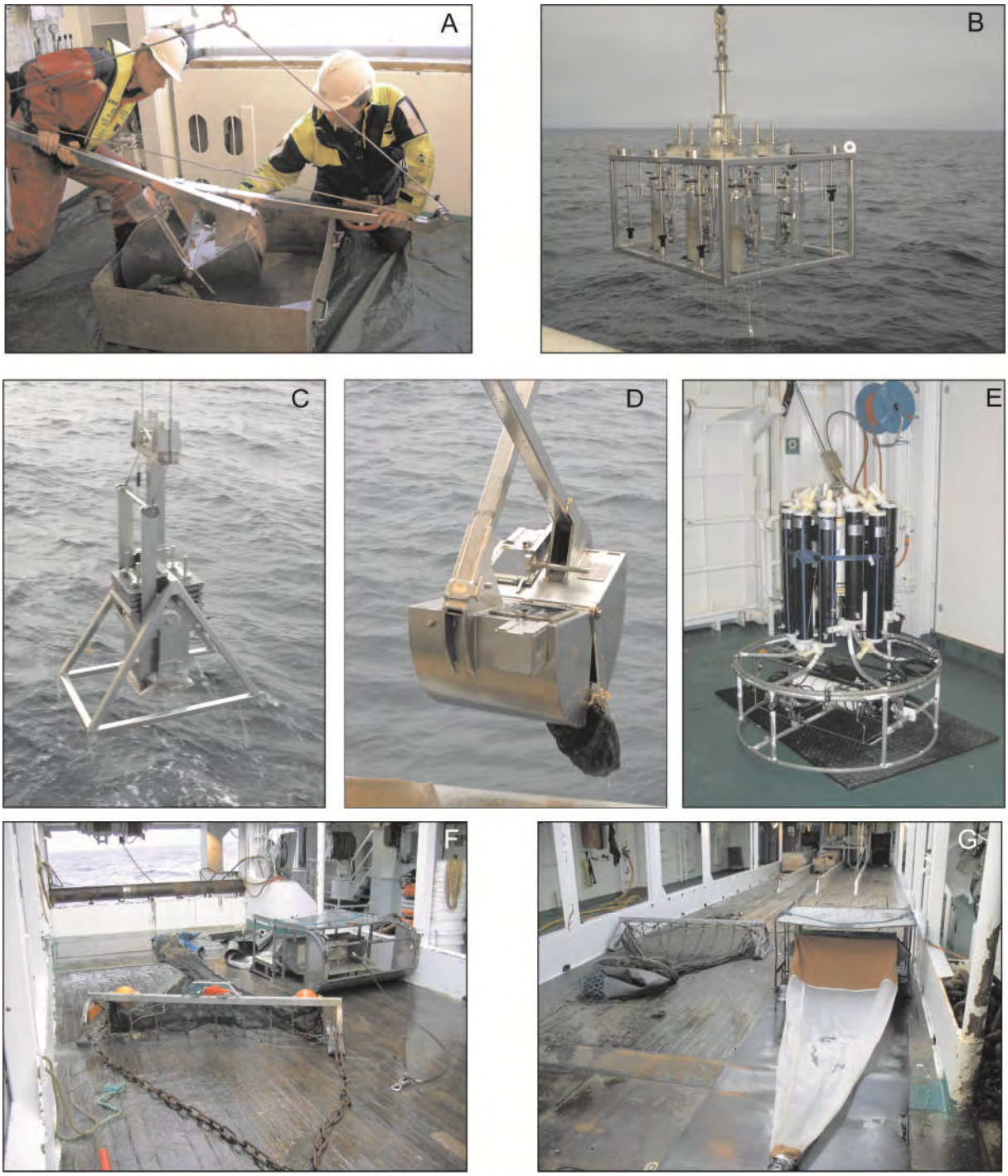

Figure 4. Equipment used for earlier investigations in the sandwave fields under the Mareano Project. A and D: van Veen Grab, B: Multicorer (6 short, undisturbed cores collected simultaneously), C: Box corer, E: CTD (Conductivity-Temperature-Depth, water column only), F and G: Beam Trawl (with chains, left) and Sled (right). The two latter are primarily biological tools dragged across the seabed for about 500 m. In the case of the sandy fields the biological specimens are sieved, with little sediment brought to the surface with the exception of cobbles, if traversed.

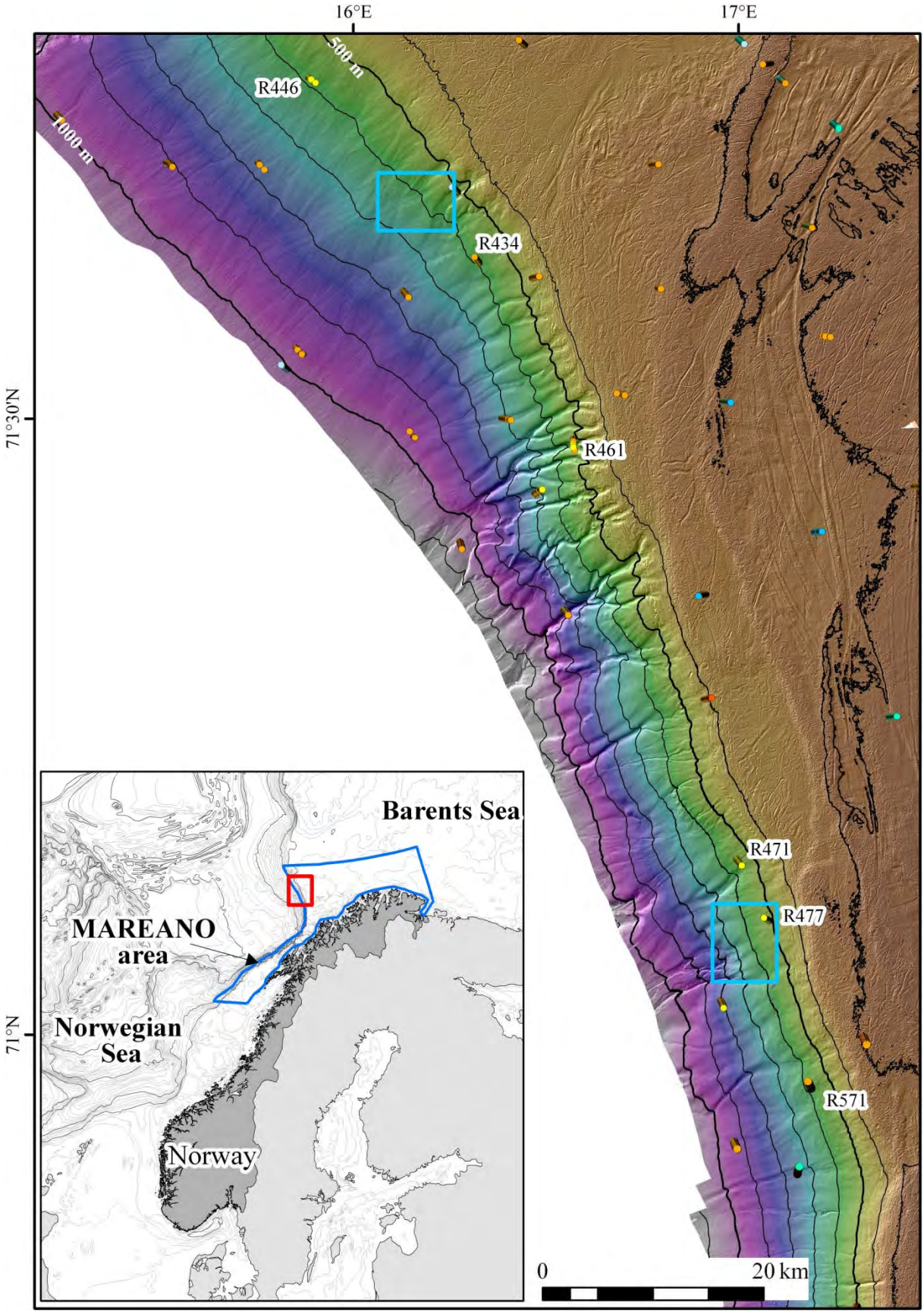

Figure 5. Location of MAREANO stations. Numbers refer to video/sampling stations discussed in this report.

4.1 Bathymetry

The continental shelf break occurs at around 400 m water depth in the study area (Figs. 1 and 2). In the south, the distance between the shelf break and the glacial bank Tromsøflaket, to the east, is only a few kilometres. Northwards the distance increases. Water depths on Tromsøflaket vary from ca. 160 m in the shallowest area in the south to ca. 350 m in the north. The western margin of Tromsøflaket is characterized by N-S-trending very long and elevated moraine ridges.

The Bjørnøya Trough stretches eastwards from the shelf break in the north, with water depths on the shelf of 300-400 m. The slide escarpments of the Bjørnøya Slide (Fig. 2), that cuts into the shelf, are up to 100 m high. West of the shelf break, water depths increase gradually towards deeper water. The chutes on the slope west of Tromsøflaket are 30-40 m deep, while the braided and anatomising channels on the sea bed further north are generally less than 1 m deep. Slide escarpments on the slope present up to 40 m relief.

4.2 Oceanography

The strong Norwegian Atlantic Current (NAC) has two cores - one trends along the continental slope, while the other is more variable and occurs in deeper water. The NAC splits in two branches west of Tromsøflaket. One branch follows the continental slope north-northwestwards towards Svalbard, while one branch follows the Bear Island Trough into the Barents Sea. Modelling results show that the strongest mean current (ca. 30 cm/s) occurs along the shallowest parts of the continental slope (Ådlandsvik & Ostrowski 2010). The NAC is stronger and goes deeper during the winter.

Results of the oceanography studies portion of the sandwave project are reported elsewhere but the setting is provided here because it is one objective of the project that the two disciplines (geology and oceanography) will find common ground. The sandwaves lie at the water depth range where a marked (and migrating) thermocline marks the boundary between the main contour currents. This co-location is clearly not coincidental and the processes giving rise to the driving currents for the sandwaves require a detailed field study and perhaps modelling reconstructions of this situation. Suffice it to note that the Norwegian Atlantic Current (NAC) upstream in the Svinøy section show mean near bottom currents of ~20 cm/s (Orvik et al., 2001). The fluctuations of the current velocity field off the shelf break are related to the wind field and topographic Rossby waves (Skagseth and Orvik, 2002). Based on satellite altimeter data, a large scale coherent mode of variability is prominent over most of the continental slope (Skagseth et al., 2004). Earlier year-long records of current meter mooring data from the 600 m isobath at Gimsøy and Bjørnøya show, for the instruments 20 m above the bottom, a strong topographic steering with mean velocity of about 20 cm/s and amplified currents during winter with maximum speed of ~ 1 m/s. Such velocities, though episodic, are more than sufficient to set the sandwave sands into traction.

4.3 Backscatter (MAREANO)

The sandwave fields on the continental slope are clearly visible in the 5-m backscatter grids (Fig. 6) due to lower backscatter in the sandwave field than the surrounding seabed.

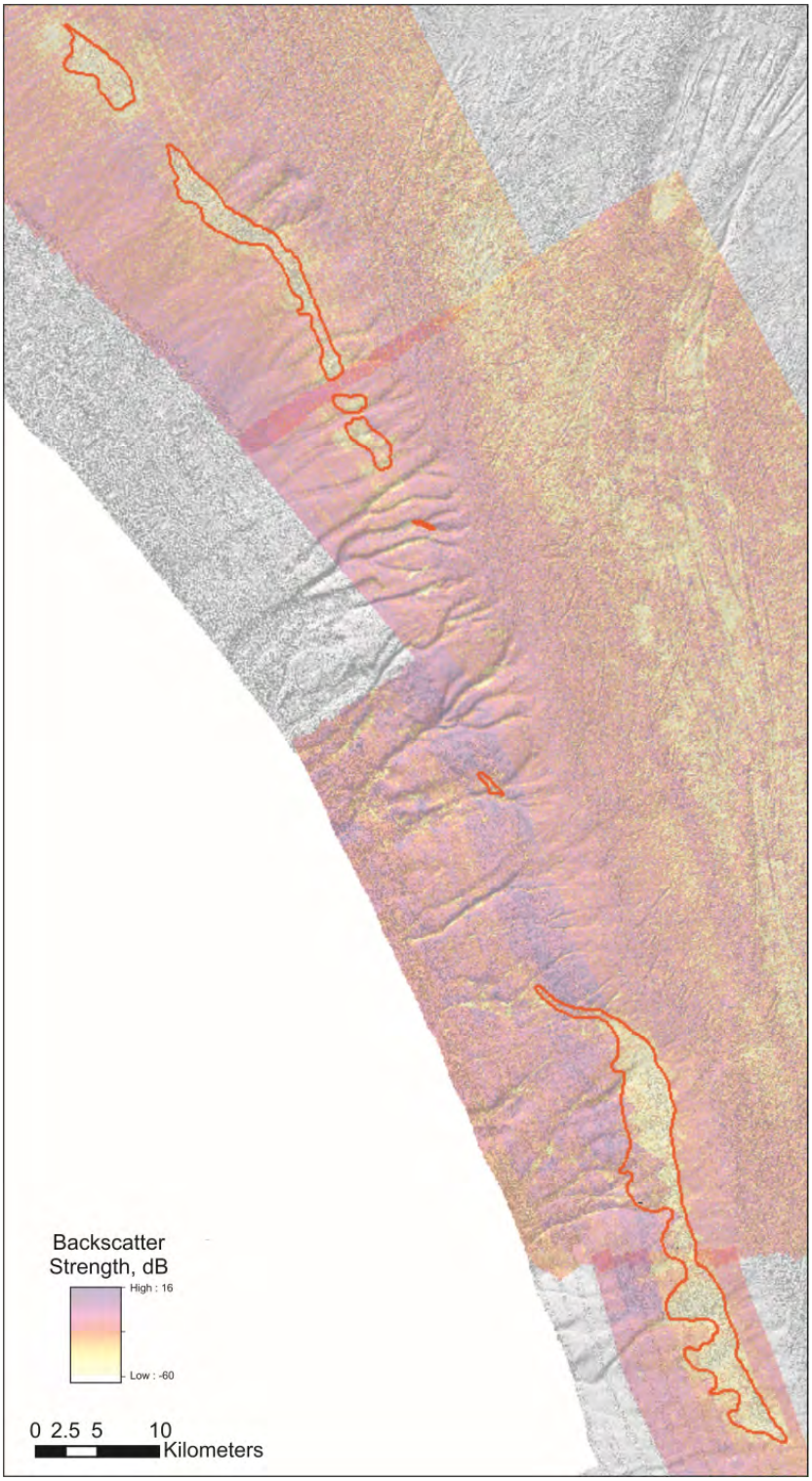

Figure 6. Backscatter strength across all the sandwave fields showing a markedly lower average backscatter in the vicinity and just beyond the boundaries of the fields. It is likely that the sands beyond the field boundaries, shown here in red, also have small but unresolved bedforms (<15 cm high).

Nevertheless, local backscatter variations within the field also show some systematic backscatter patterns. There is no simple relationship between backscatter amplitude and surficial sediment type but this signal is a primary proxy for seabed texture. The acoustic return from outer-beam transducers (those at low seabed incidence angle, outside about 20°), is sensitive to seabed-roughness (scattering), with stronger signal for rougher seabed. Coarse gravels and cobbles tend to be locally rough and return high-amplitude while sands and finer grained materials can be locally smooth with a much lower backscatter. Accordingly, loose sand in the sandwaves absorbs echosounder signals to a larger degree than the troughs. In addition, the uneven seabed caused by the sandwaves reflects echosounder signals in various directions thereby causing weaker backscatter detection. Sub-bottom profiler (TOPAS) data show that the troughs can reach down to the gravel lag on top of the glacially derived deposits, thus exposing the gravelly glacial sediment (stronger backscatter) below. However, much of the backscatter signal is independent of the sandwave morphology (see Section 6.3), and in this older dataset, subject to considerable noise levels with telltale “stripes” oriented parallel and normal to the ship’s tracks.

4.4 Video observations (MAREANO)

Several MAREANO video stations are located within the sandwave fields (Fig. 5). In the following we describe seabed sediments and structures at each station (from north to south) based on individual video lines.

4.4.1 Video Line R446-VL467

This video line (587-584 m water depth) was run in east-southeast direction, perpendicular to the crests of the large sandwaves seen in the multibeam data (Fig. 7). Approximately 14 large and small sandwaves were observed in the video matching those seen on the multibeam. However, the smallest bedforms (ripples) have too small wavelengths or amplitudes to be observed.

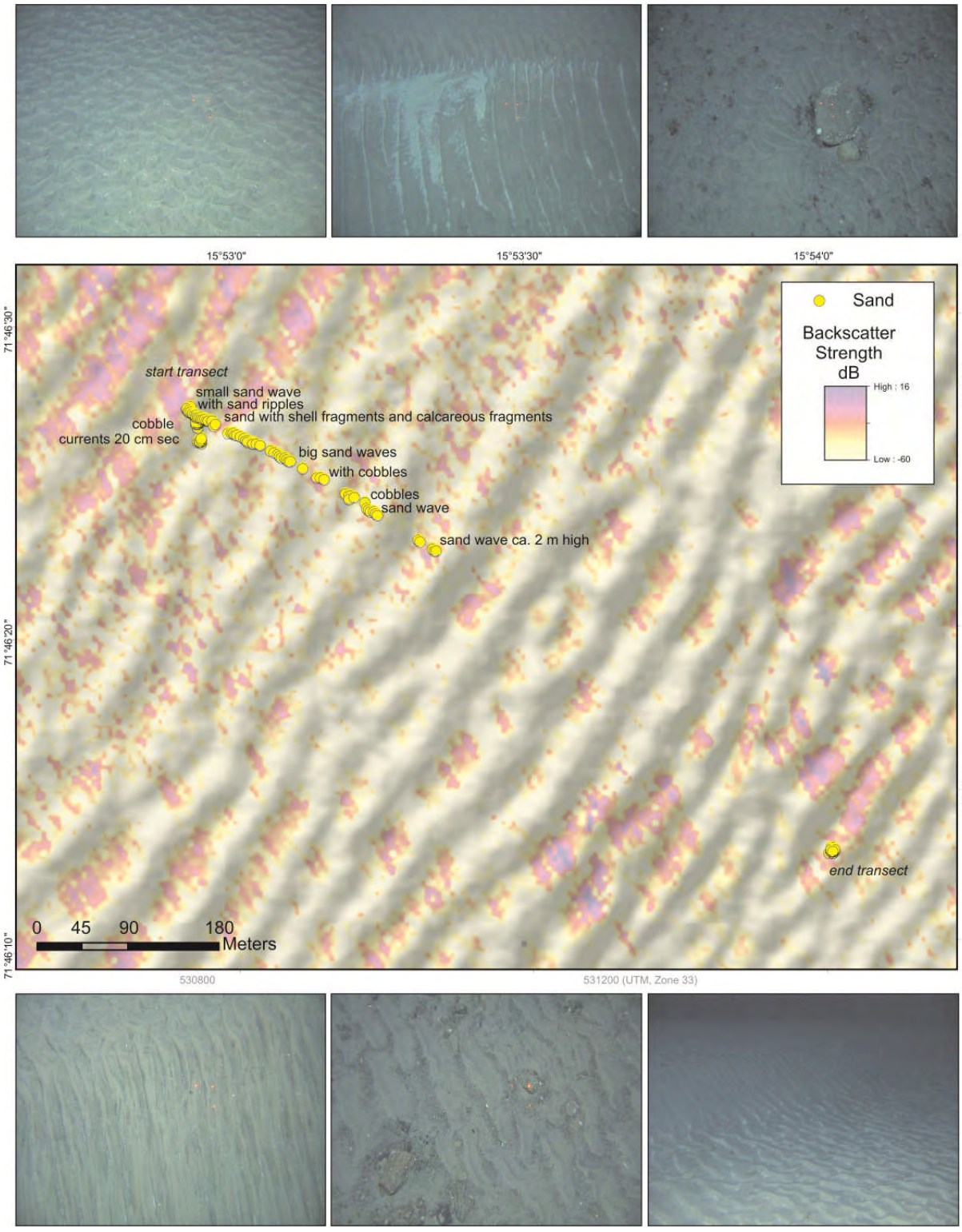

Figure 7. Video station R446 (cruise 2010110) with real-time notes superimposed on a backscatter image, with representative excerpts from the video. Note the 3-D versus 2-D ripples on the crest versus the lee and trough respectively and the near normal orientation of the two ripple sets. Note also the local directional and scouring effects the boulder (upper rightmost photograph) has on the currents. Navigation communication problems erroneously placed more than half the location points at the end of the transect; in fact they should be evenly distributed across the transect.

Sandwaves appear to be 0.5-2 m high and are covered by sand ripples. Several types of ripples occur; most frequent are 3-D linguoid ripples, but there are also transitions to lunate and sinuous ripples. Ripples on the lee side of sandwaves are straight-crested (2-D) and semi-perpendicular to sandwave crests. Ripples in troughs immediately downstream from sandwaves are frequently sinuous out of phase. Ripple wave length is typically around 10 cm (occasionally up to 20 cm) and ripple heights are 1-4 cm.

The sandwaves are dominated by grey, fine-very coarse grained sand, while also pebbles, cobbles and boulders up ca. 0.5 m occur in the wave troughs. Light coloured bioclastic shell fragments of coarse to very coarse-grained sand and fine gravel are common, especially on the lee side of sand ripples and in ripple troughs. The seabed between sandwaves is sand starved, and often only a thin layer of sand ripples covers the underlying gravelly unit. The gravel probably represents an erosional lag partly covered by sand.

4.4.2 Video Line R434-VL455

This video line (584-590 m water depth) was run in a northwest direction, perpendicular to the crests of the large sandwaves seen in the multibeam data (Fig. 8). Approximately 14 large and small sandwaves were observed in the video, which is more or less the same number as counted in the 25-m multibeam data grid along the video transect.

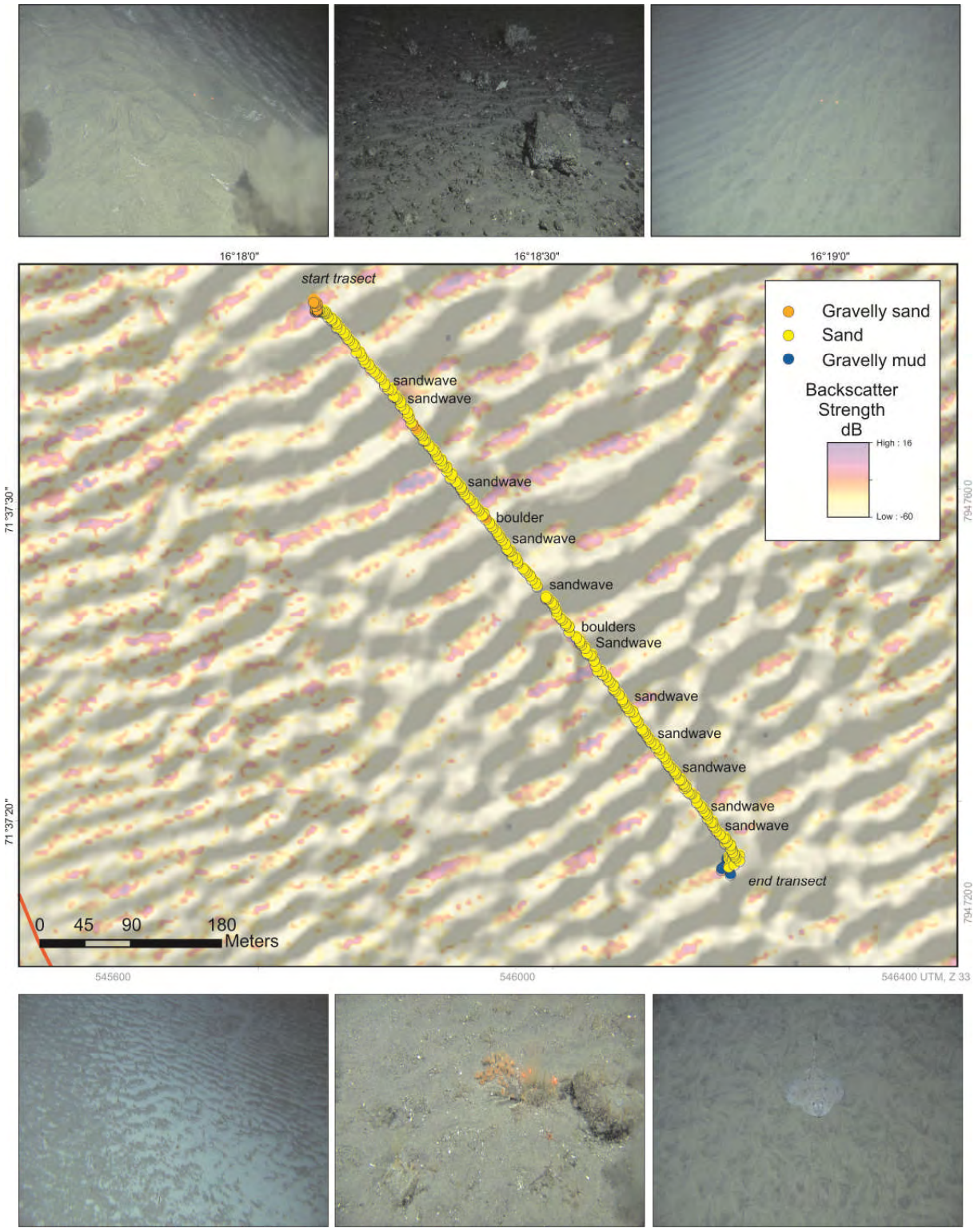

Figure 8. Video station R434 (cruise 2009105) with real-time notes superimposed on a backscatter image, with representative excerpts from the video. The gravelly lag with a thin, partially rippled sand cover in the troughs contrasts with the fine or medium sand on the sandwaves. The upper left and right photographs depict a sharp crest to lee side transition with a marked change in ripple type and orientation. The lee flank in the lower left photograph is rich in shell sand.

Sandwaves are up to 1.5 to 3.5 m high and 60 to 100 m wavelength and are covered by sand ripples. Several types of ripples occur; most frequent are linguoid ripples, but there are also transitions to lunate and sinuous ripples. Ripples on the lee side of sandwaves are straight and semi-perpendicular to sandwave crests. Ripples in troughs immediately downstream from sandwaves are frequently sinuous out of phase. Ripple wave length is typically around 10 cm (occasionally up to 20 cm) and ripple highs are 1-4 cm.

The sandwaves are dominated by grey, fine to very coarse grained sand, while also pebbles, cobbles and boulders up ca. 0.5 m occur in wave troughs. Light coloured bioclastic shell fragments of coarse to very coarse-grained sand and fine gravel are common, especially on the lee side of sand ripples and in ripple troughs. Accumulations of shell fragments are common especially on the lee side of sandwaves. The seabed between sandwaves is sand starved, and often only a thin layer of sand ripples covers the underlying sediment unit. The gravel probably represents an erosional lag partly covered by sand.

4.4.3 Video Line R471-VL493

This transect (around 550 m water depth) crossed 13 sandwaves that traverse across one of the glacigenic debris flow channels/chutes. Across the whole transect the sand was rippled in 2-D and 3-D forms (10-15 cm wavelength), more subdued in height in the troughs. On the stoss and crests, many were highly asymmetric while some were more rounded and nearly all produce a complex colour pattern where darker coloured fine grains (perhaps up to 15%) are sorted on the stoss and troughs of the ripples. Shell hash was common in troughs as was some “fluffy” organic material occasionally accumulated in the troughs, suggesting more still conditions than during active current formation. A current of about 1.3 kts (0.7 m/s) was observed. Boulders (up to 40 cm) and gravel were observed in four of the troughs as were occasional trawl marks. Apparently very steep lee sides were observed; possibly the steepness is exaggerated by spherical aberrations. These flanks generally had 2-D ripples with crestlines oriented nearly normal to the sandwave crestline. Brittle stars, crabs, hermit crabs, bivalves and occasional demersal fish were observed.

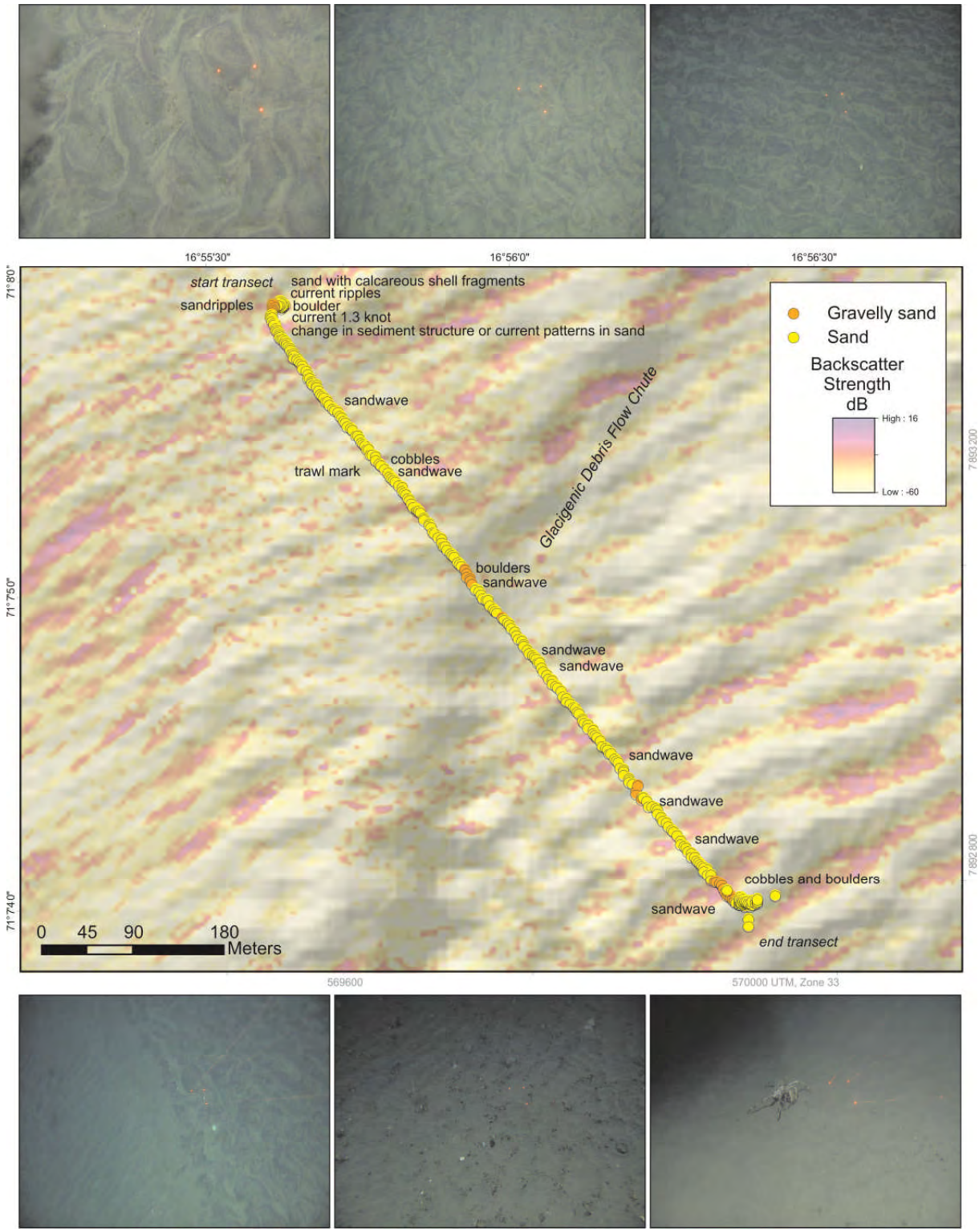

Figure 9. Video station R471 (cruise 2009111) with real-time notes superimposed on a backscatter image, with representative excerpts from the video. The ripples on the sand crest and stoss slope are complex, enhanced by the sorting of the dark grains, presumably more dense heavy minerals. The lower left photograph show an apparently very steep lee flank.

4.4.4 Video Line R477-VL499

This transects was at around530 m water depth. Troughs show a combination of flow-parallel bands of rippled, white sand and adjacent gravelly sand with normal scale and miniature comet marks and a strong preferred orientation fabric. This suggests currents occasionally stronger than ripples will survive and some planar bed grain transport. Boulders (up to 40 cm) and gravel were observed as were ripple-filled trawl marks, apparently having ripped up cohesive material below the sand. Ripple troughs were commonly filled with shell hash of fine gravel to sand size. Sharp crests and steep lee side flanks with 2-D ripples at very steep oblique angles suggest a complex but active current regime. Cables and net debris were present as were rare crabs, fish and relatively abundant sponges on the gravels.

4.4.5 Video Line R571-VL595

This transect (around 590 m water depth) crossed 14 sandwaves with most troughs exposing deeply embeded and fauna-covered glacial gravels and boulders (up to 50 cm). Again, 2-D and 3-D ripples are ubiquitous and shell hash of fine gravel size is common. Crestlines are sharp with very steep lee flanks. Trawl marks cut the stoss side ripples and are beginning to show healing by sand transport. Flat groundfish were relatively common and redfish and crabs were observed.

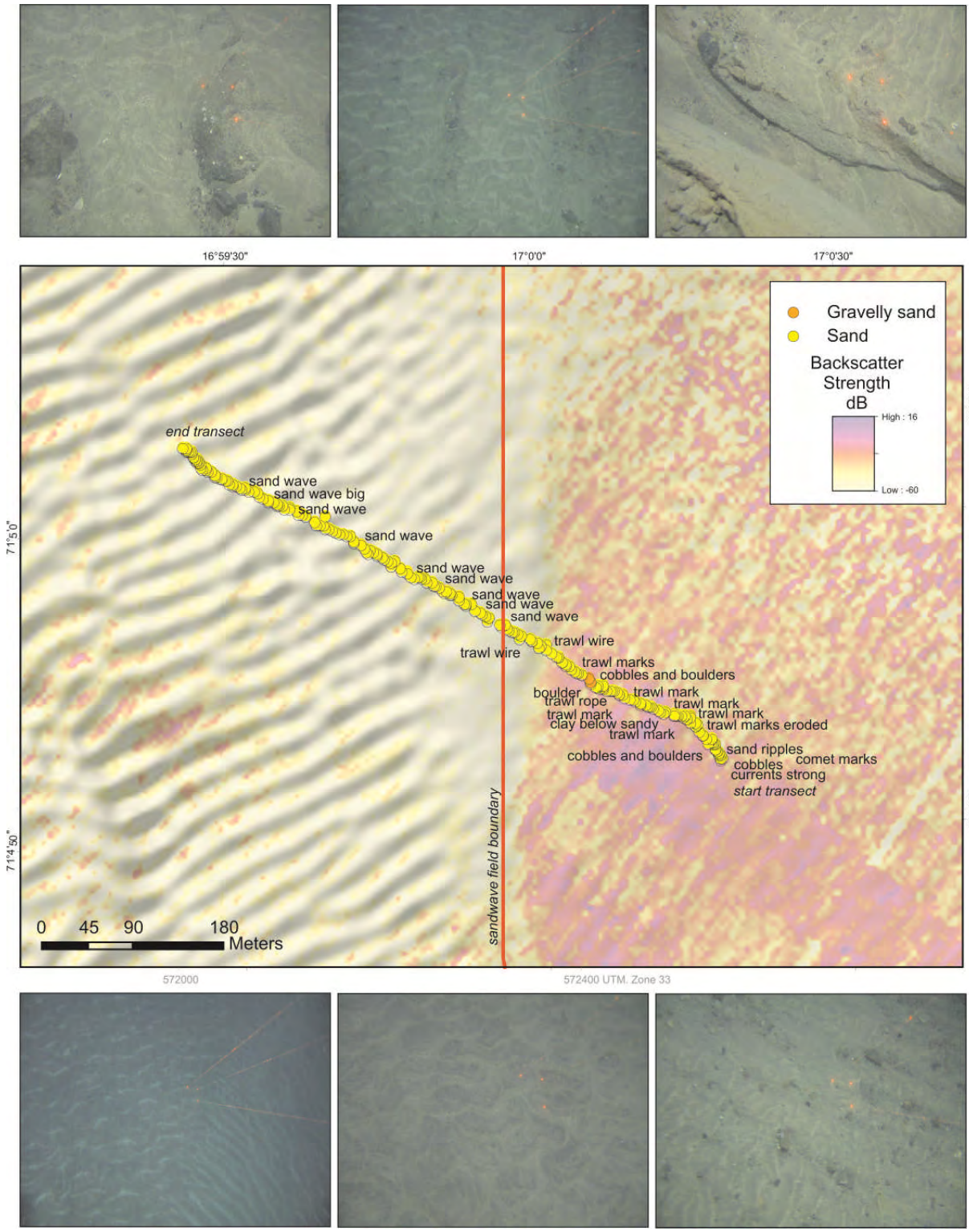

Figure 10. Video station R477 (expedition 2009111) with real-time notes superimposed on a backscatter image, with representative excerpts from the video. The ripples are strongly affected by perturbations in the seabed, including boulders and cobbles, and troughs cut by trawling action (upper right). Note the exposure of a more clay rich diamict beneath the sand.

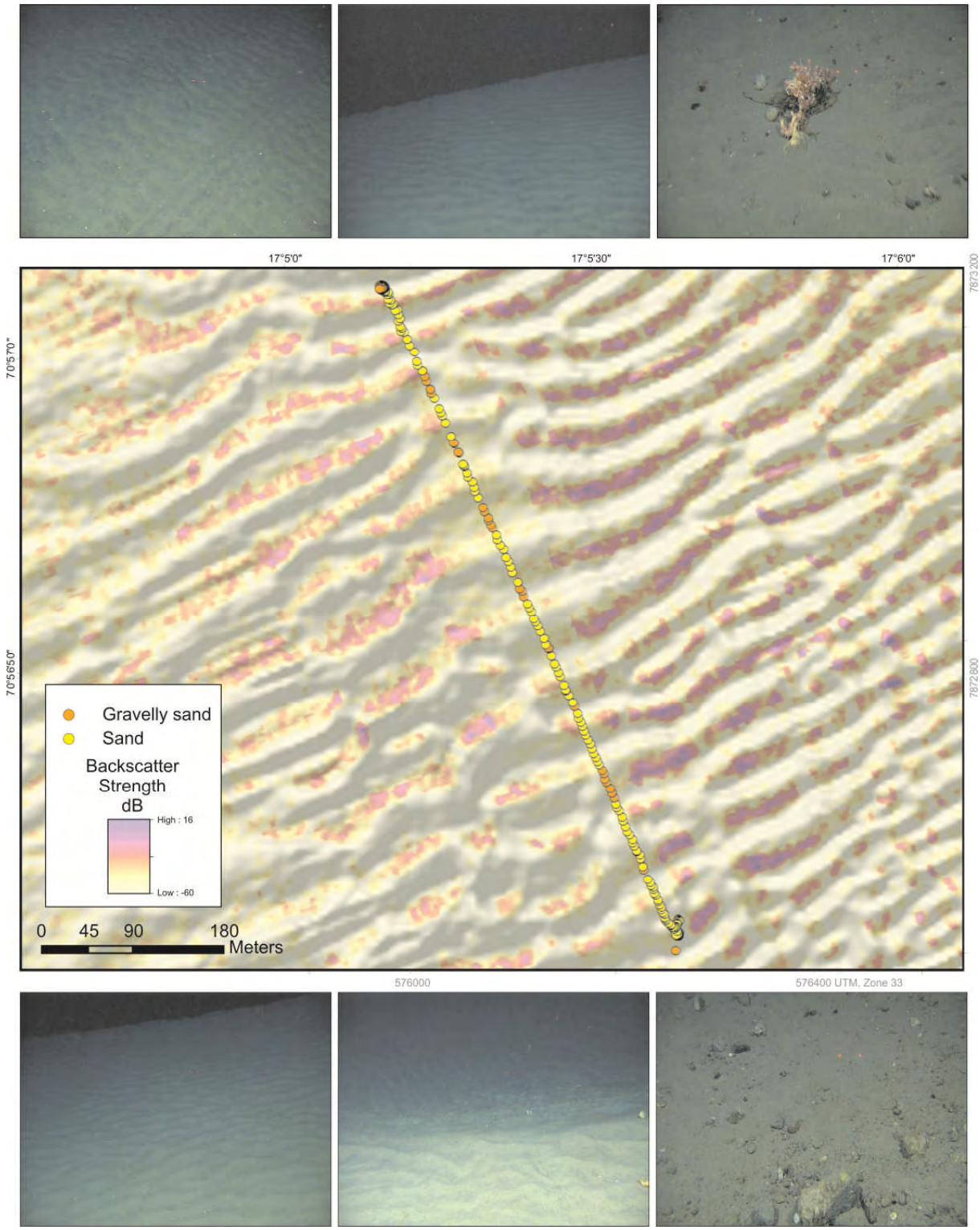

Figure 11. Video station R571 (cruise 2010110) location superimposed on a backscatter image, with representative excerpts from the video. Three of the photographs show a sharp crest-lee side transition, sometimes with the same marked ripple orientation difference seen at other sites. Note the trawl mark (upper left).

4.5 Seabed sediment samples (MAREANO)

As part of the MAREANO project several types of seabed samples have been collected at three sites within the sandwave fields (Fig. 5).

Figures 12 to 16 show the location and setting of the sample stations with respect to the video transects and sandwave forms. As expected from the backscatter signals and the video transects, most samples were sandy but some encountered gravel and cobbles. At Station R571 (Fig. 12), located in the N-1 sandwave field, all sampling techniques were attempted.

The grab sample site resulted in two trials recovering only gravel in the jaws but moving station location about 150 m enabled a sand sample. This was a sandwave trough site sampling the relict glacial gravel whereby the new location was over the sandy bedform. The box core recovered a few centimetres of well sorted sand. Station 571 multicorer recovered 10-15 cm sand, grey on top transitioning to olive grey at 2 cm depth, with clear concentrations of the denser (dark coloured) minerals associated with ripple structures. These were sub-sampled (7- 1 cm thick slices) for further grain size and geochemical analysis. Analyses of the uppermost slice show 100% sand (63-2000 µm).

Station R471, from the S-1 sandwave field, grab and box core samples yielded up to 17.5 cm of fine sand (Fig. 13). A box core subsample was taken where some foraminifera were observed. The beam trawl yielded a small but diverse fauna.

Station R434, from the N-2 field, yielded small grab and box core samples of fine to medium sand, the former with traces of the coarse(?) sand size shell hash which concentrates in the sandwave lee sides and ripple troughs (Fig. 14).

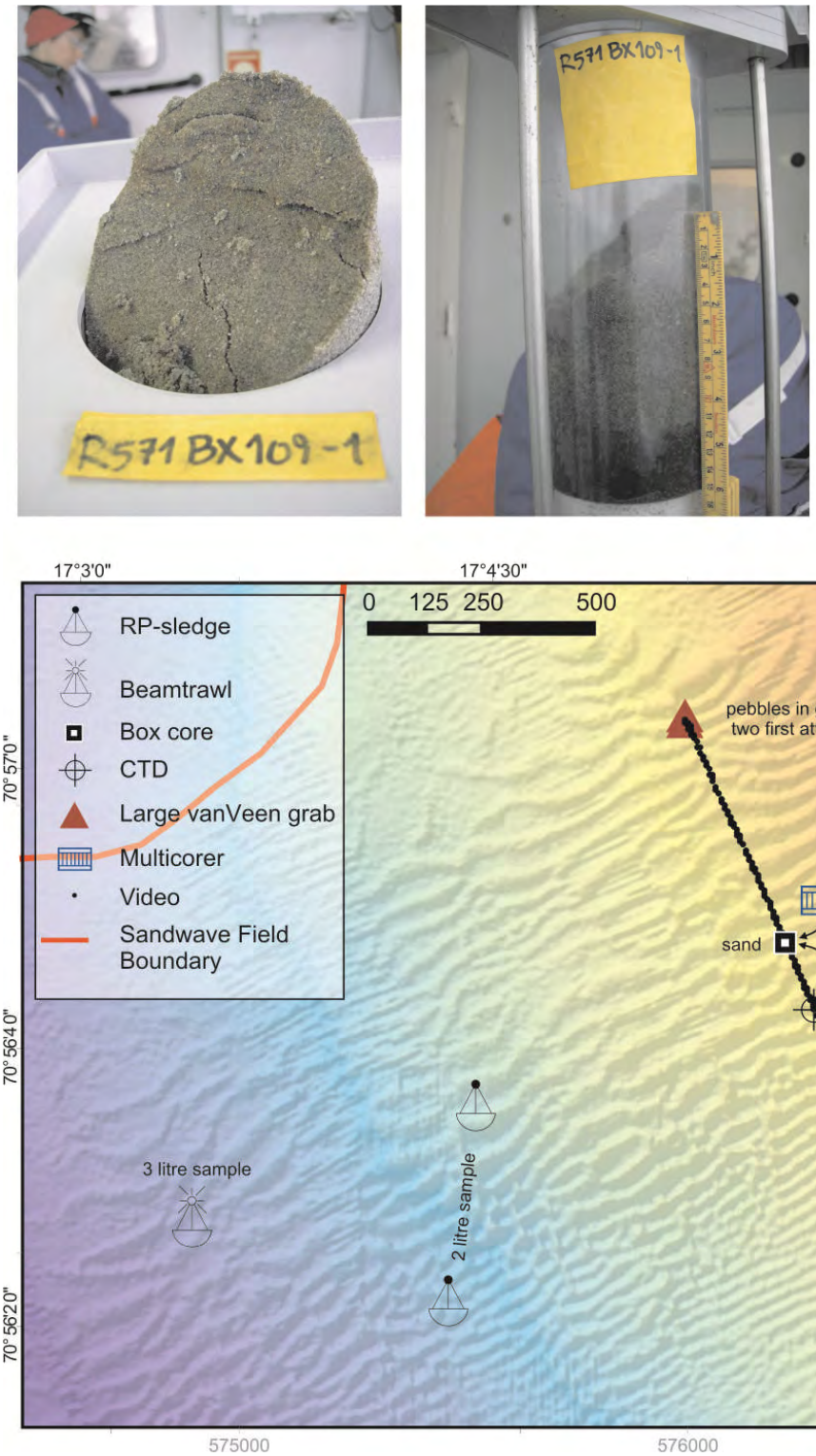

Figure 12. Seabed stations at MAREANO reference site R571where all the equipment in the previous figure was deployed. Sand is generally difficult to sample to any appreciable depth with the boxcorer and multicorer but 15 cm sand was recovered comprising a fine to medium, well sorted, siliciclastic sand.

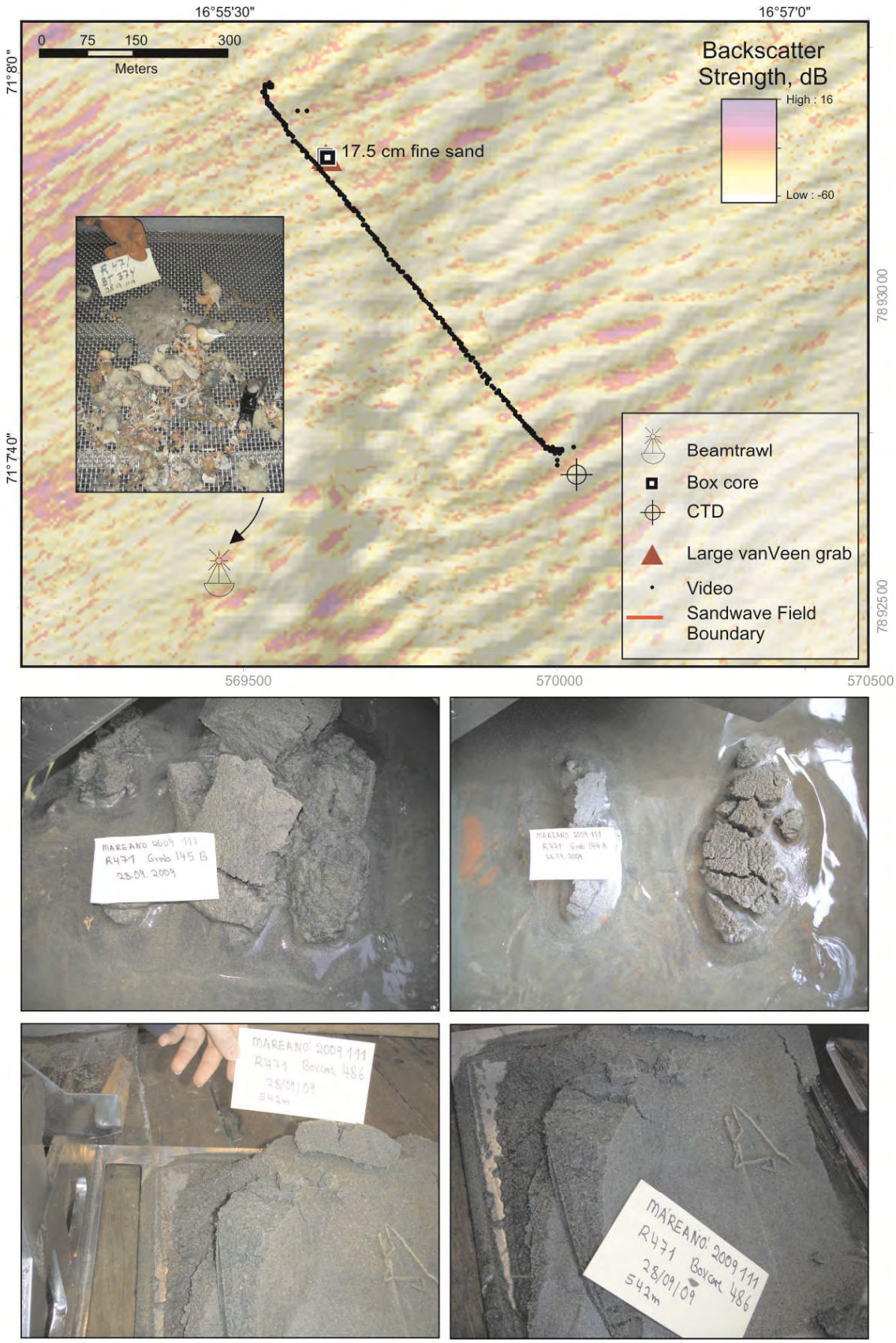

Figure 13. Seabed stations at MAREANO reference site R471. A well sorted, fine to medium grained sand was recovered.

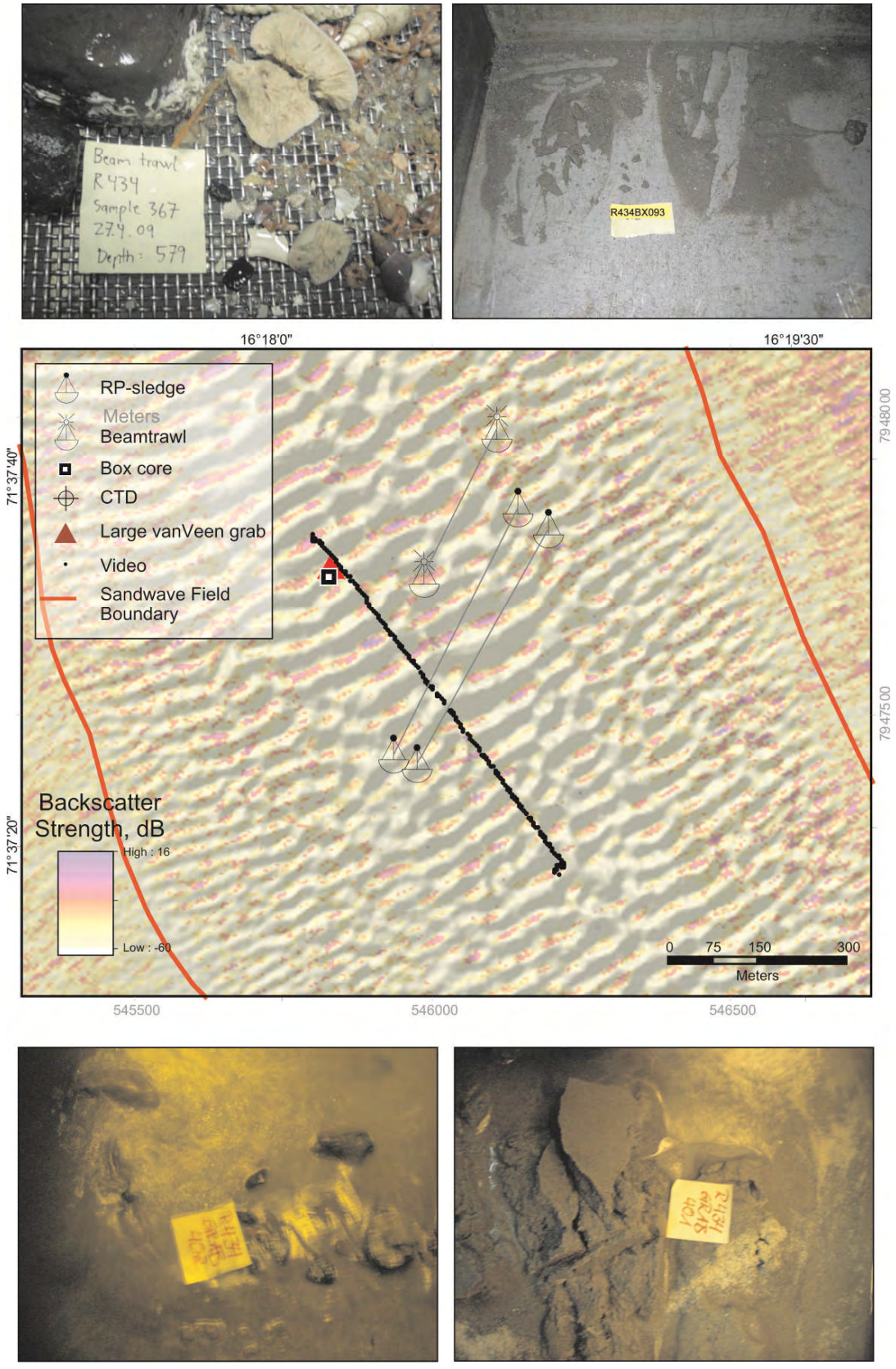

Figure 14. Seabed stations at MAREANO reference site R434. A well sorted, fine to medium grained sand was recovered. The sorting pattern of medium to coarse carbonate (shell hash) grains associated with ripples seen in the video is recognized in the grab sample (lower right photo).

4.6 Surficial geology

As part of the MAREANO project, the surficial geology has been mapped in the area. Figures 15 and 16 shows portions of the genesis and texture maps, respectively.

The slope area consists mainly of gravelly sand and sandy gravel with the exception of the sandwave fields where sand, of course, dominates. The sand locally extends beyond where sandwaves are recognized on the multibeam images, especially outside the N-1 field. The gravel is of glacial origin, generally muddy and diamict (poorly sorted mud with sand and gravel) detritus that has flowed downslope from the shelf-break. Some component must be ice rafted detritus (IRD) as late glacial age icebergs scouring the seabed dominate the shelf down to present day water depths of 450 m (occasionally 470 m).

Demarcated geo-features include glacial moraines of various scales and large scale fluting (on the shelf) and MTD features on the slope, including traces of the dendritic gully-like chutes as well as the escarpments of large gravity-driven slides. The chutes commonly are sandy-bottomed, contrasting with gravelly interfluves. The slides are generally translational (sliding along one or several glideplanes corresponding to presumably weaker strata) and many include a retrogressive component (progressive step-wise up-slope migrating failure as headwalls loose sediment gravitational support at their base and subsequently fail further). Note that nearly all occurrences are relatively “old”, many covered with glacial-age sediments and presenting a somewhat subdued morphology. In the following section the stratigraphy is presented in order to view the sandwave occurrences in a better time context.

5. STRATIGRAPHY - A PRESERVED HISTORY OF THE SANDWAVES?

Better understanding of the hydrologic process, sand provenance, and the timing and flux of the sandwave fields are major goals of this project. The existing sub-bottom profiler data, though not targeted for such investigations, nevertheless provides the basis for an initial stratigraphic framework. Figure 17 shows the extent of TOPAS data and those survey lines investigated in this study. Most survey lines crossing the sandwaves are illustrated in this report.

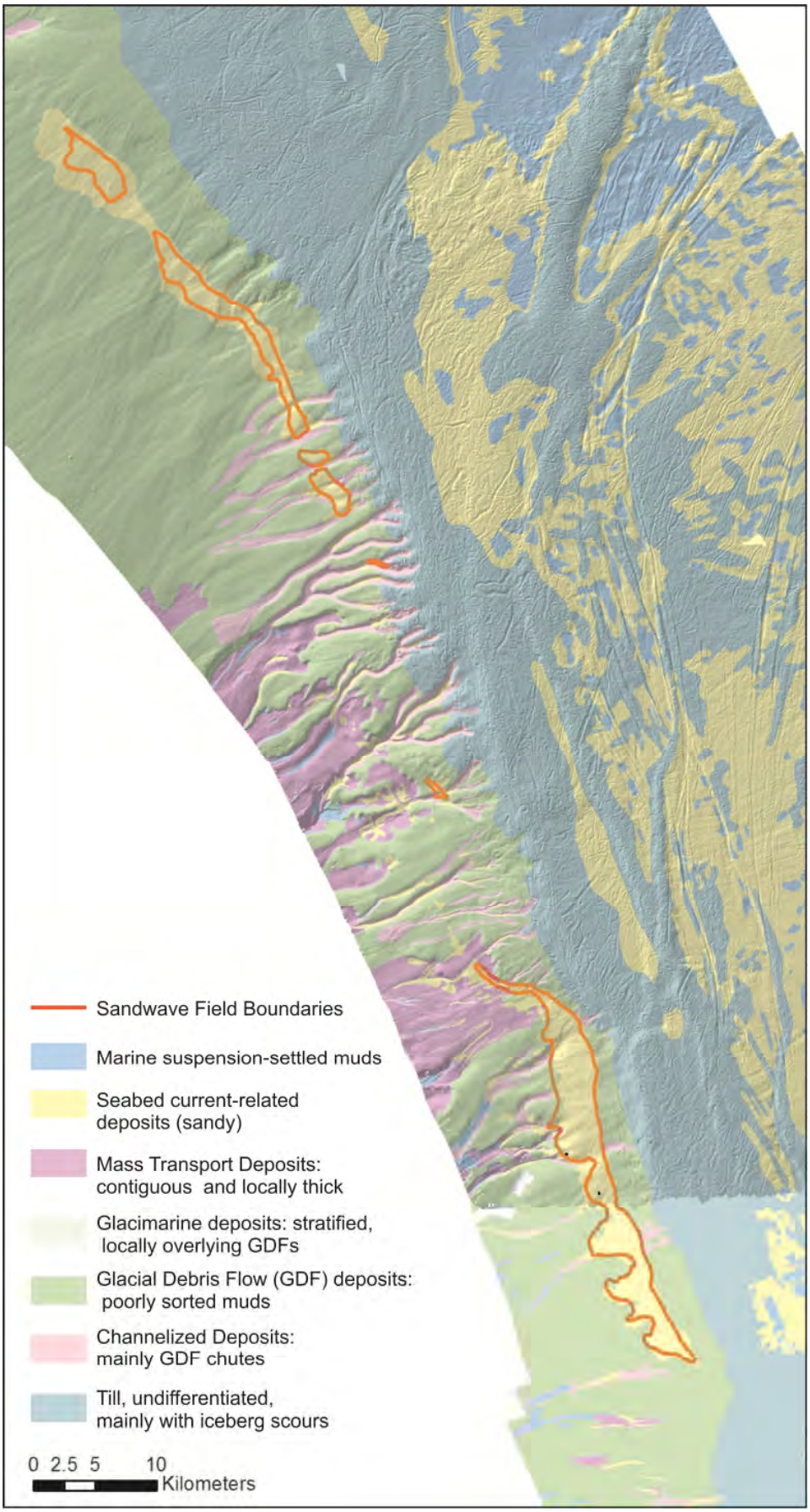

Figure 15. The sandwave fields (red outline) in the context of the MAREANO surficial geology (genesis) map.

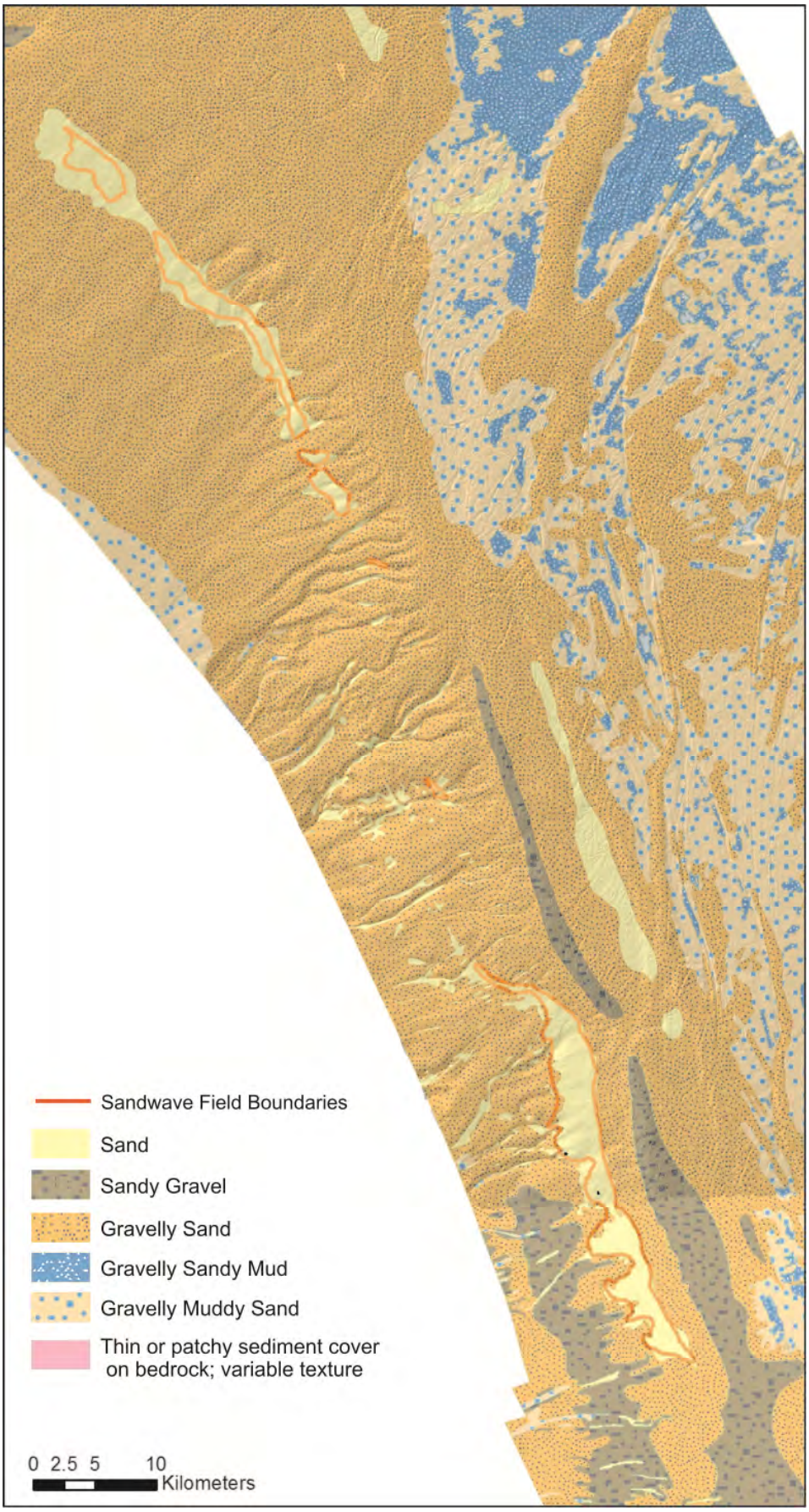

Figure 16. The sandwave fields (red outline) in the context of the MAREANO surficial texture (grain size) map.

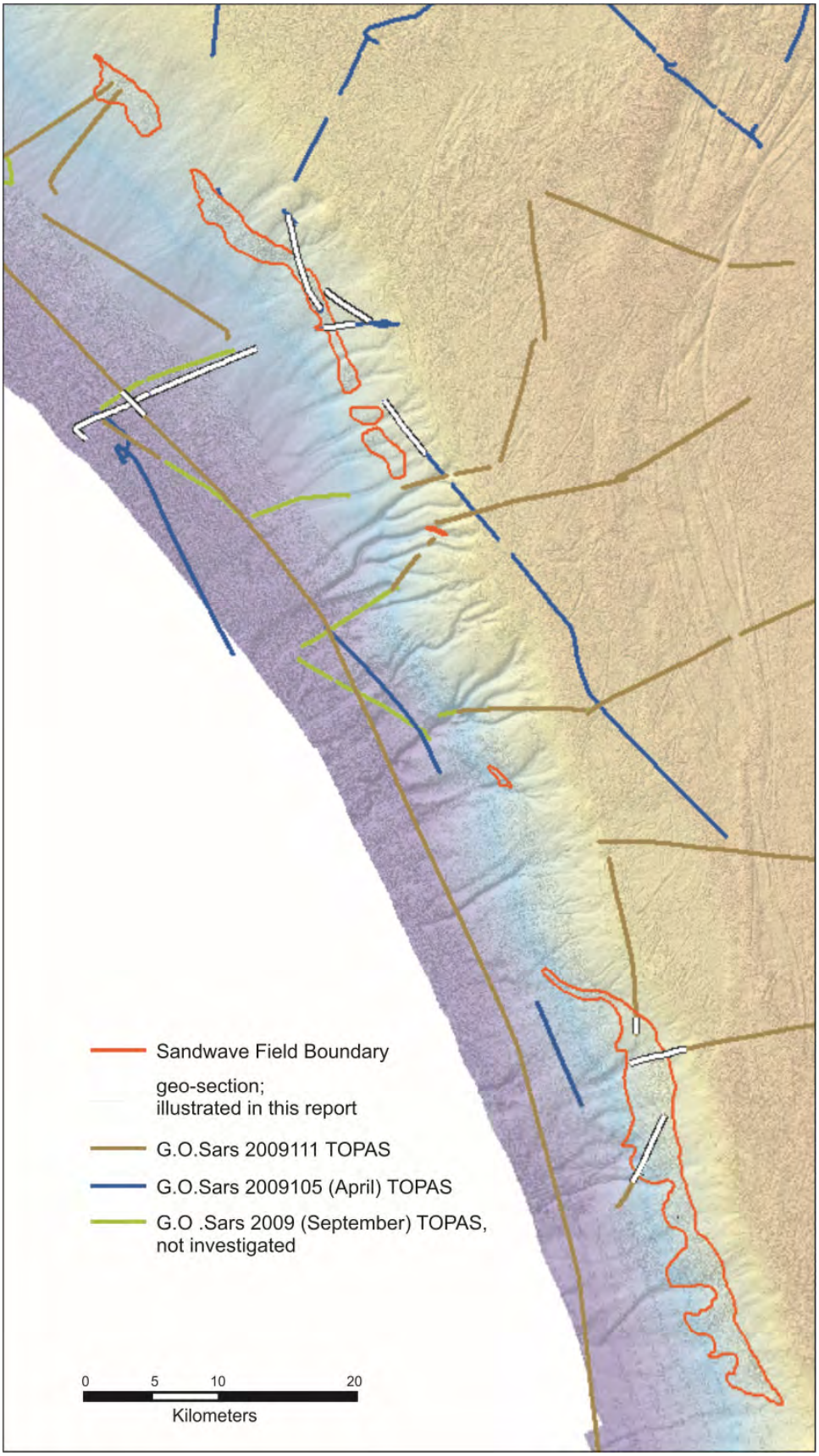

Figure 17. TOPAS sub-bottom profiler coverage (to 2010). Most transects within the sandwave fields are interpreted and illustrations included in this report.

The numerous gully, chute or canyon-like troughs which cut the slope along most of the margin demonstrate no clear spatial relationship to the location of the sand wave fields. Rather, the fields follow a narrow range in water depth and given that this is coincident with the thermocline, it is clear that the oceanographic regime of today governs the location and degree of sand mobility. What is less clear is for what period of time this has been the case.

With the post-glacial onset of Holocene age (last 10-12 000 years) oceanographic patterns, the sandwave field was generated but the timing of this is unknown. Yet, the potential for constraining this from a geological viewpoint lies in the stratigraphic relationships of the sand with older and younger events. Generation of the sandwave field implies that there must excist a source and a sink for the sand. Furthermore, if there is a net flux of sand (presumably downstream, ie. northwestward), then this source-sink relationship should be evident in the geology. The longer-lived the field and the more sand flux, the more evident it should be.

Conceivable sources and sinks are numerous. If the sands are not very far-travelled (many 10’s of km) then the evidence should be within the area already mapped yet initial investigations fail to show this clearly. This might simply be because the process is of such a small magnitude that our (sonar) investigation techniques are not capable of resolving it (ie. centimetres of erosion and deposition rather than metres). However it may also be due to failure to recognize (interpret) the evidence at this early stage in the project or because appropriate data coverage in key areas is lacking. The following section provides a stratigraphic framework of the sandwave field setting which sets constraints, however broad, on the timing and processes. This is an initial investigation of this aspect of the project; further fieldwork will be designed to approach the problem with better and more varied datasets.

5.1 Succession of geologic events

This section presents a series of sub-bottom profiler transects, Figures 18 to 25, which are meant to document the geometry of the sandwave areas, demonstrate the nature of the sediments beneath the sandwave sands and in so doing, confirm the 3-D dimensions of the sand bodies. This and further estimates based on the bedform sizes provide a setting within which the bedform morphometrics (Section 6) can be evaluated.

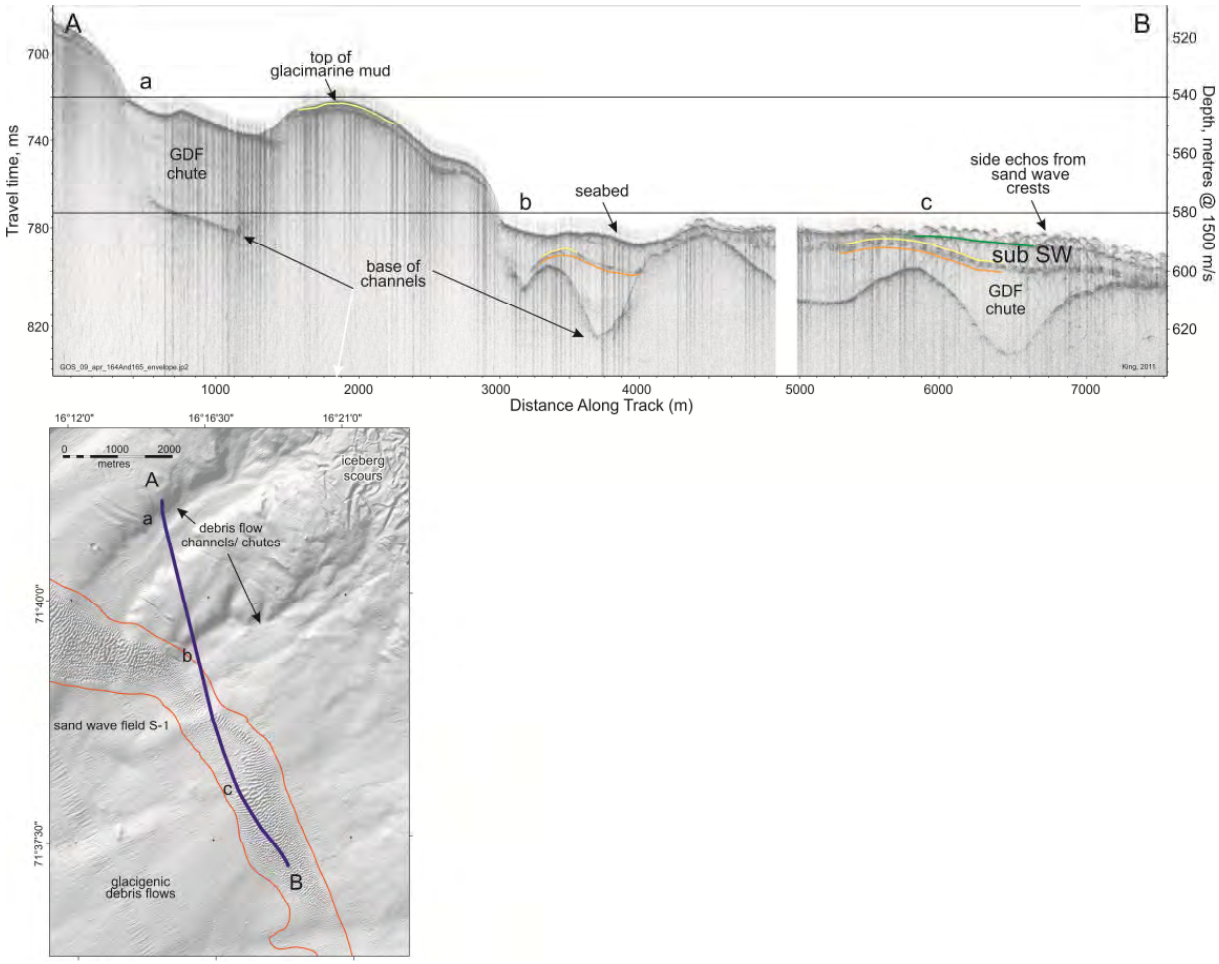

Figure 18. TOPAS sub-bottom profiler transect across the southern sand wave field. Glacigenic Debris Flow (GDF)-filled channels (eg. positions a and, b, flow tops locally shown in orange) are overlain by a blanket of glaciomarine muds about 3 m thick (top shown, yellow). This blanket is covered with later deposits demonstrating an homogeneous internal acoustic character (labled sub SW, top, green) in the sandwave field that are not present, for example, on the channel interfluve farther upslope. It is in turn covered with the present-day sandwave sands with a gravelly base marked locally in green. Stratigraphic relationships elsewhere in the region are similar (Figs. 19 to 22 and 25). The question arises as to the genesis of this upper deposit (sub-SW). Is it a later debris flow event or does it have an earlier sandwave genesis? Strategic core sampling is planned; the two alternative interpretations would imply cohesive and non-cohesive sediments respectively.

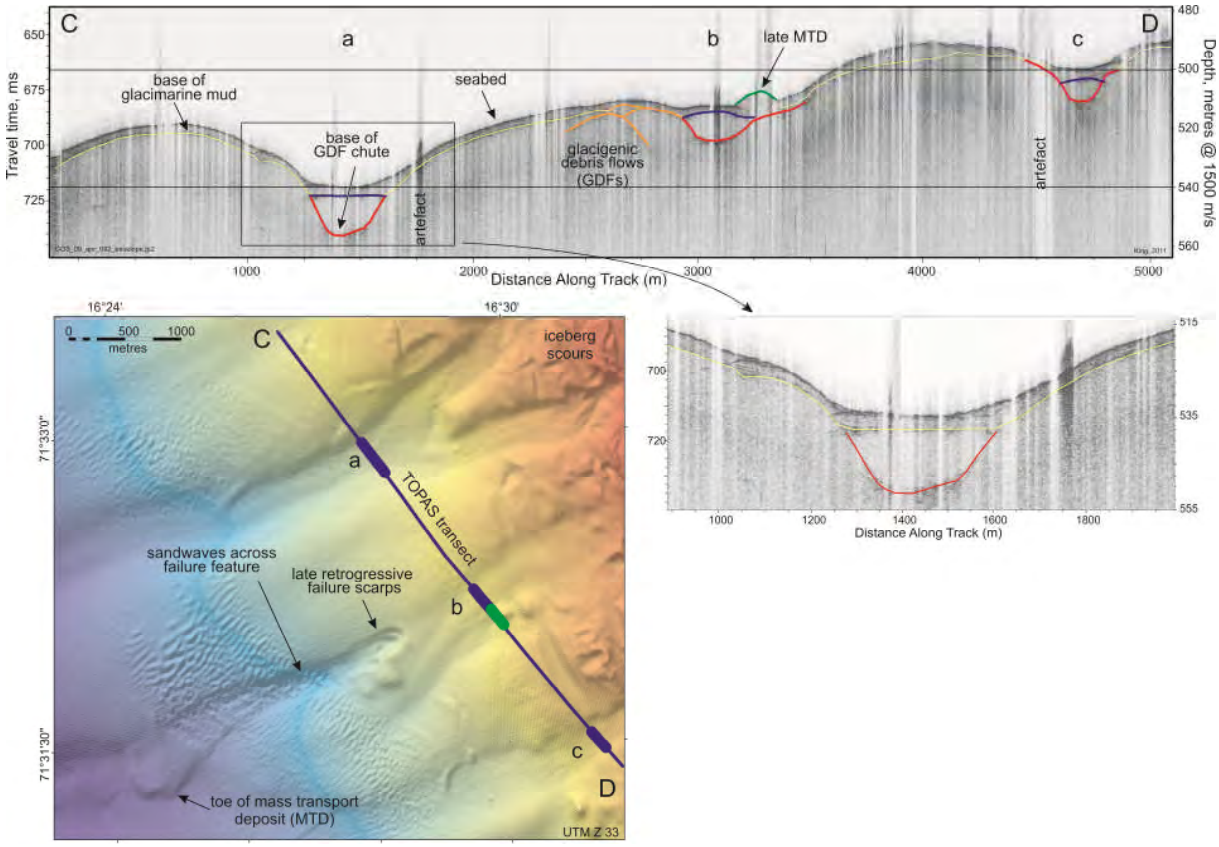

Figure 19. TOPAS sub-bottom profiler transect across the southernmost north sandwave field. Mass Transport Deposit (MTD)- filled chutes (channels a, b, c) between sets of stacked or en-echelon glacigenic debris flows (GDFs) themselves contain debrite-like mass transport deposits. These likely deposited while the ice sheet was at the shelf-break. They are overlain by a blanket of glaciomarine muds about 3 m thick. Relationships suggest that sandwaves initiation postdates both this and a later, retrogressive MTD event, displaying a stepped headwall and a corresponding depositional lobe. Noise artefacts on the TOPAS transect arise from air under the transducer with excessive ship heave.

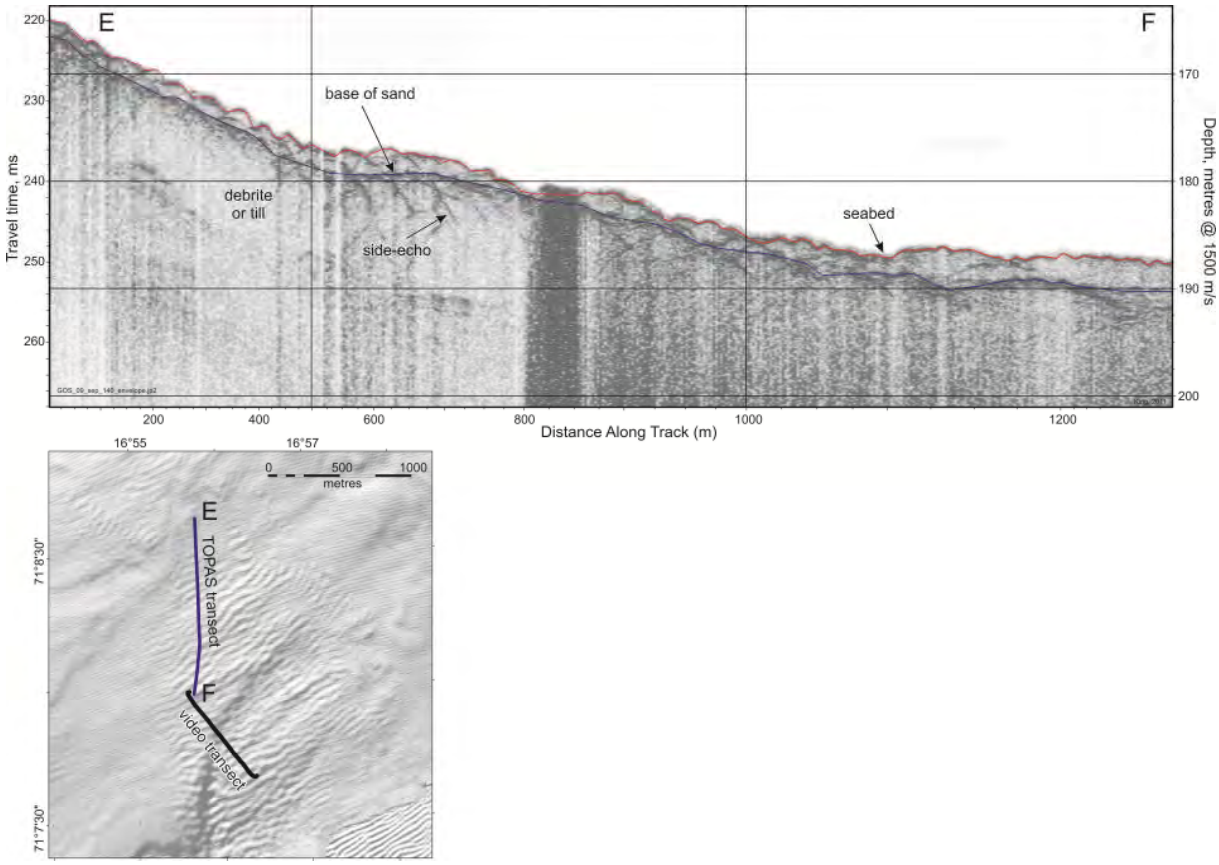

Figure 20. TOPAS sub-bottom profiler transect across the northern area of the southern sand wave field. The relatively steep bedform faces create hyperbolic side-echo artefacts. The base of the sand field is glacially-derived diamicts. Sand here is between one and four metres thick with bedform amplitude about one metre. Note the variable horizontal scale as the ship decelerated toward video station R471, also leading to excess background noise.

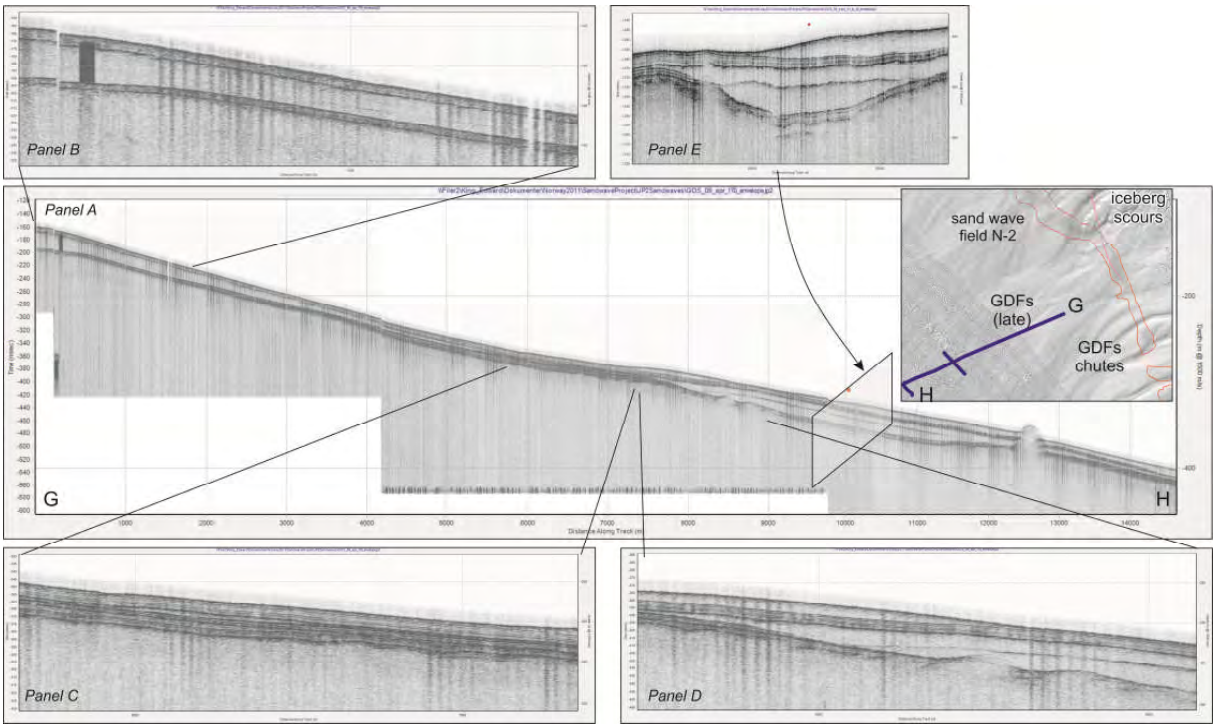

Figure 21. TOPAS sub-bottom profiler transects located below the sandwave N-2 field. Glacigenic Debris Flows (GDFs) (flow tops locally shown in orange) are interbedded with glaciomarine muds (top shown, yellow). A thick GDF is buried by stratified glaciomarine mud on the upper slope (Panel B), while the latest of the GDFs crop out on the lower part of the slope (Panels C, D and E), with little or no glacimarine mud cover. The stratigraphic relationships are thus identical to those in the sand wave field (Figs. 18 to 21), with a seismically homogeneous body under the sand. However, the alternate interpretation, whereby all the acoustically homogeneous wedges and lenses represent GDFs, is more demonstrable than within the GDF chutes farther up the slope, in the previous illustrations. The implication is that the outcropping GDF is analogous to that immediately underlying the sand waves. Thus the argument that bed "sub-SW" in Figure 18 has a genesis in older sand waves is weakened.

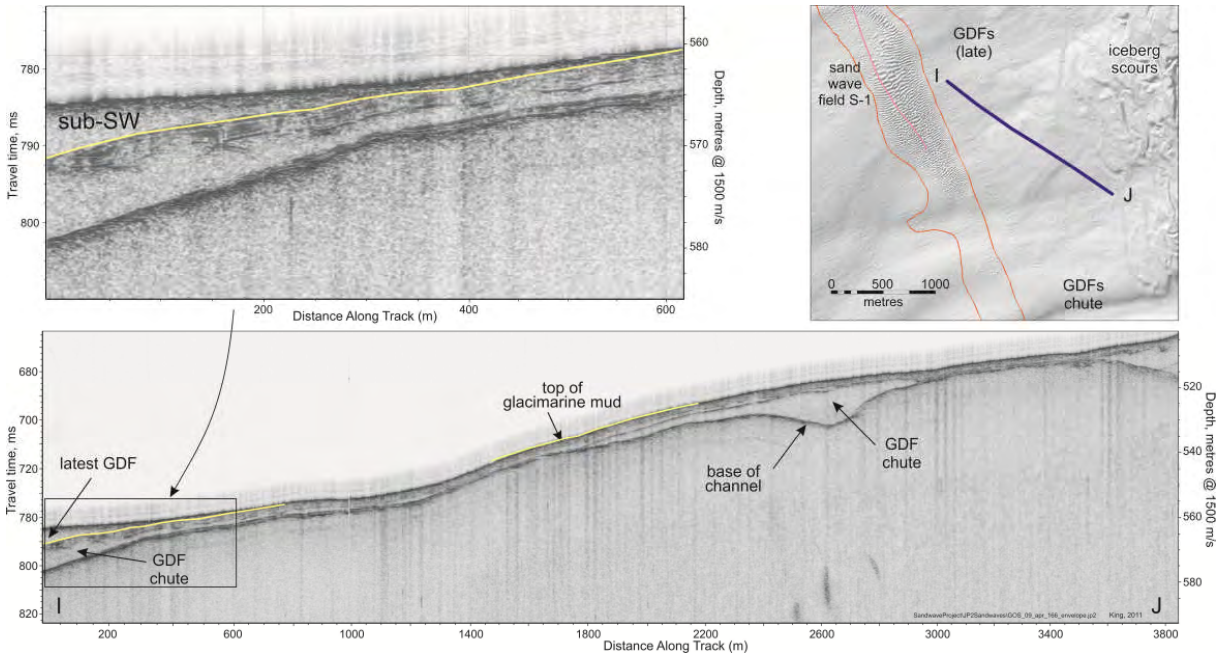

Figure 22. TOPAS sub-bottom profiler transect located above the sand wave S-1 field. Glacigenic Debris Flows (GDFs) and associated chutes are interbedded with a glaciomarine mud blanket. The latest of the GDFs (sub-SW) here is the same depositional body directly underlying the sandwaves immediately downslope. Thus, the series of illustrations (Figs. 18 to 22) demonstrate that this sandwave field has not generated a body of stratigraphically distinct immobile sand since its inception. The seabed engineering implication is that without any long-term aggradation, this system will continue to simply bypass sands across the slope in this area. Further regional sub-bottom profile surveying in the other fields should be conducted to substantiate this conclusion. Note that this finding provides little constraint in terms of bedform movement or flux.

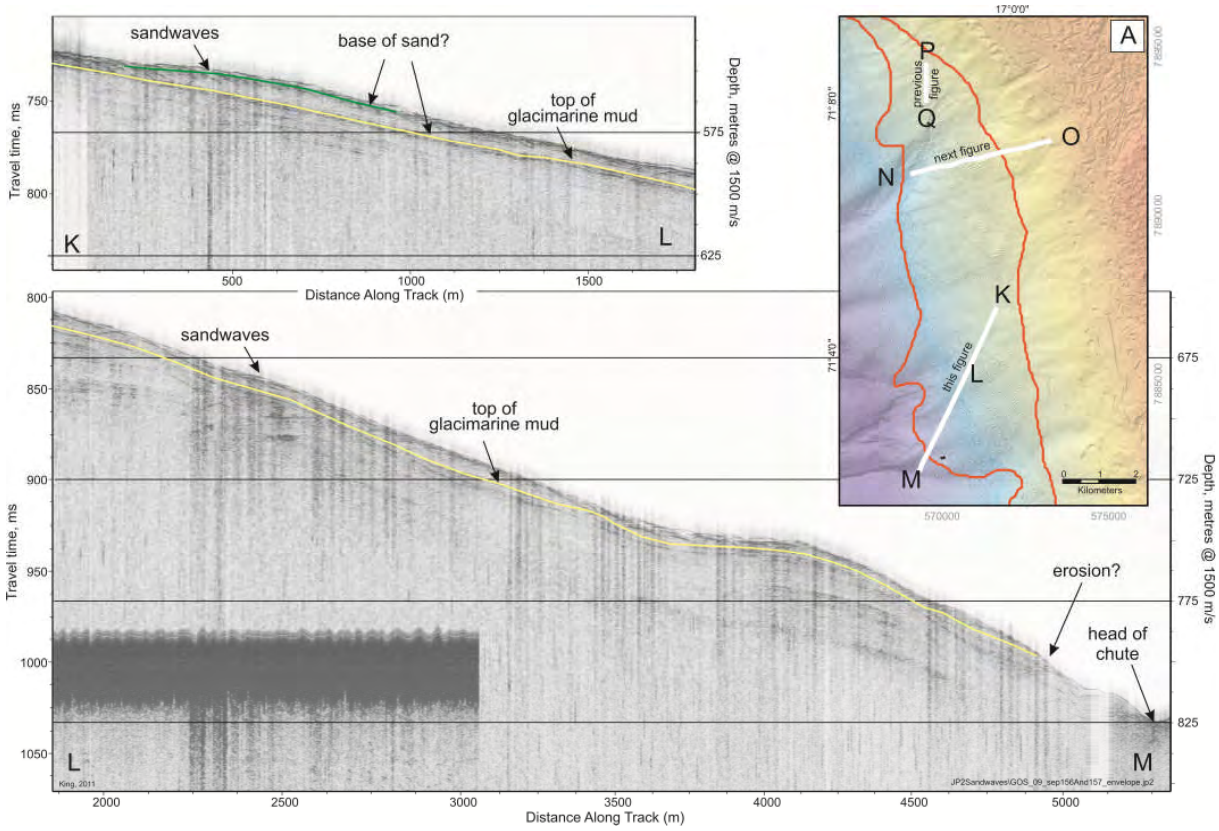

Figure 23. TOPAS sub-bottom profiler transect across the sandwave S-1 field. The upper panel (K-L) connects with the lower (L-M) with a small data gap at point «L» on the map. Small sandwaves lie on top of stratified glaciomarine sediments. There is some uncertainty if the sandwave sand is thin or thicker (green versus yellow base, panel K-L). Planned TOPAS surveying across the fields in 2012 will better confirm the stratigraphic continuity of the base of the sands, somewhat hampered here by isolated survey lines. The chute at the base of the profile is a possible conduit for sandwave-migrated sands out of the system, that is, a pathway to a sand sink much farther downslope.

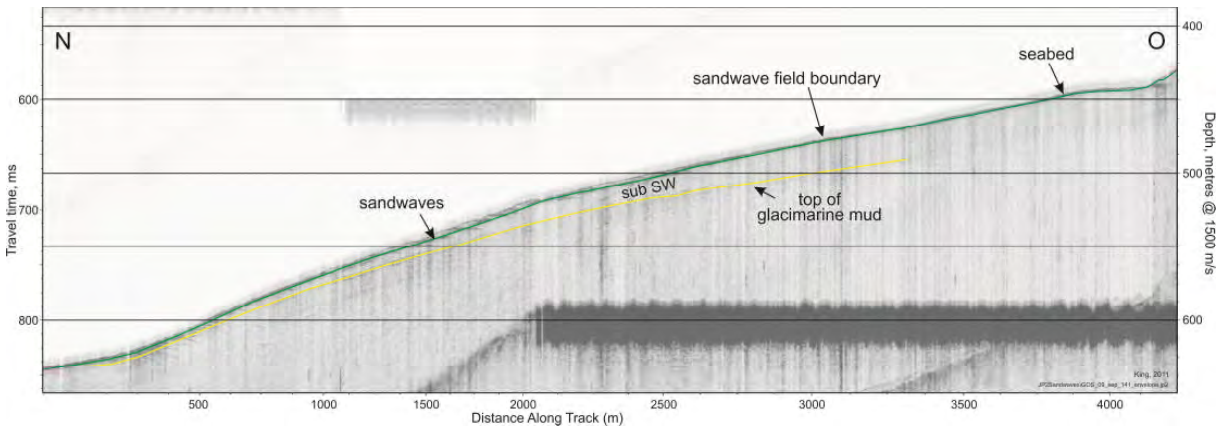

Figure 24. TOPAS sub-bottom profiler transect from near the shelf-break to the sand wave S-1 field. Small sandwaves make up a very thin bed lying on top of un-stratified glacial sediments (sub-SW unit). Location and setting, see previous figure.

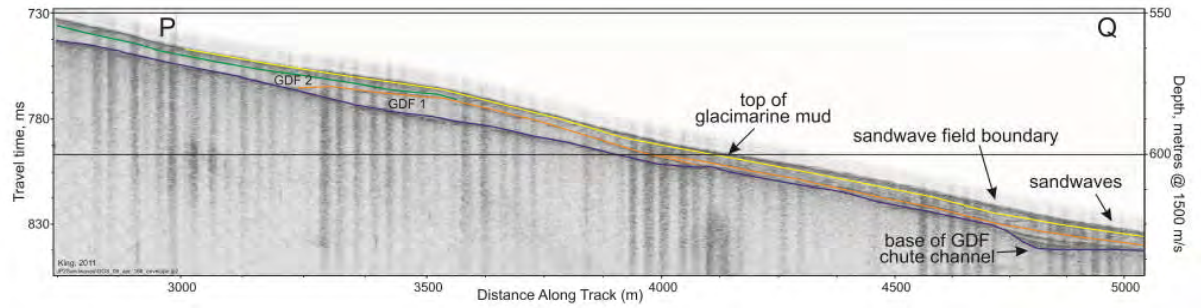

Figure 25. TOPAS sub-bottom profiler transect across the sand wave N-2 field. The sandwaves lie on top of a stratified glaciomarine mud blanket.

Figures 18 and 19 are TOPAS transects along the slope immediately upslope of the S-1field and N3-4 fields respectively. Both show channel cuts and lens shaped infilling bodies (in profile) characterized by an acoustically semi-transparent, incoherent and homogeneous signal. These are locally stacked and demonstrate migration of successive stacked lobes (stacking best seen in Fig. 21), though limited acoustic penetration generally precludes definition of the older deposits. Sections 4.4 and 4.5 show video and grab samples depicting gravel and cobble-rich material where bedform sands are so thin as to expose the underlying deposits. These coarse sediments can only have been transported by glacially related downslope processes, early post-glacial iceberg rafting, or later translational slides. The latter are very evident elsewhere and can be largely discounted here, at least for the time frames relevant to the upper tens of metres of deposits. These are typical channel-fill bodies (King et al. 1996, Laberg and Vorren 1995, Vorren et al. 1998, Laberg et al. 2010), interpreted to represent cohesive mass transport, debris flow type processes under late glacial conditions while the ice margin remained very close by at or near the shelf break. They may have been responsible for channel cutting also but pre-debris flow cutting by non-cohesive flows cannot be discounted. These flows are typically covered or interbedded with the same semi-stratified blanket across this part of the upper slope. In this case, it is uniformly about three metres thick, with little differential intra versus extra-channel sedimentation rate. Though not sampled here, this is an identical setting to large parts of this margin and these are the product of deglacial plume and IRD processes. This blanket gives a subdued, smoothed character to the shaded-relief images of the slope which contrasts with the sharp topography of the sandwaves. This suggests that most (perhaps not all) MDT processes pre-date most of the latest deglaciation.

In Figure 18, the glaciomarine mud blanket is in turn covered with later deposits with an homogeneous internal acoustic character lying just below the sandwave sands. The genesis of the homogeneous unit below the sand might be interpreted as debris flow event or an earlier, and now buried, sandwave generated body. Strategic core sampling is planned in the 2012 summer season. The two alternative interpretations would imply cohesive and non-cohesive sediments respectively.

Stratigraphic relationships are difficult to establish directly because the survey lines did not cross the sand wave field. However, Figure 19 shows that the sandwave field passes, largely uninfluenced in distribution, across both the path of the slightly buried MTD deposits as well as a small but much more recent failure scarp and depositional lobe. These sandwaves sit upon the glaciomarine blanket as they are only decimetres in amplitude here and they pass over the even more recent (though undated) failure event. This establishes that they are, geologically speaking, the latest "event". Sampling and dating of the most recent MTD has not only the potential to establish its age, an important goal in other geohazards-related studies at NGU, but it would also place a maximum age on the sandwaves. Thus cross-cutting relationships alone indicate a relatively recent age, perhaps as old as the inception of contour currents driving the sandwaves. See section 8.6.

Figure 21 demonstrates the nature of the GDFs on the mid slope. Typical of these deposits, they present as wedges and lenses in profile, in this case interbedded with stratified glaciomarine muds. Acoustic character alone is not sufficient to interpret them as cohesive (muddy) debris flows. Their geometry, in section combined with plan view shows that these are typical examples of GDFs as established through more complete studies elsewhere on the Norwegian margin (cf. King et al. 1996, Laberg et al. 2010). The nature of the downslope and apparent upslope pinchout of such flows is important in the context of the sandwave fields where, further up on the slope and within the GDF chutes, the GDF genesis is not as clear. Comparison between GDF chutes and flows in figures 21 and 22 show that the later site, located just upslope from sandwave field S-1, also comprises GDFs just below the sandwaves and not older and inactive sand, as might be suspected. Planned coring can help confirm this interpretation. A short core penetrating into the sub-sandwave (sub-SW) unit would encounter cohesive muds in the case of GDFs and sands otherwise. Some indication of the underlying material was gained at video station R477, where grey, glacial-like mud was exposed, apparently through bottom trawling (Fig. 10). At this location, however, we lack the TOPAS control to establish the seismic-lithologic link.

Figures 23, 24 and 25 complete the documentation of TOPAS coverage in the sandwave fields. Lacking a strong sub-bottom reflector beneath the sandwaves, the central part of the S-1 sandwave field (Figure 23) apparently has sand thicknesses up to several metres (typically 7 to 10 m and under 13 m). This exceeds the sandwave heights in this area which are typically under 1 m high, maximum 2.5 m at this site. If, in fact the entire seismic unit comprises sand, as suggested here, then this represents a significant sand volume and suggests volume estimates by the technique in Section 6.7.2).

5.2 Sand thickness and a sand sink

A stratigraphic interpretation of the TOPAS transects was conducted using the Canadian-developed seismic viewer, SEGY JP2 Viewer (Courtney 2007). Figure 26 shows the spatial and frequency distribution of sand thickness.

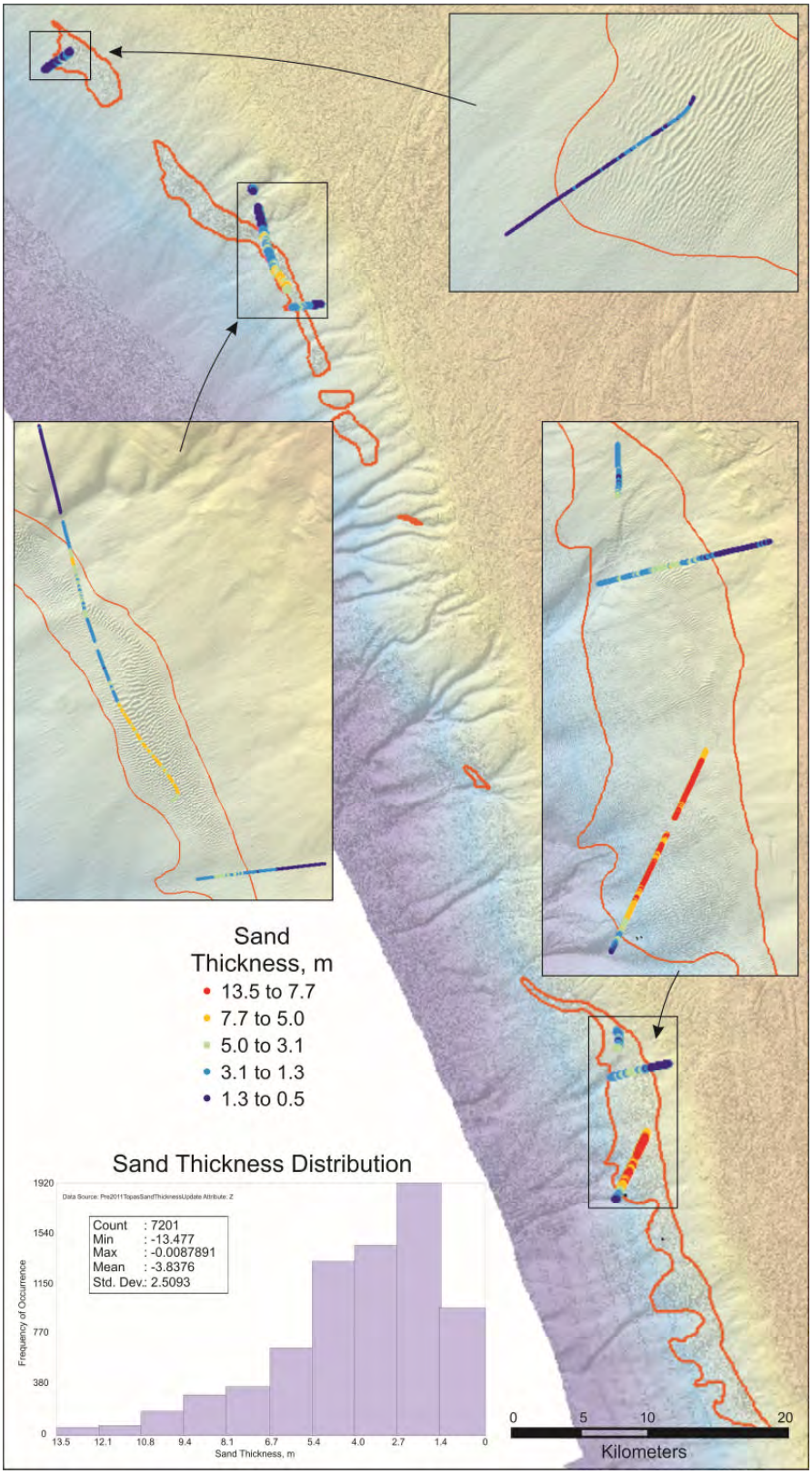

Figure 26. Thickness of the uppermost seismic unit, interpreted to be sand comprising the sandwaves or sand previously activated by sandwaves. The thickest sands are in the mid S-1 field (red dots where the interpretation is somewhat uncertain; it may be considerably thinner. Further surveying as part of this project (planned summer 2012) will confirm or refute this interpretation.

This is a preliminary and very incomplete picture. The values plotted here represent seabed to first sub-bottom reflector, which, in the previous sections, has been demonstrated to represent the sands associated with either presently active or (less?) active deposits immediately below the bedforms themselves. Note that there is some uncertainty in this interpretation but this arises more from the lack of continuity of the TOPAS data than the geological concept. As such, further planned surveying will clarify and provide much more detail on the sand thickness. It will also help establish if sites with sand thickness significantly exceeding the bedform heights actually represent inactive sand. If this is the case, then this sand below the bedform troughs represents a sediment sink in itself and mitigates the "need" to look outside the sandwave fields for sink deposits (eg. in the GDF chutes). Further estimates of the sand thickness (volume) are presented in Section 6.7.2 and in Table 1.

5.3 Summary and Implications of the Stratigraphic Findings

Mass transport chutes and infilling GDFs provide the general setting of the slope area. They are interbedded with stratified (waterlain) glaciomarine sediments and represent downslope processes while glacial ice was near and at the shelf break. Superimposed on these are the sandwave fields. They cross both the glacial deposits and a younger mass transport deposit (MTD) apparently unimpeded.

The sand waves lie directly on top of the glacial deposits with little sign of erosion or aggradation. Such relationships might exist elsewhere and should be investigated with further TOPAS surveying. Their overall distribution shows little dependence on the down-hill oriented GDF chutes; fields dip into and out of these depressions. There may be some local hydrographic (or geologic) affects, as suggested in later sections, but only the small N-5 field is entirely within a GDF chute, and this may be largely coincidental (Fig. 27).

Though most TOPAS traverses depict very thin sands, about equivalent to the heights of the sandwaves, there is local evidence of thick sands (generally under 10 m).

Further sections will demonstrate some level of present day activity/mobility of the sand but all evidence to date suggests that the sandwaves developed after glacial activity ceased, during the Holocene, perhaps well into this chron, and they have not preserved multiple phases or migration and preservation of the sand, and that there is no clear process relationship with the older downhill chutes, ie. the gullys are not trapping or guiding sands down their axes.

It follows from above that no voluminous sand source or sink is readily apparent. This suggests that small scale and fairly local erosion of the glacial deposits releases enough sand to keep the field supplied in a dynamically stable situation with little bypass of sand. The

most apparent sink for the sand is within the field itself, in locally thicker deposits superimposed with sandwaves that no longer activate these sands.

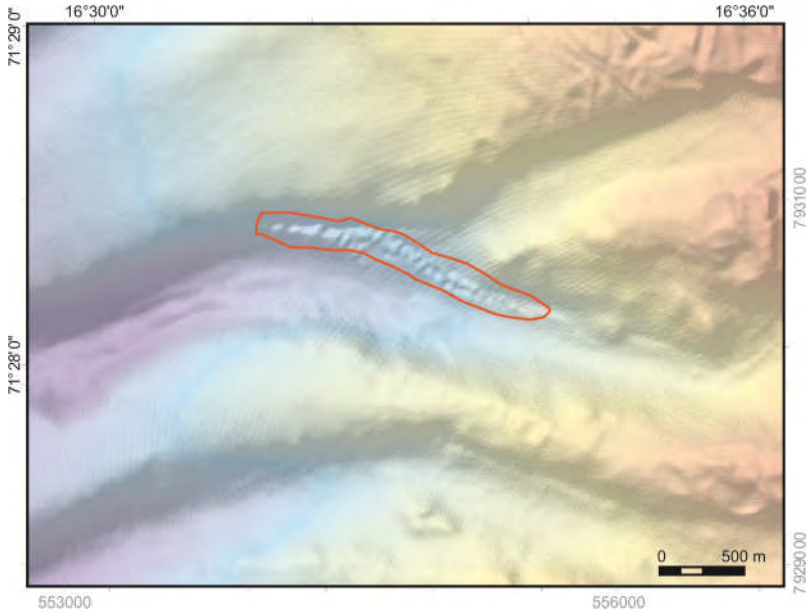

Figure 27. The small N-5 field is the only example of sandwaves confined to a gully or GDF chute, possibly because the chute orientation steers and accelerates the flow locally.

6. SANDWAVE MORPHOMETRICS

Measurement of sandwaves is a routine technique to describe and assess their potential direction and magnitude of movement. Parameters such as heights, slopes and symmetry can be derived and potentially indicate level of bedform activity and transport directions.

6.1 Methods

Sandwaves metrics were derived from the bathymetric grid for each of the fields to fully characterize the amplitudes, wavelengths, symmetry, steepness and setting with respect to regional topography. This was accomplished through a combination of extraction, filtering, auto-picking of troughs and crests and subsequent filtering in both GIS and spreadsheet environments. The ESRI ArcMap and ArcInfo GIS products (Version 10) were utilized in this study. Most feature classes, including foundation data, such as DEMs and derivative shaded relief, curvature, slope rasters as well as all the compilation point line and polygon data and all the spatially-related morphometrics and statistical derivatives were assembled in a file geodatabase called EggakantenSandwaves.gdb. All data are stored and displayed as UTM projections at Zone 33 (MAREANO project standard). Many of the interim data derivatives were assembled in a series of Microsoft Excel™ spreadsheets derived from the GIS data, where autopicking of key morphometrics components of the sandwaves and calculation of the metrics was performed. A separate document was assembled outlining the rational and the

step by step procedures along with some discussion of their strengths and weaknesses. This document was not fully evolved and edited to be incorporated into this report; it is an internal NGU reference only, but can be made available from the authors (entitled King EggakantenSandwaveObservationsProceedures.docx).

For each of six separate fields with a coherent crestline orientation (within 20 degrees), depth profiles were derived along crestline-normal lines at 100 metre spacing. Bathymetric values along all lines were extracted at 5 m intervals from the 5 metre binned DEM and assembled in spreadsheets. Figure 28 shows an example of the lines and points.

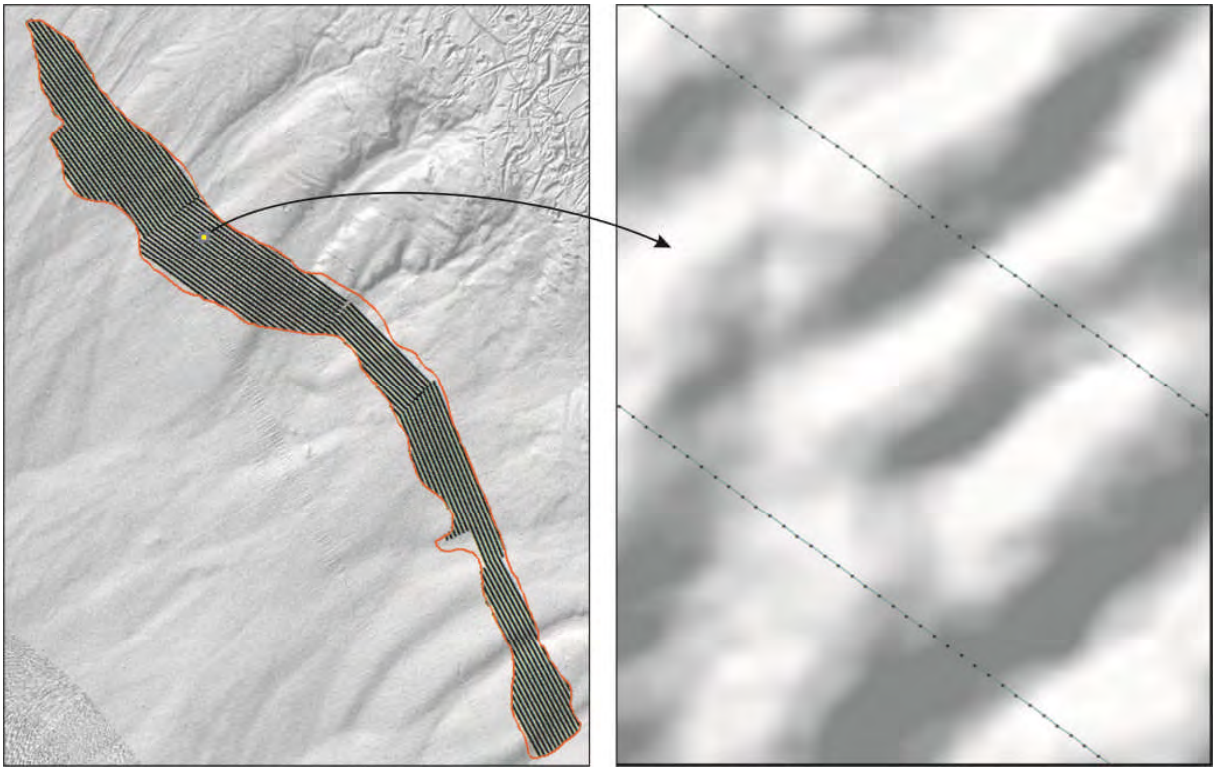

Figure 28. Lines constructed at 100 m spacing normal to the crestline trends and, truncated at the sandwave field boundaries were used to generate points along the lines at 5 m spacing. These were attributed with the multibeam DEM water depths, assigned UTM coordinates (zone 33) and then imported into a spreadsheet for further manipulation.

An auto-picking routine to recognize minima and maxima (troughs, crests, and flanking slope maxima) was performed on a slightly smoothed derivative of the bathymetric profiles. Techniques are shown graphically in Figure 29.

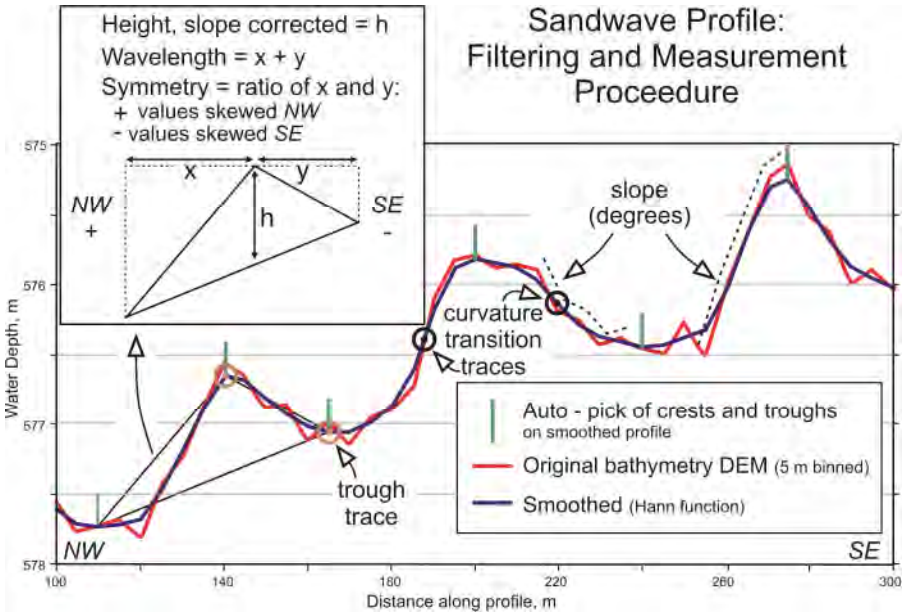

Figure 29. Selected bathymetric profile from sandwaves in the northernmost field demonstrating procedure for derivation of the metrics. Bathymetric profiles were generated across the entire field, normal to the sandwaves, at 100 m spacing. The original bathymetric profile (red) was smoothed (blue). Symmetry calculation involved computing x/y which produced positive values for northwest-skewed forms and fractional values for southeast-skewed forms. For the latter (south), an inverse function produced negative values of comparable magnitude, allowing generation of simple histogram distributions ("+" for NW skew and "-" for SE skew). Height/wavelength ratios were calculated for each form. Slope and backscatter values (seabed micro-roughness) were generated as a grid from the DEM at full (5 m) horizontal resolution and then attributed to the auto-pick points. Slope was calculated for both bedform flanks as was their ratio and the same negative inverse function applied to fractional values (as for skew).

Smoothing of the bathymetric profile was necessary to minimize small perturbations, presumably both noise and superimposed bedforms, whose measurement locally excluded recognition of the larger (> 1 m high) bedforms. The smoothing utilized was a Hann function, adapted for this specific Excel spreadsheet use. It maintained bedform relief more faithfully than a running average. Figure 30 displays a comparison of pre and post smoothing (red and blue depth profiles).

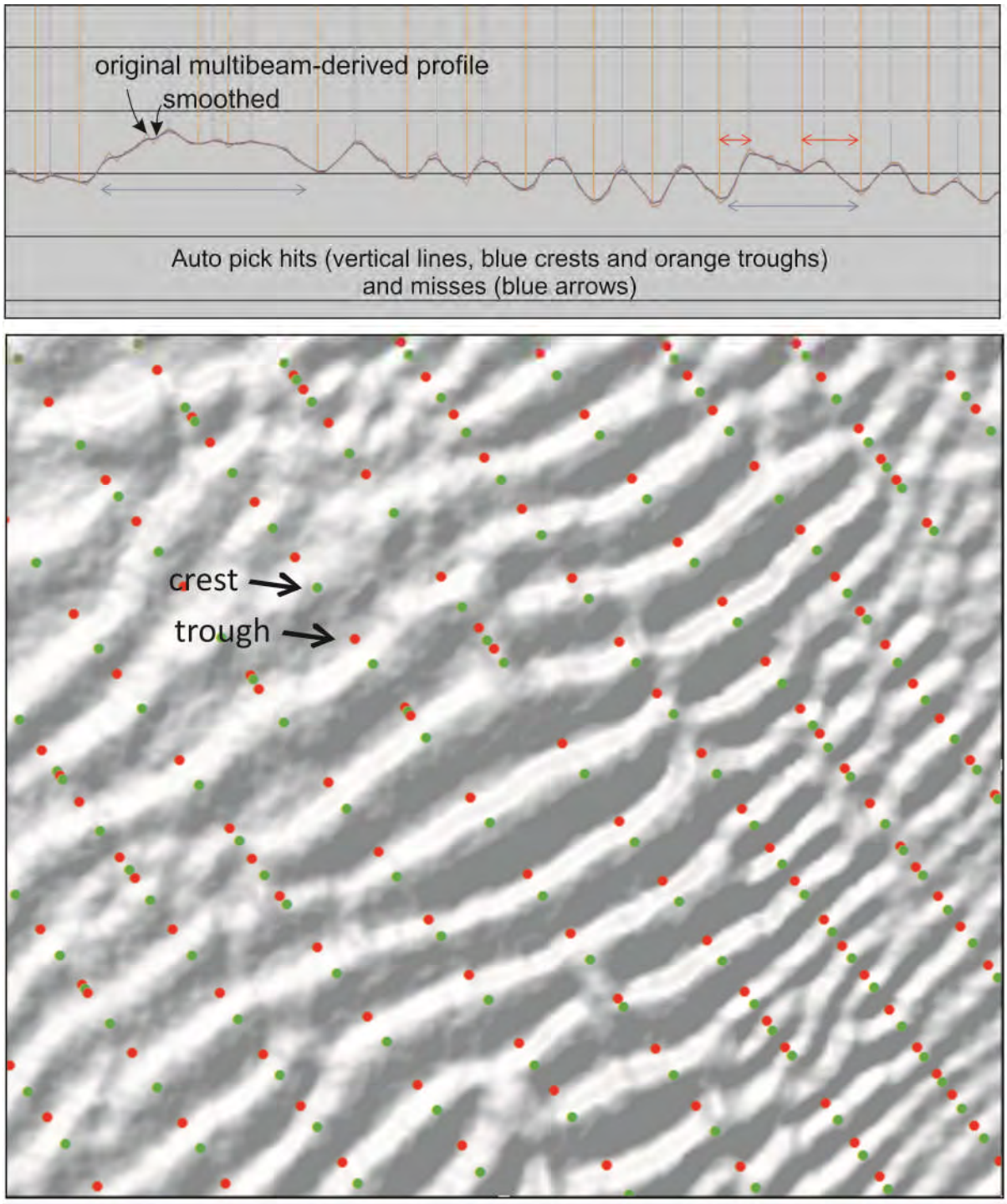

Figure 30. Example of spreadsheet derived auto-pick results for recognition of bedform troughs and crests. Upper panel shows a profile excerpt where the vertical lines mark the auto-pick of troughs and crests. The goal was to derive large enough samples to generate robust statistics. In all nearly 30 000 bedforms were identified using this technique. The lower panel shows these results fed back into the GIS display. The trough sites were assigned the morphometric attributes (e.g. height, width, symmetry, slope, curvature, backscatter, height/wavelength ratio). A small percentage of auto-pick "misses" relate to the larger bedforms, either where they are compound (near crestline bifurcations) or have smaller, superimposed bedforms. This was deemed so seldom as to have little statistical effect.

The auto-picked values were filtered to eliminate low amplitude (<10 cm) and very short and long wavelength (>1000 m) forms which represented noise and non-bedform morphology such as small-scale glacigenic debris flow channel flanks. This required a limited manual filtering by visual inspection of the points with respect to non-bedform features.

Sandwave slopes were derived in GIS from the DEM as gridded values at original 5 m resolution; better resolution is unlikely given hull-mounted surveys in 600 m water depth. This bin size is critical, as discussed in further sections. The suspicion is that some of the features critical to process understanding may be too smoothed to recognize their presence and thus significance.

These measurements provided the basis for robust statistics of the bedform metrics, including *height*, *wavelength*, *profile symmetry*, and stoss and lee flank *slope* and crest and trough *sediment texture*. Figure 29 outlines the derivation of these parameters.

All measurements preserved data point location coordinates such that their spatial distributions within and among the fields could also be investigated by re-entering values in the GIS environment and enabling visualization of their spatial relationships.

By convention in this report the authors refer to the SSE-facing flank of the sandwaves as the stoss (erosional, experiencing current acceleration toward the crest) or the upstream face and the NNW flank as the lee (depositional, slip-face) or downstream. Note that the video observations Section (4.4) do not have compass orientation information and as such there is an implicit assumption that the lee faces, sometimes easily recognized, are facing NW or NNW. This may be incorrect. Similarly, in this section the stoss-SE and lee-NW terminology is used rather interchangeably and strictly speaking too loosely; it is precisely this relationship that some of the measurements attempt to confirm or refute.

6.2 Water depths

Figures 2 and 3 show the apparent water depth constrictions that the sandwave fields follow. The hypothesis is that their spatial coincidence with the thermocline indicates some causal relationship. Figure 31 shows the detailed frequency distribution of all measured bedforms with respect to water depth.

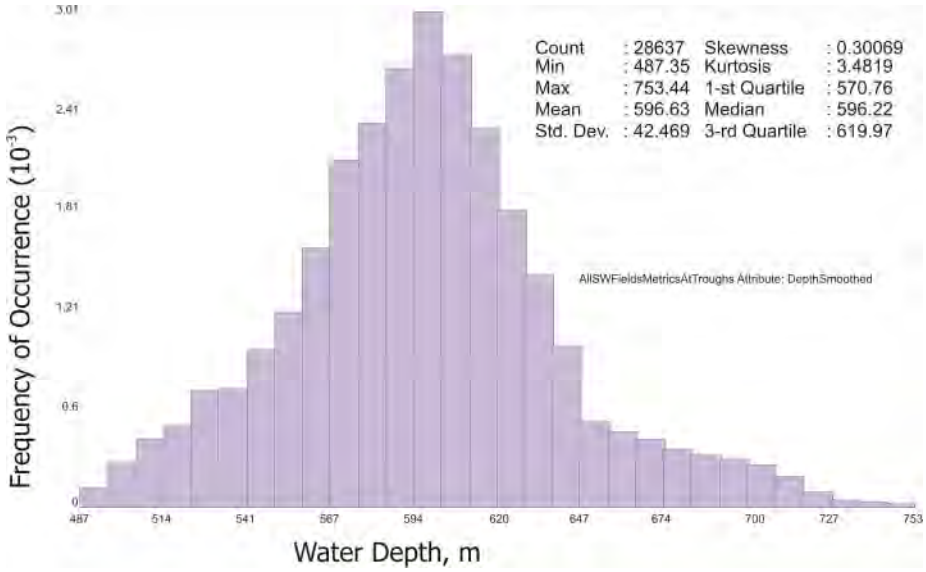

Figure 31. Distribution of water depths for all measured sandwaves.

Definition of this distribution and the link with oceanography may be significant later in the project when the seasonal upslope-downslope migration of the thermocline is better understood.

6.3 Bedform texture

Information on bedform texture is largely from the backscatter images but the sampling is invaluable as control (Sections 4.4 and 4.5). Cursory observation of the backscatter images in the sandwave fields reveals that some of the troughs exhibit higher backscatter and therefore have a coarser texture than the crests. The video and sampling confirms gravel and cobbles, often with a sand dusting while the crests are always sandy, with ripples and a variable amount of fine shell hash. Figure 32 shows an example of the elevated backscatter in the troughs.

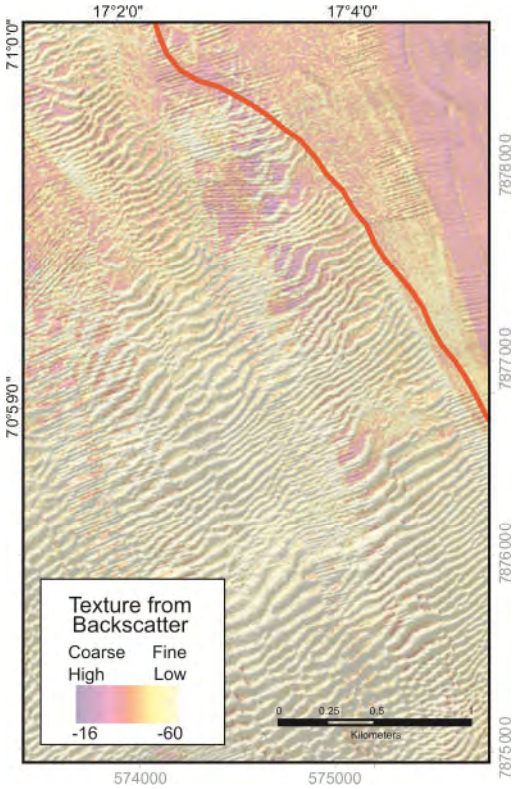

Figure 32. This site in the S-1 field shows a clear dominance of high backscatter in the troughs of some sandwaves. Video observations indicate that this is generally a lag deposit sitting directly on glacially-derived muddy debris flows. All the trough and crest auto-pick points were assigned backscatter values extracted from such multibeam images to demonstrate the propensity of this phenomenon.

Other areas show a clear streaking of high backscatter normal to the bedform crestlines, generally suspect as noise inherent in the collection of these data. Still others show a propensity for higher lee-side backscatter. Though not tested here, small ripples approaching gravel and cobble dimensions should also give rise to increased backscatter (observed commonly on low frequency sidescan images). Thus an erroneous interpretation of gravel might arise where ripples are common, as on these sandwaves. A statistical evaluation was undertaken.

6.3.1 Technique

Two compilation techniques were used. The first, later abandoned, was to manually trace troughs and crests in GIS and extract backscatter values. The other was to use the auto-picked trough and crest locations and attribute these with backscatter values extracted from the multibeam-derived images.

6.3.2 Results

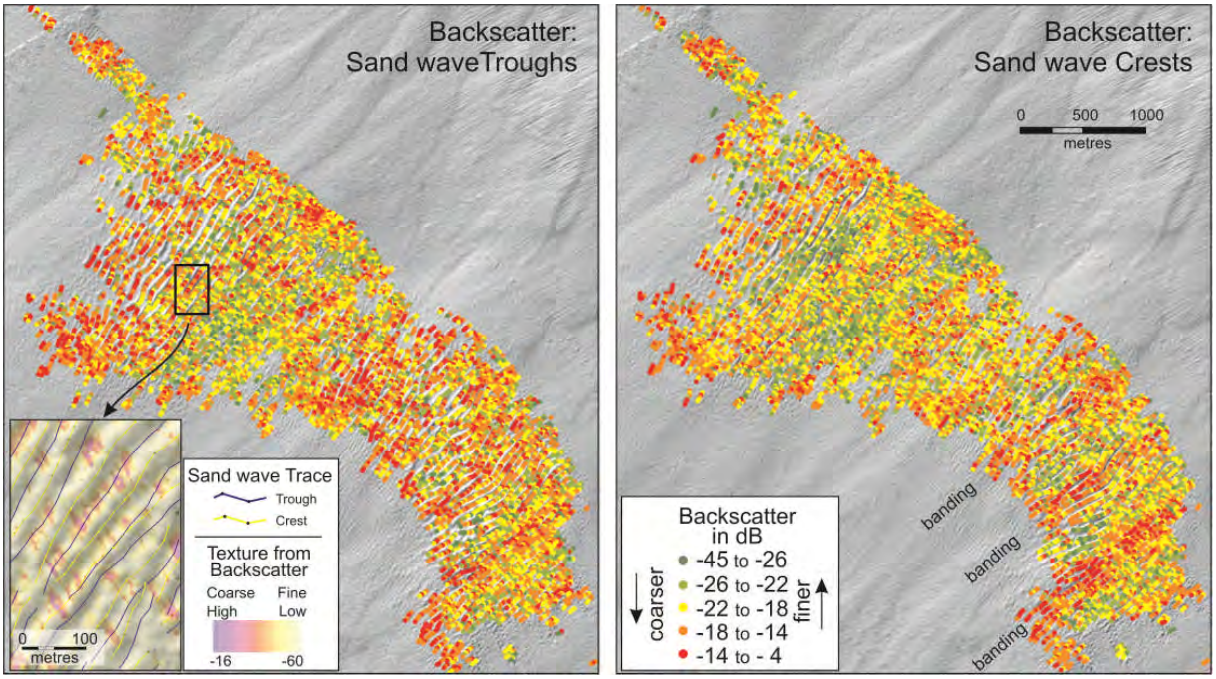

Figure 33. Seabed texture in the troughs (left) and at the crests (right) of sandwave in the N-1 field, superimposed on a shaded relief image (illumination from 315°). The insert (lower left) shows how this was derived from traces of the troughs and crests superimposed on the backscatter image. A strong trend towards coarser troughs than crests is demonstrated. Bands of coarser (higher backscatter) crest texture are apparently due to imprecise balancing of backscatter values from line to line or across the multibeam sonar lobes. Thus they introduce considerable noise in the analysis. The original backscatter grid exhibits an along slope (current parallel) pattern of coarse texture (normal to the troughs). This might be noise but it might represent ribbon-like development between sandwaves or blow-outs.

Figure 33 shows crest versus trough backscatter results using the manual trace technique, conducted only on the N-1 field. Clearly there are more abundant red and warm colours associated with troughs but examples are common on crests also. However, colour banding across the field suggest a high level of backscatter value noise (parallel to survey line orientations). Statistical comparisons of the backscatter values (Fig. 34) for the N-1 field only show little crest-trough difference for the overall field; a nearly negligible trend towards more frequent coarse than fine grained troughs.

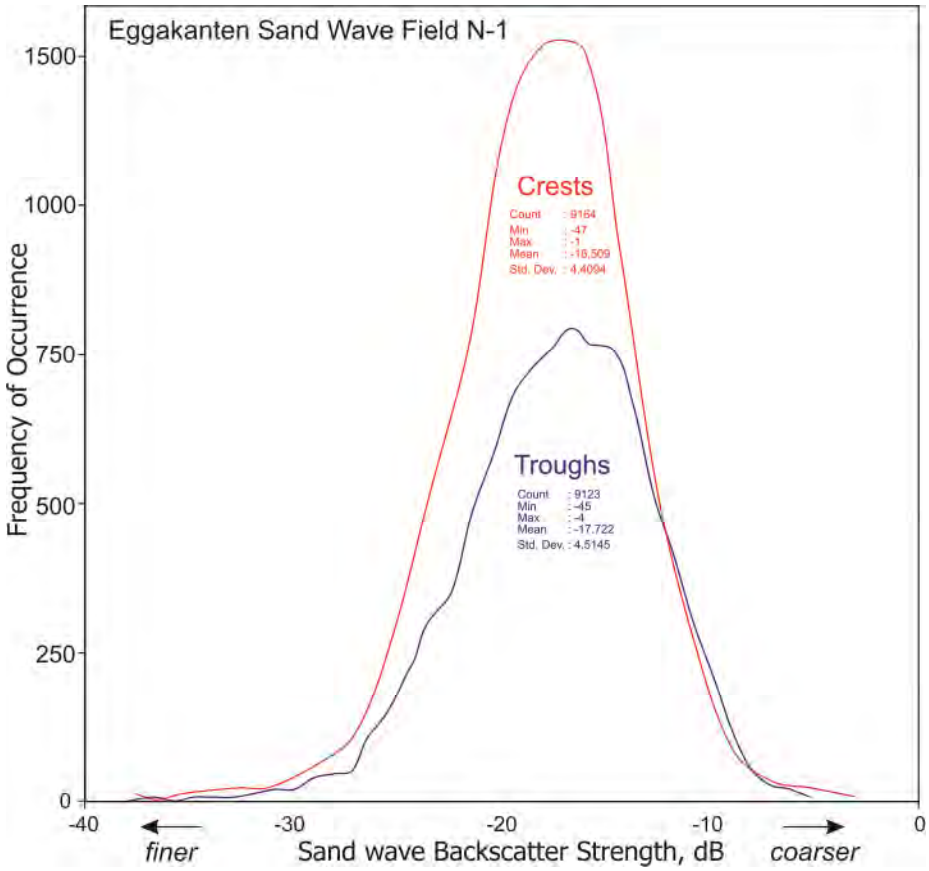

Figure 34. Comparison of crest versus trough backscatter values for the N-1 field, derived from along manual traces of the sandwaves. Despite clear examples of the differences in a spatial sense as demonstrated in Figure 32, these populations are not unique. This is partly due to some noise in the backscatter values which is independent of the bedforms and because of averaging of the smaller forms where crest trough backscatter differences are negligible.

Backscatter values for troughs and crests were also compiled for the other sandwave fields. Figure 35 compares trough versus crest values for the northern part of the S-1 field. It is clear that values are much affected by noise; the patterns follow ship's tracks to a large degree. The same is largely true for the N-2 to N-4 fields (Figure 36) but here there some spatial clustering of abundant coarse troughs and fewer coarse crests.

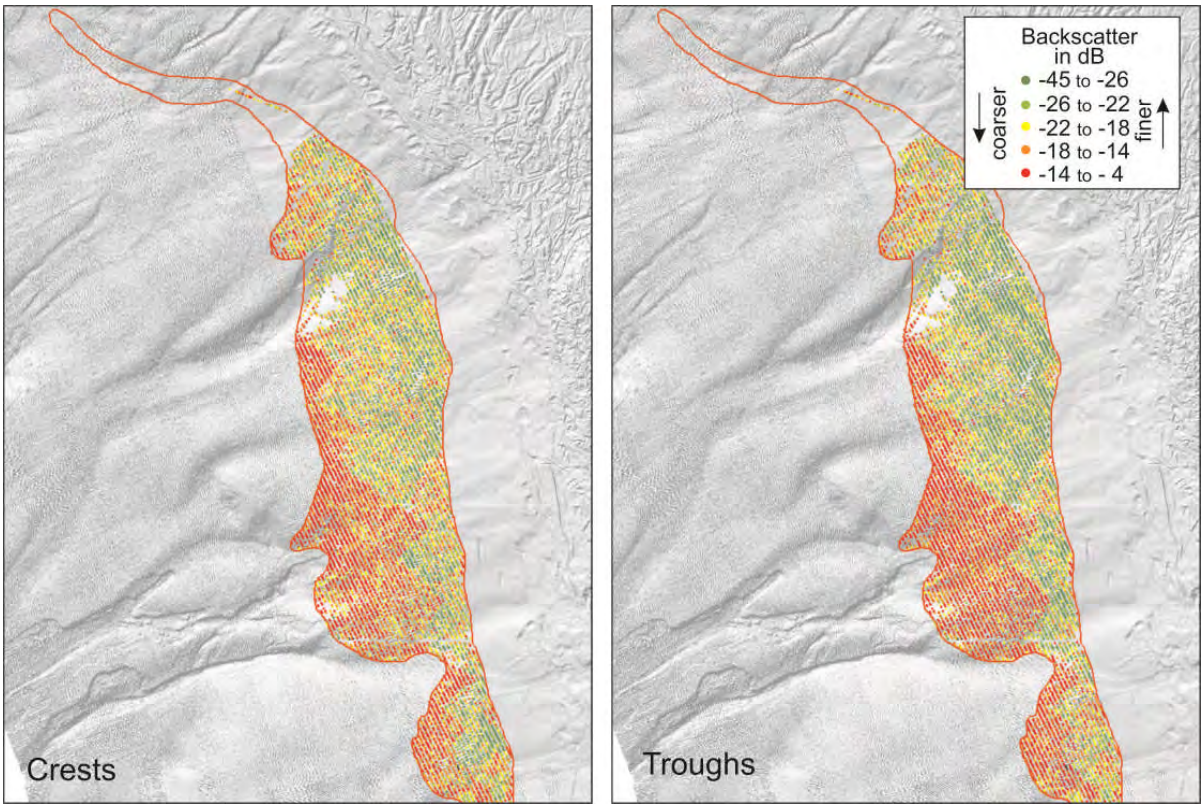

Figure 35. Backscatter comparisons for troughs and crests in the S-1 field. The rectilinear pattern reflects ship's tracks and highlights the noise levels in the data more than it does bedform-related relationships.

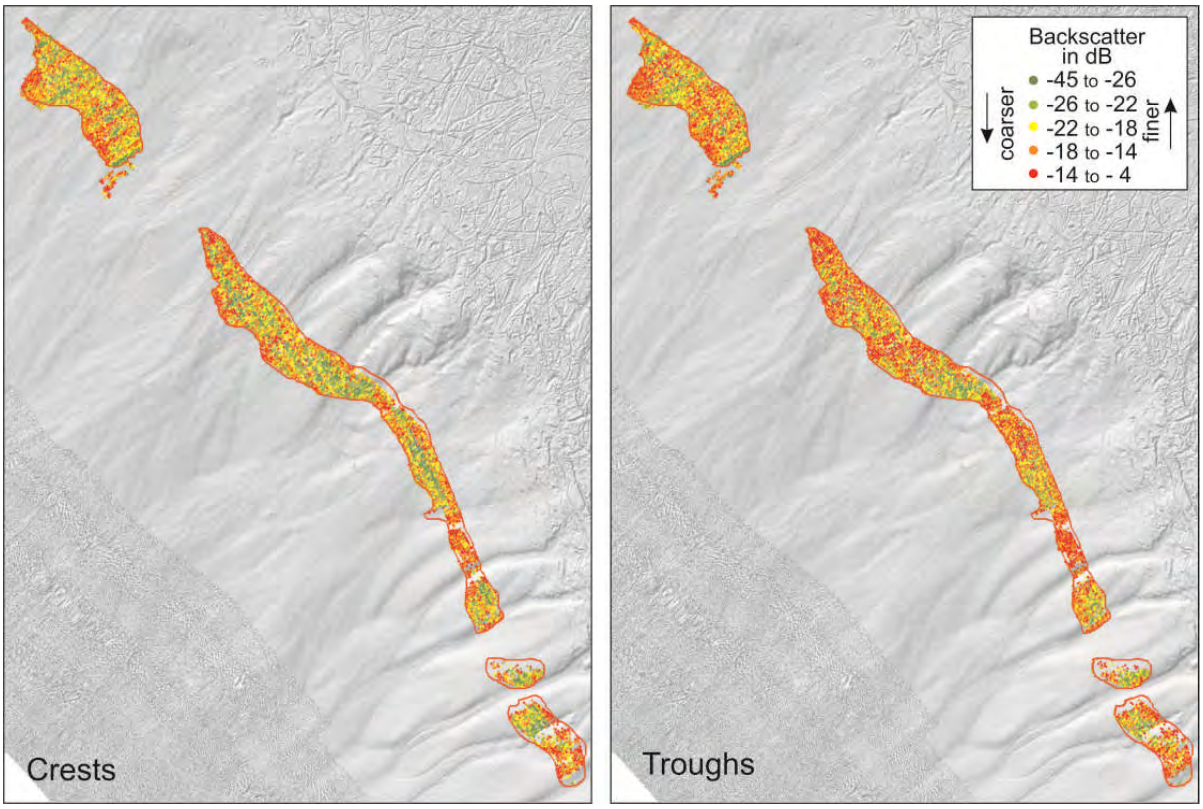

Figure 36. Backscatter value comparisons for troughs and crests in the N-2 to N-4 fields. Some colour banding is noise-related but overall warmer colours (coarser sediments) dominate in the troughs.

Crest versus trough backscatter comparisons based on the whole dataset (all measured sandwaves) are even more evenly matched. Figure 37 shows essentially identical distribution curves (blue and black curves). With the reasoning that only the troughs of the larger sandwaves potentially reach to the glacial gravel lag surface, those bedforms larger than 2 m height were isolated but their frequency distribution is also are indistinguishable (Fig. 37, green curve).

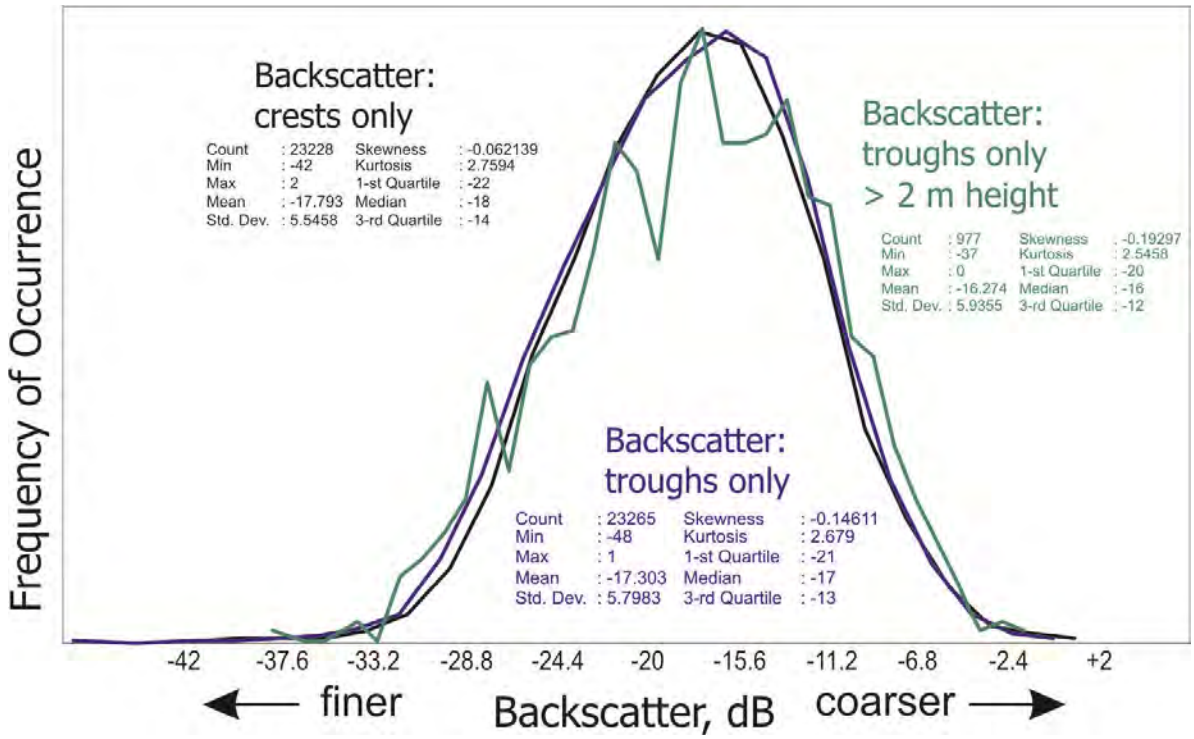

Figure 37. Comparison of backscatter values for troughs (blue) and crests (black) for most bedforms in the study area. The curves are largely indistinguishable. This is counterintuitive given the observations of gravelly troughs in the video and in local areas (e.g. Fig. 32). Even the larger bedforms (green) follow the same trends. The main interpretation is that most troughs are sandy but data noise and perhaps an elevated signal from ripples may contribute.

Interpretation of these findings is that, 1. Backscatter noise levels are relatively high and this tends to mix high values on both crests and troughs, 2. Most troughs are, in fact, sandy and do not reach to and expose the lag surface, 3. Both shells and small ripples are ubiquitous on the sandwaves and both are known to cause elevated backscatter signals in sidescan sonograms. This is scale and sound frequency dependant but it is conceivable that ripples on the scale of gravel (cms relief) give rise to elevated backscatter such that the usual gravel - high backscatter proxy degrades.

6.4 Heights and wavelengths

6.4.1 Technique

Height and wavelength measurements were derived from the auto-pick function as illustrated in Figure 29. A simple crest to trough measurement was unrepresentative because meso-scale morphological features (mainly glacigenic debris flow chutes) within the sandwave fields cause significant local up-hill and down-hill changes. Therefore, the height was defined as the elevation difference between the crest and the average elevation of adjacent troughs. Wavelength measurements were both from crest to crest and trough to trough; only the trough wavelengths are presented.

6.4.2 Results

Figure 38 shows the relationship between height and wavelength for all bedform measurements. There are some outliers, but the bulk of occurrences are less than 3 m high and 120 m across. Figure 39 presents a field by field separation of heights and wavelengths.

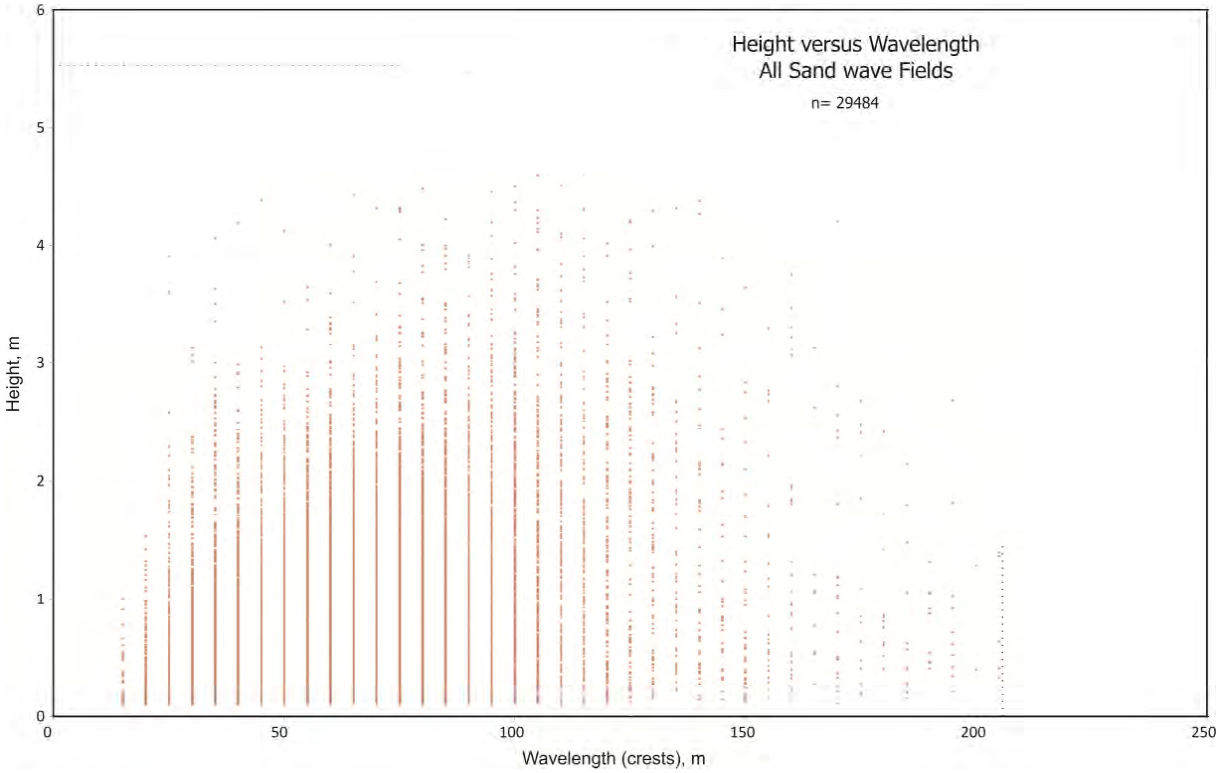

Figure 38. Wavelength versus height for all measured bedforms. Note that the high number of measurements tends to be hidden in overlapping points representing forms less than about 3 m height and 120 m wavelength. Dotted lines mark the extremes at 5.5 m height and 210 m wavelength.

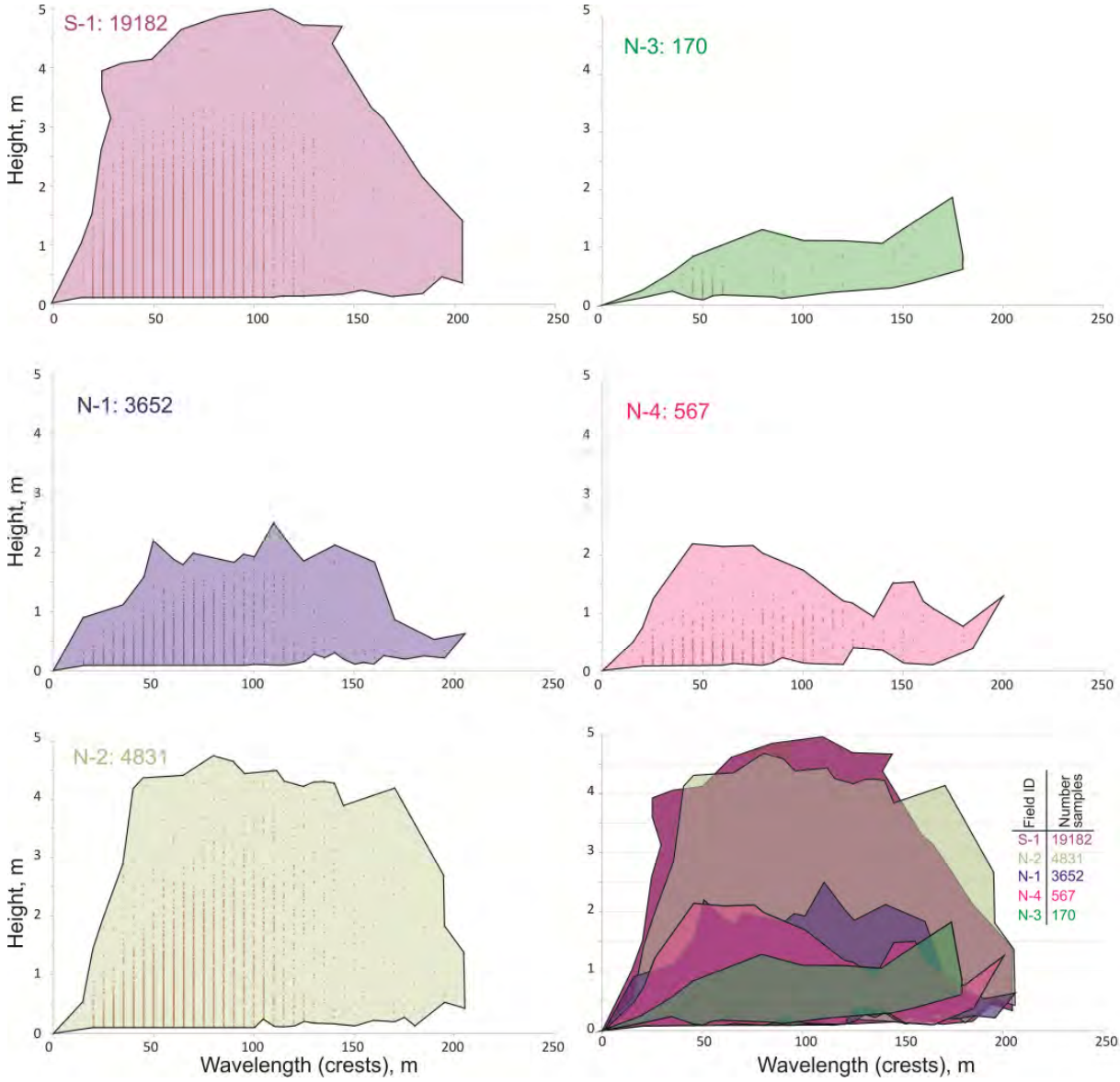

Figure 39. Height versus wavelength points and envelopes for individual fields.

Figure 40 shows the distribution of sandwave heights and wavelengths. Heights show a uniform exponential (normal) distribution with an average of 0.75 ±0.62 m. This is compatible with the video observations. Wavelengths are similarly exponentially distributed (tail less than 30 m wavelength is likely due to limited sampling resolution). They are on average 39±16 m across with maxima in the 130 m range.

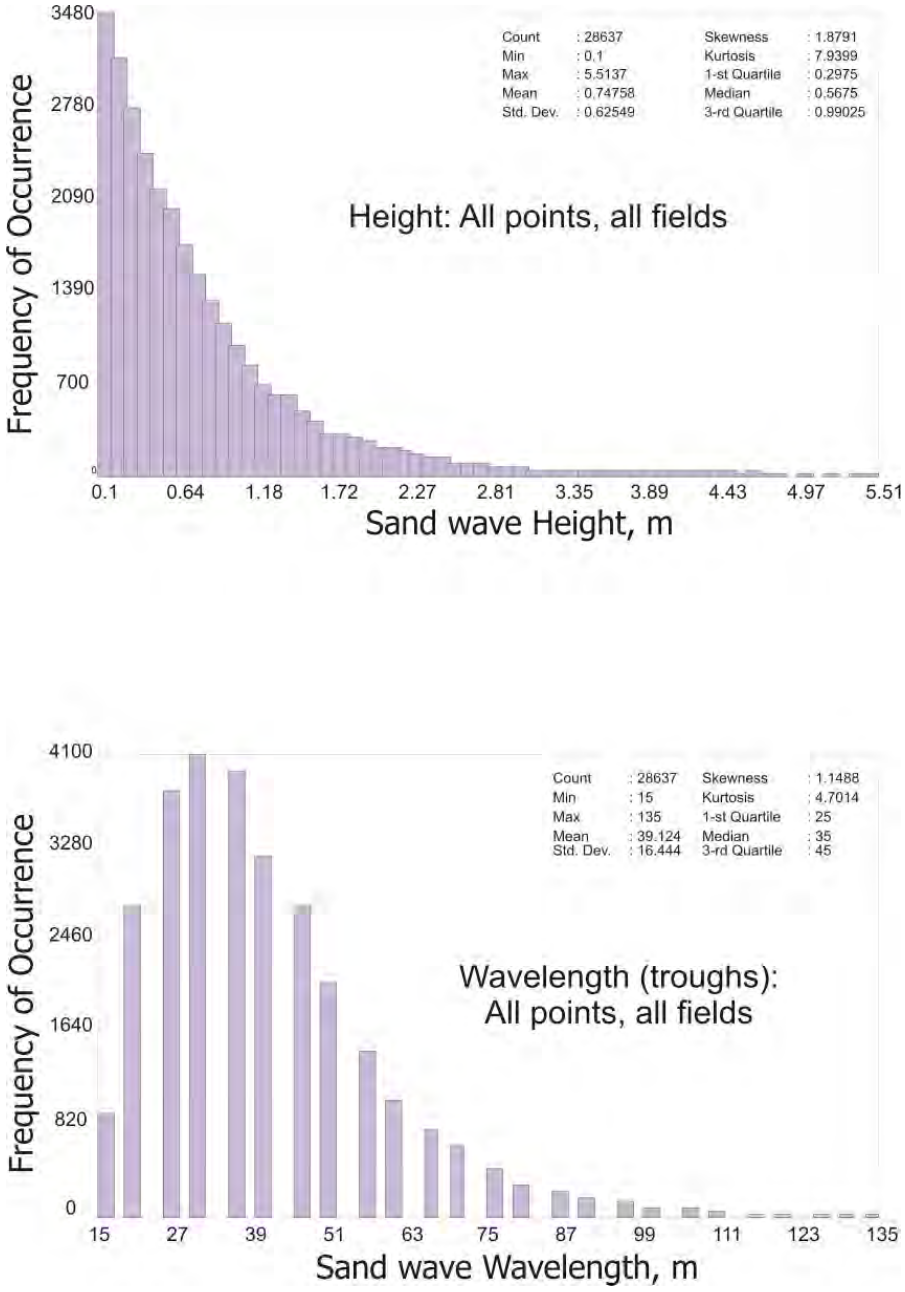

Figure 40. Distribution of sandwave heights and wavelengths for all fields.

Figures 41 to 46 show the map distribution of wavelengths and heights for the various fields. Bedform size varies strongly within the field, mainly in an along-slope sense. Clusters of larger forms have some spatial affiliation with the larger changes in topography, generally near the flanks of the debris flow chutes/channels but this is not always the case. Figure 42, for example, shows the higher sandwaves on one large interfluve at the southern end of the N-3 field but few on the next interfluve. Similarly, the northernmost part of the field shows two higher fields on the interfluves but just south of this a large and continuous cluster of high sandwaves straddles two interfluves and the channel in between.

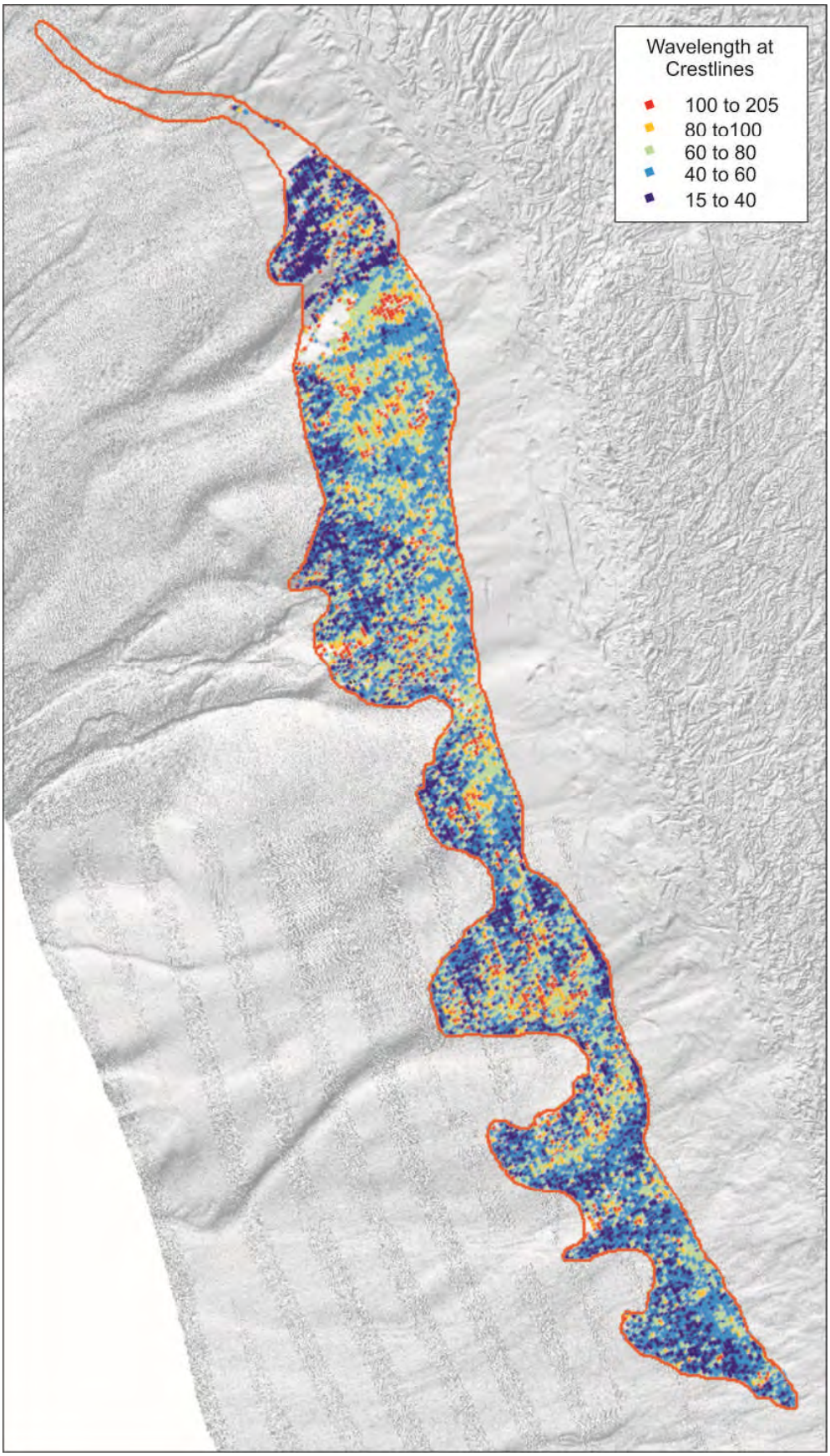

Figure 41. Wavelength distribution of sandwaves in the S-1 field. The greatest values are commonly in the vicinity of the downslope gullies/chutes associated with regional along-slope topographic changes.

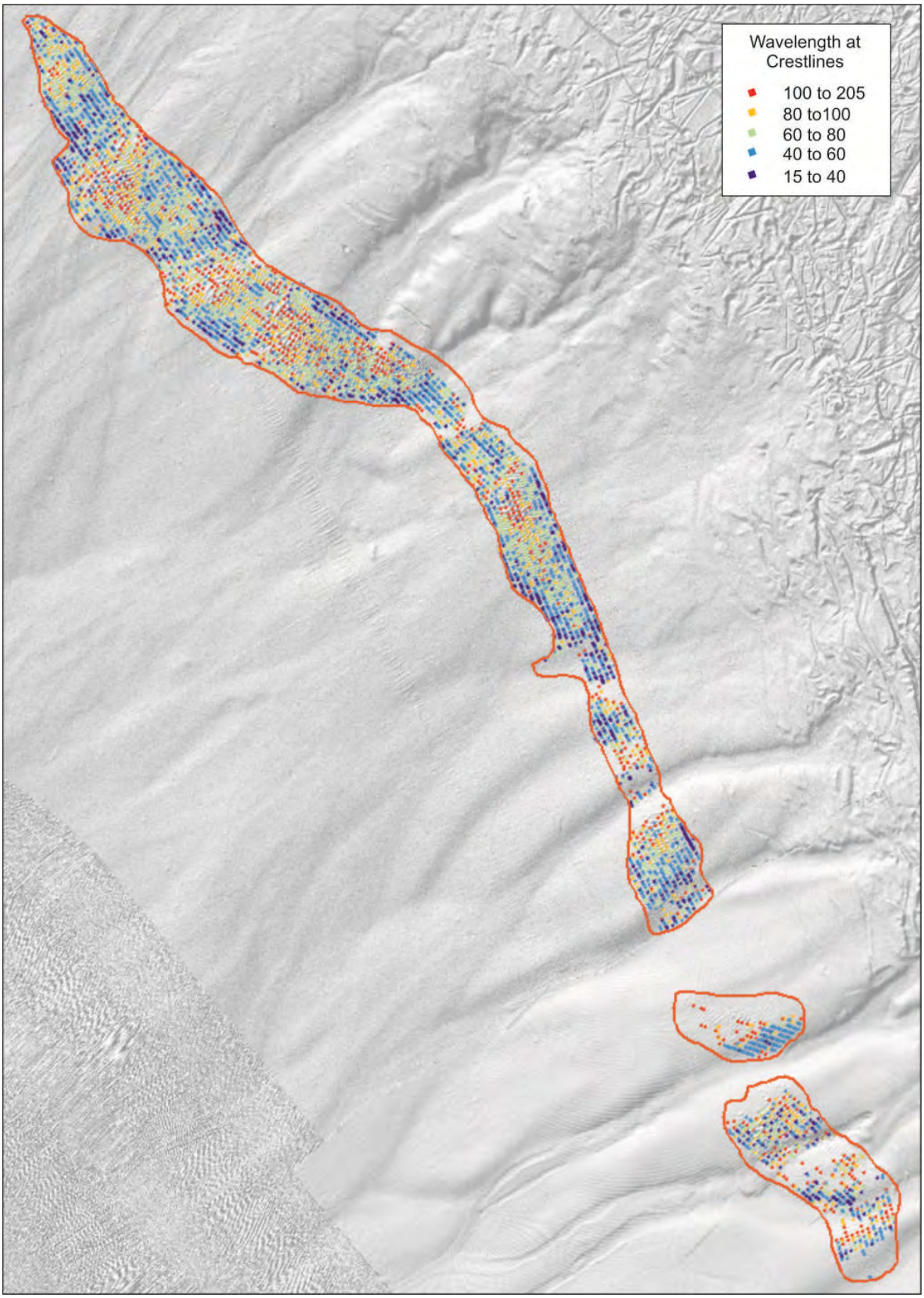

Figure 42. Wavelength distribution of sandwaves in the N-2 to N-4 fields.

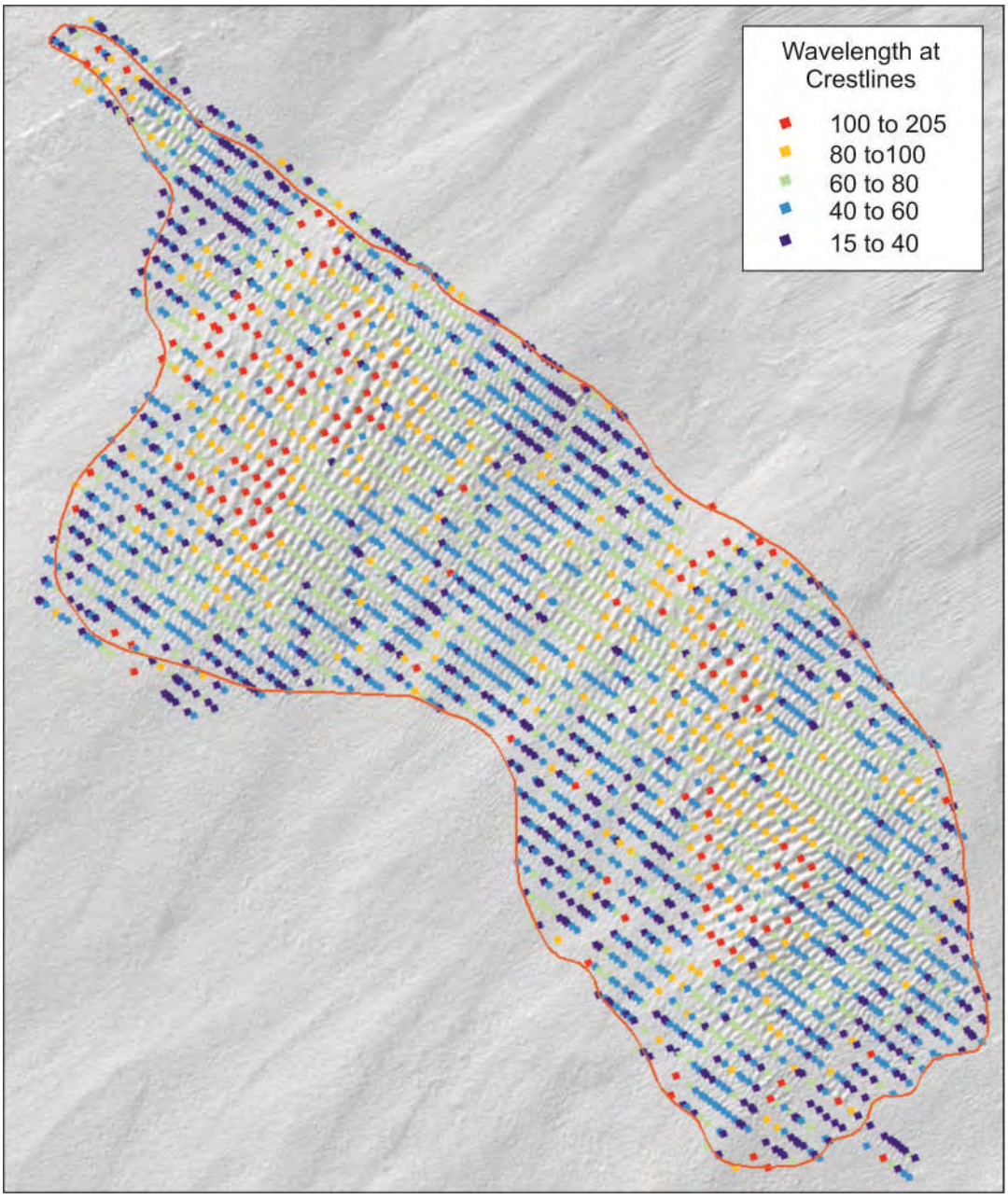

Figure 43. Wavelength distribution of sandwaves in the N-1 field

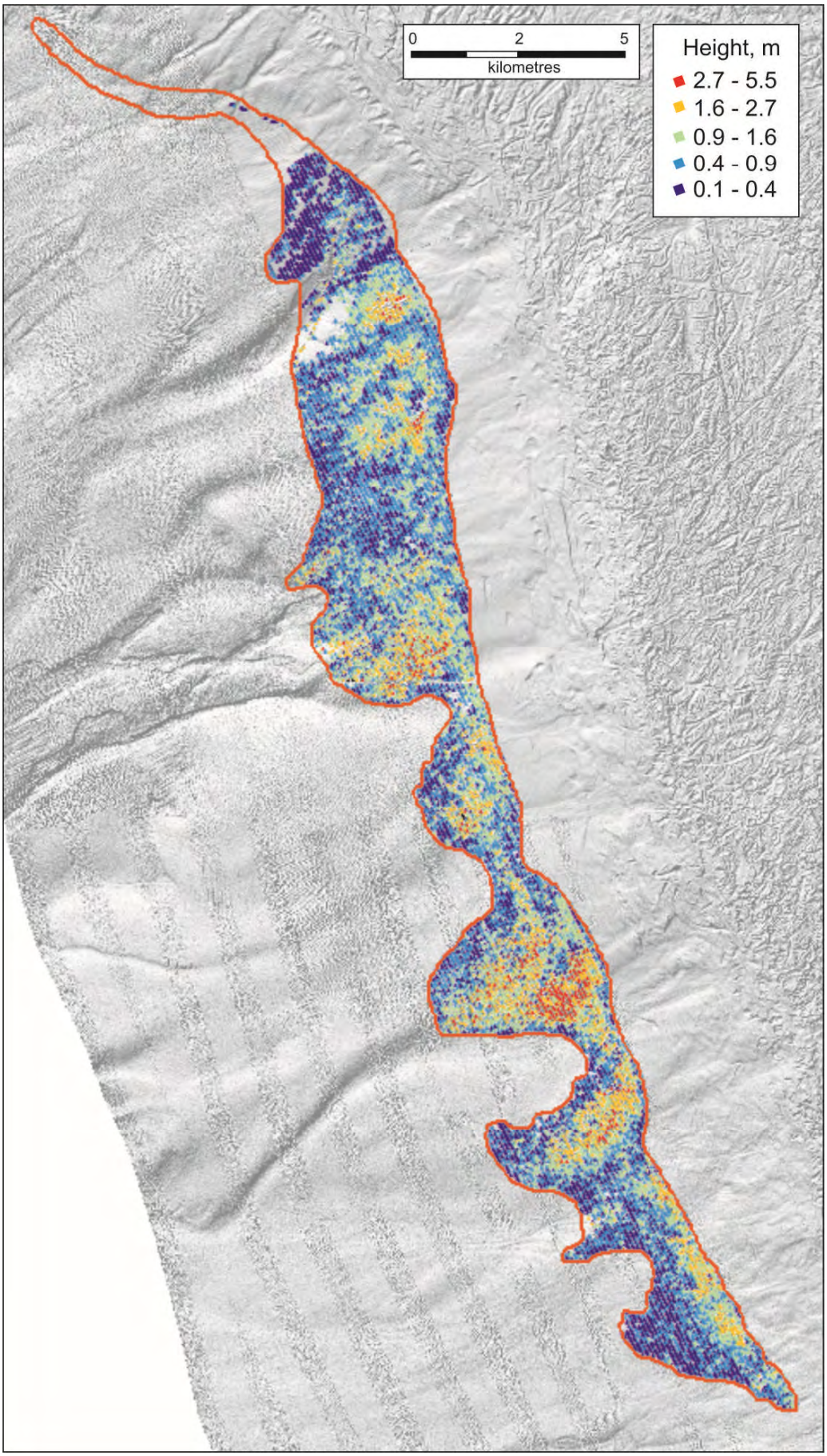

Figure 44. Height distribution of sandwaves in the S-1 field.

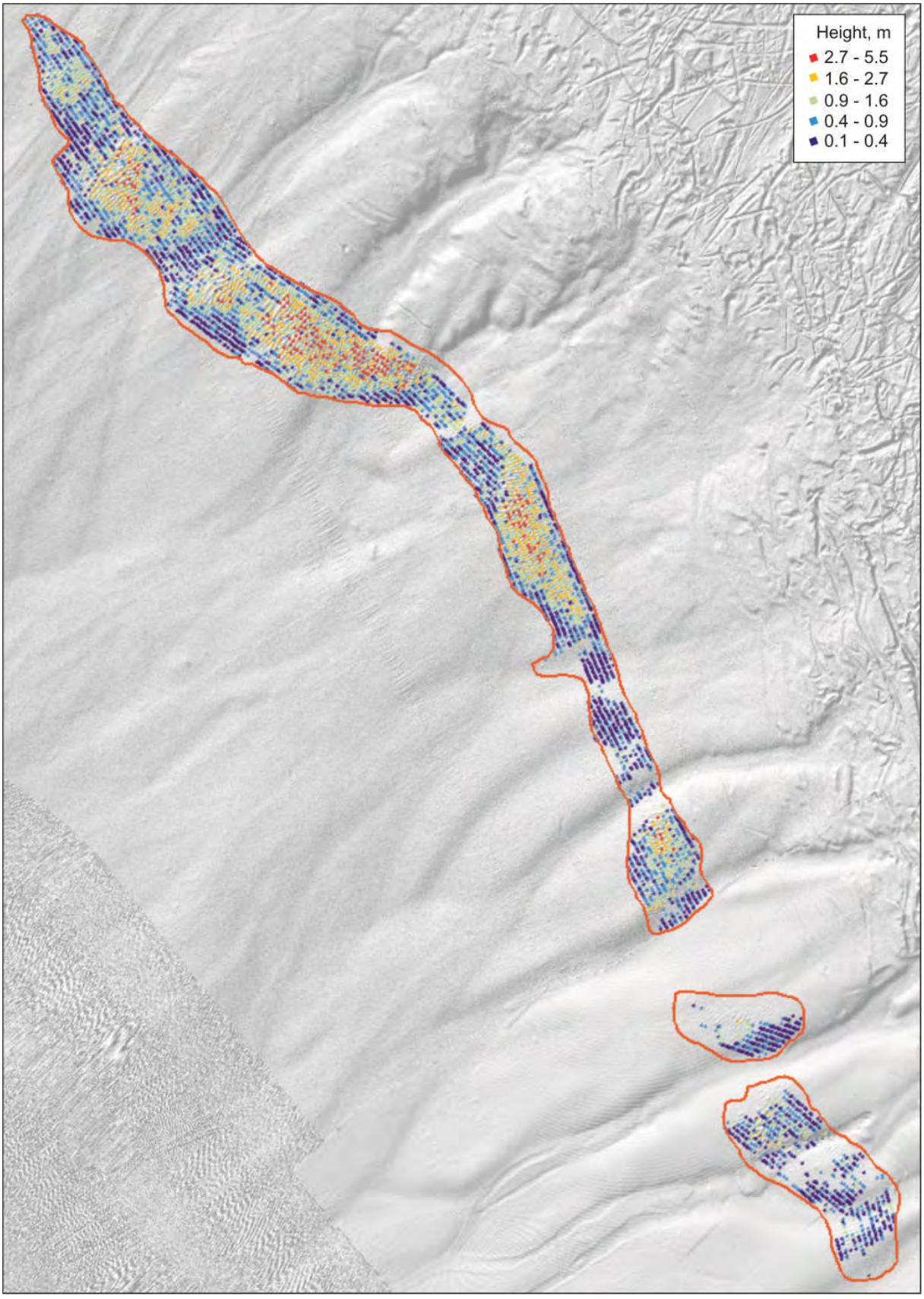

Figure 45. Height distribution of sandwaves in the N-2 to N-4 fields.

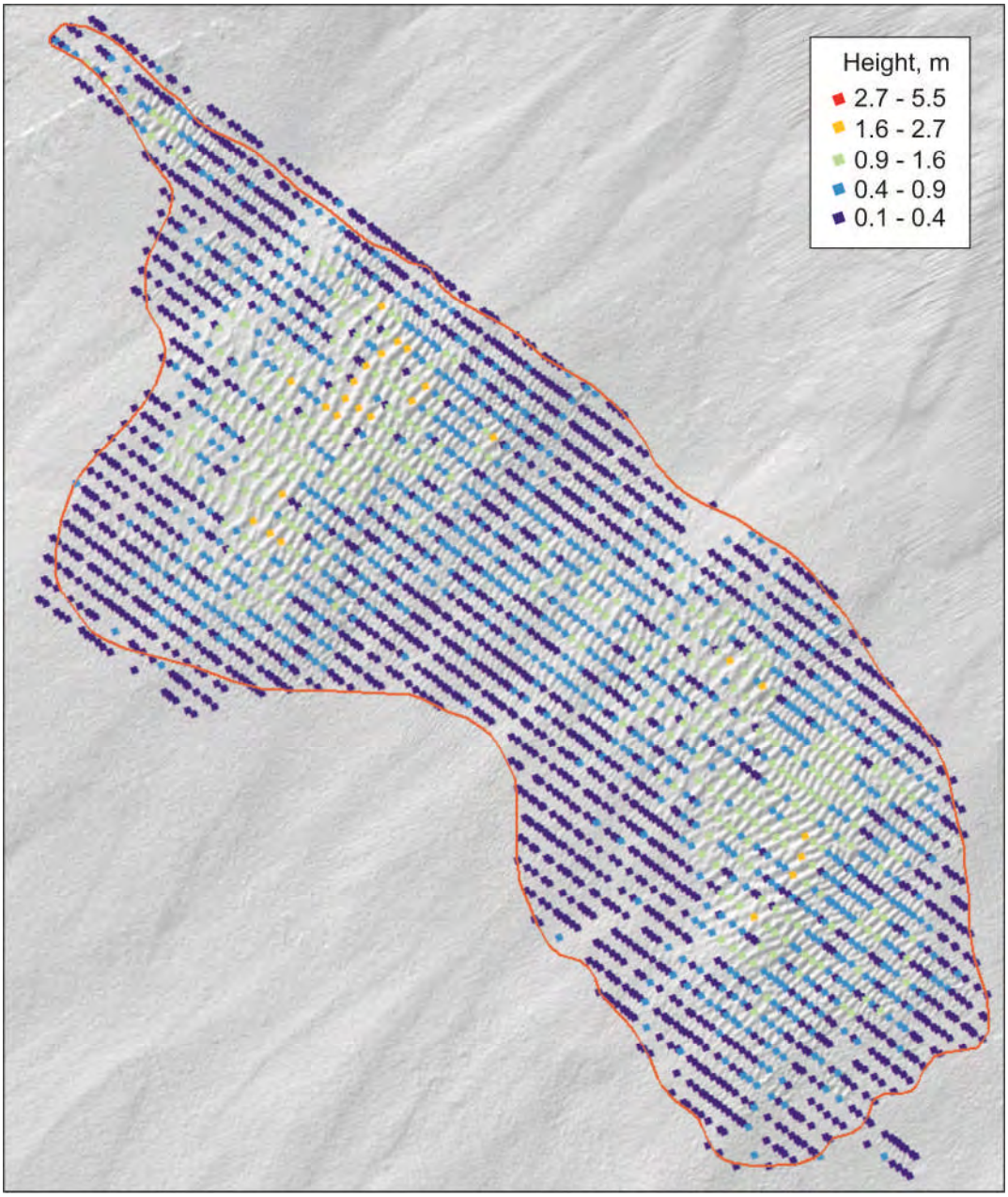

Figure 46. Height distribution of sandwaves in the N-1 field.

Bedform Height/Wavelength ratios is another common index of morphometrics. Figure 47 shows the distribution of these ratios for all bedforms. These values are relatively high, suggesting equilibrium evolution and little sand starvation. This is considered further in Section 6.7.

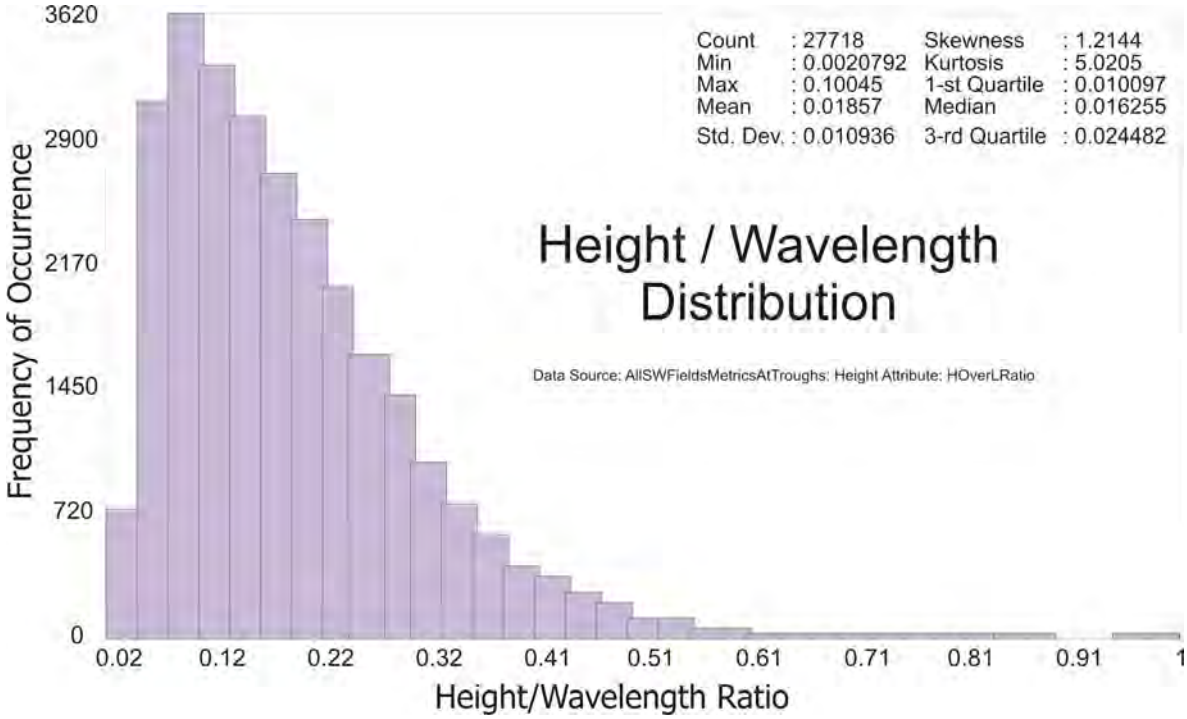

Figure 47. Frequency distribution of height/wavelength ratios for all measured bedforms. Small bedforms tend to have a mean height/wavelength ratio of about 0.1 while that of active sandwaves is around 0.03 provided the sand source and development time is not limited (Dyer 1986). These examples fall within the higher end of this spectrum.

6.5 Bedform symmetry

Profile symmetry is a commonly measured parameter to indicate dominant bedform migration direction. The lee face (flank downstream of the crest) is depositional and, in active forms, should approach the angle of repose while the stoss (face upstream of the crest) should be erosional or at least allow bypass of mobile sand in transit to the crest. A state of accretion or aggradation is relatively uncommon in marine bedforms. Unsteady and directional switching of currents is common in the marine environment and the relation to bedform size and response time (lag) to changes can be complex. Symmetry in this study was calculated as shown in Fig. 29. The symmetry ratio produces whole and fractional values so the latter were assigned negative inverse values such that frequency distribution histograms would display normally distributed (eg. the mirror image of a symmetry ratio of 2 is 0.5; so -1/0.5=-2).

Figure 48 shows a very uniform (normal) distribution of symmetry where all measurements are considered. This was somewhat unexpected given the simplified setting whereby the contour currents are generally northward and tidal influences should be minimal. The following presentation will demonstrate that there are local trends with some coherency in symmetry, though they are largely unexplained. Also, limitations in spatial resolution of the basic depth data can induce much greater symmetry in the statistics. This is discussed in connection with the slope derivations in Section 6.6.2.1.

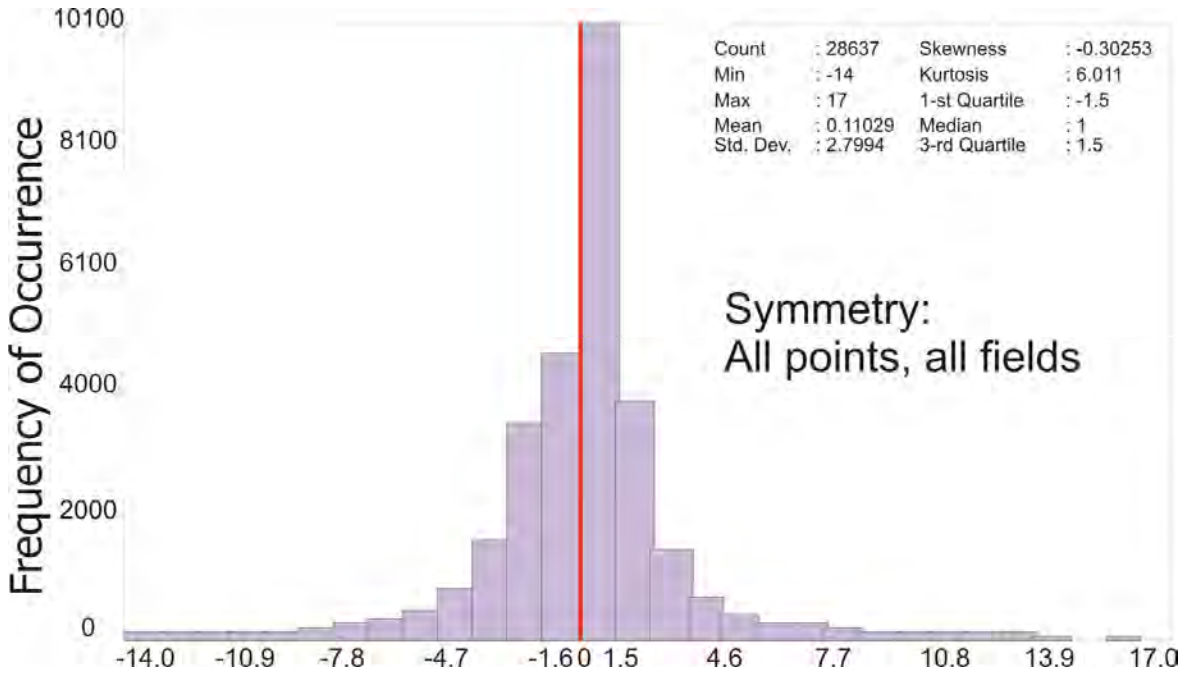

Figure 48. Distribution of symmetry measurements for all fields. The red line marks symmetric forms.

Figures 49 to 51 show the spatial distribution of the symmetry index across the various sandwave fields. The N-1 field (Fig. 49) shows a clear banding of symmetry values across the field which are spatially related to the meso-topography arising from the GDF chutes. A similar pattern is observed in Figures 50 and 51.

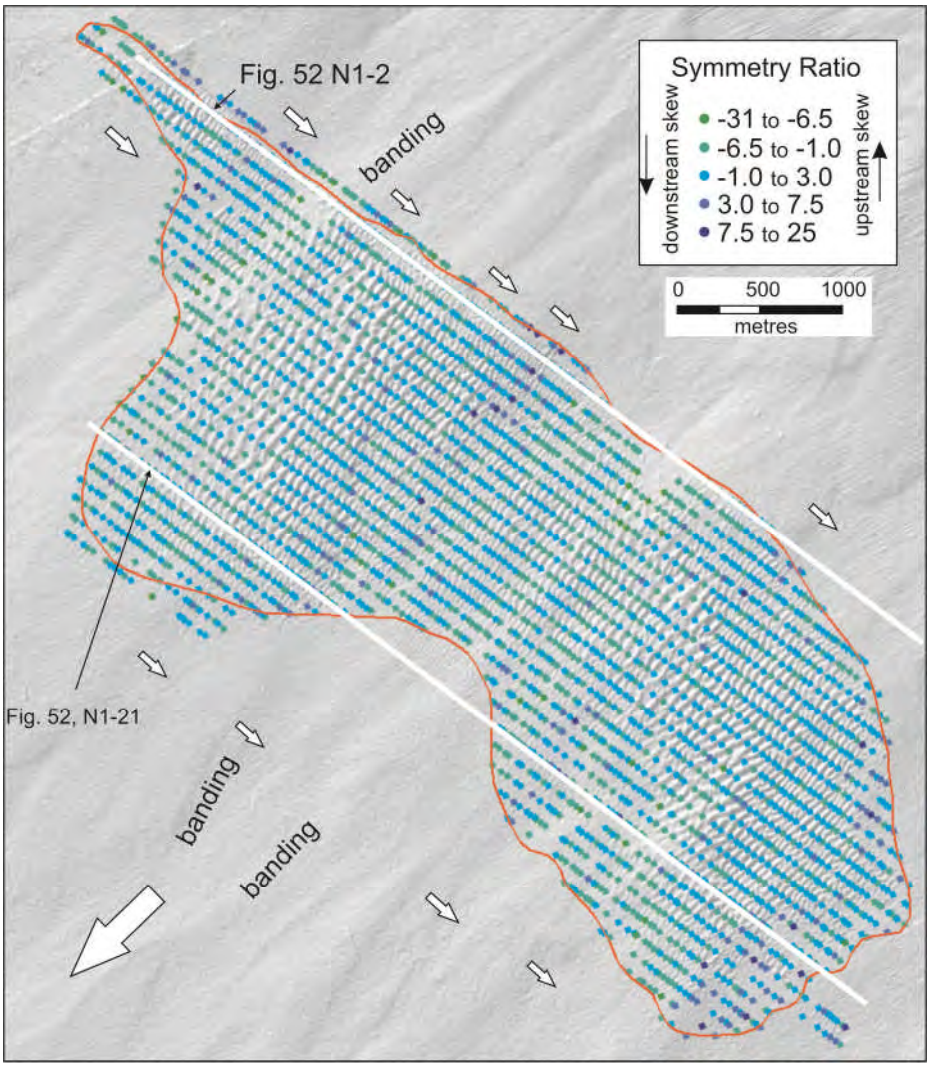

Figure 49. Symmetry of bedforms in the N-1 sandwave field superimposed on shaded relief bathymetry. The shaded relief image shows local slopes of the pre-existing glacigenic debris flow system channels and interfluves (small, down-hill pointing, white arrows) across the regional downslope direction (large white arrow). The colour banding across the field is closely related to the local channels; SE-facing slopes show a strong symmetry indicative of sand wave up-hill skewness (downcurrent), a pattern mirrored in the down-hill direction. This indicates a more pronounced up-hill migration than down-hill if skewness is recognized as a migration direction indicator. Note that the strongest trends are associated with the smaller bedforms flanking the field. White lines mark the positions of two profiles in Figure 52.

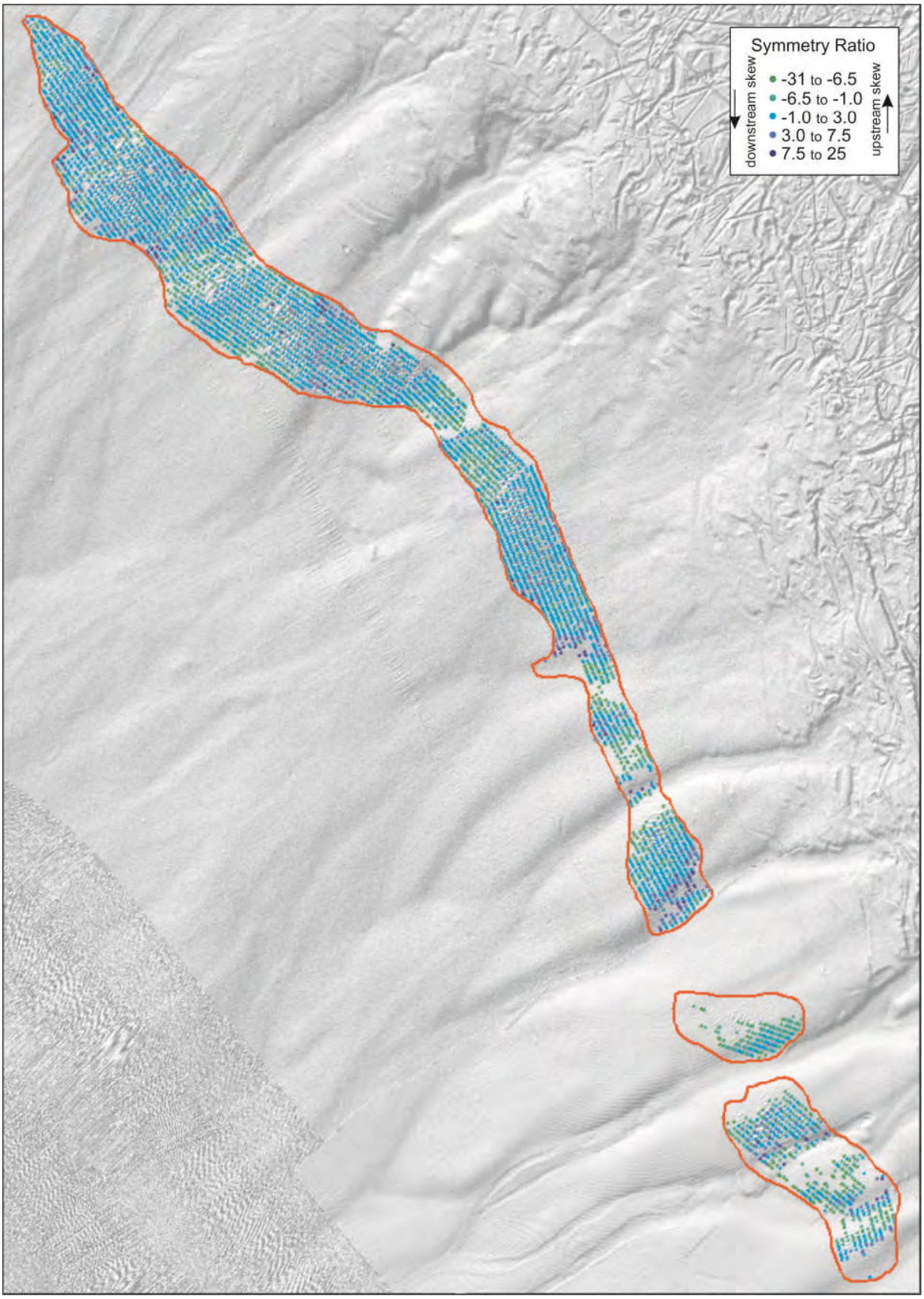

Figure 50. Symmetry of bedforms in the N-2 to N-4 sand wave fields. Note here also the across-field banding of colours (green versus blue) correlating with the GDF chutes/gullies.

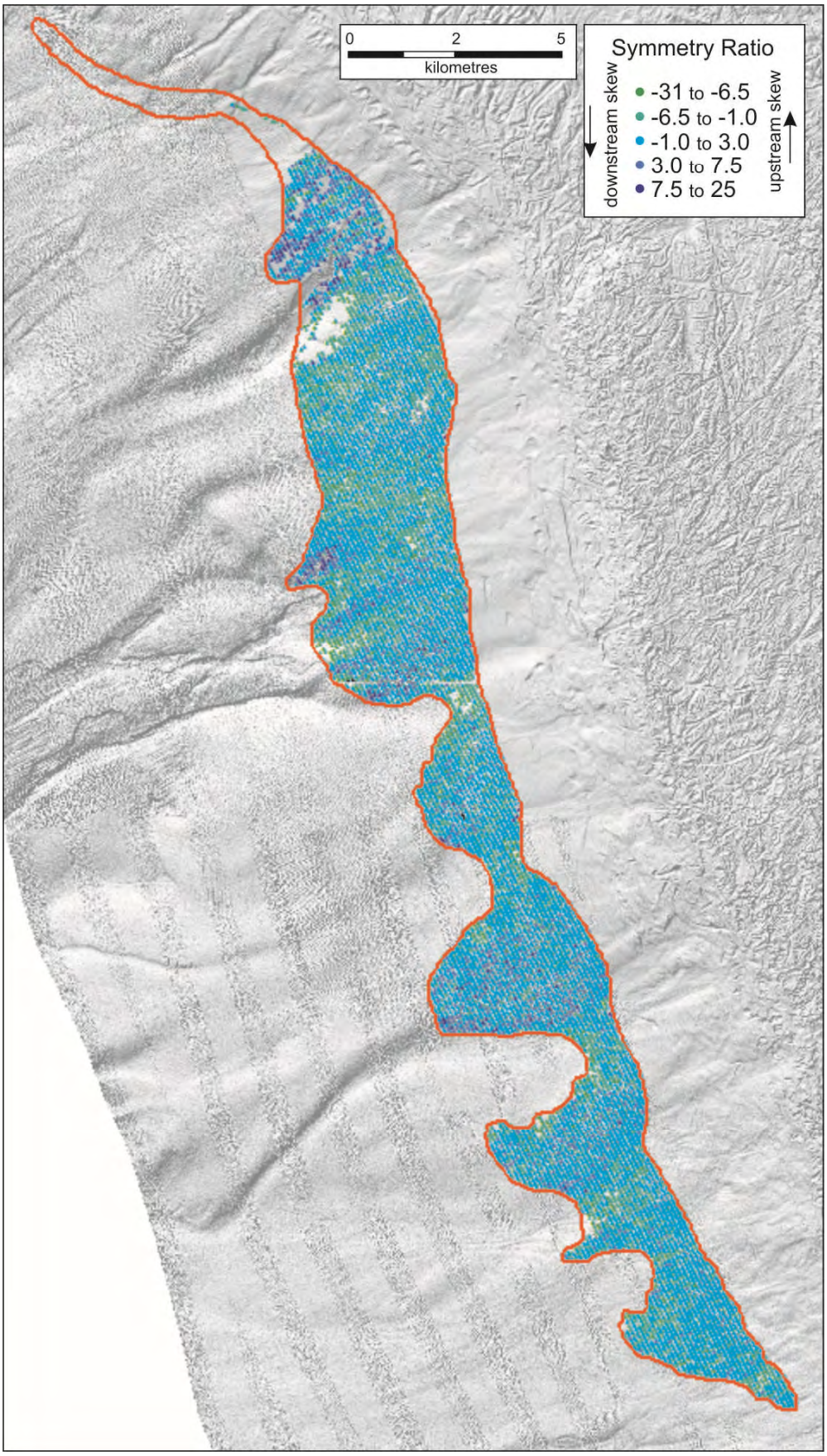

Figure 51. Symmetry of bedforms in the S-1 sandwave field.

The tendency toward spatial banding of the symmetry of the sandwaves was investigated further. Figure 52 shows two bathymetric profiles where symmetry index colours are plotted along the profiles. The three expanded views show individual sandwave auto-picks and corresponding coloured indices. The tuning of symmetry index to the meso-scale topography of the flanks and interfluves of the glacigenic debris flow (GDF) chutes is well demonstrated. Here, sandwaves with southeastward skews (greener colours) fall on the northwestward sloping GDF chute flanks while the opposite skew (bluer colours) characterizes many of the SE facing meso-scale slopes. The inference is that NW facing flanks of the GDF chutes are the sites of comparatively higher southeastward-directed bedform migration.

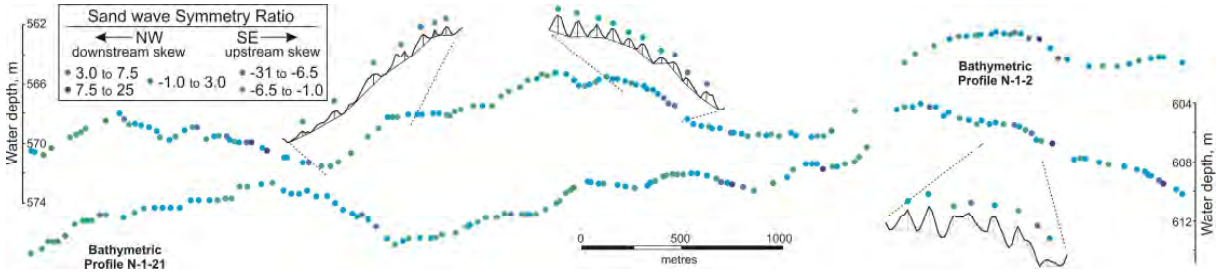

Figure 52. Symmetry of bedforms in the N-1 sandwave field. Profile locations in Figure 49. Glacigenic debris flow system channels and interfluves generate a regional relief to which the sandwave symmetry is tuned. A more pronounced up-hill than downhill skew suggests preferential migration up the SE-facing channel flanks (downcurrent).

The symmetry values are more uniformly distributed than expected, assuming that the driving contour current is more or less unidirectional. This is partly due to incomplete (too low resolution) imaging of the sandwaves discussed later) but Figure 52 shows clear trends despite this drawback. It was suspected that symmetry may be also a function of bedform size so symmetry distribution plots of various size classes were generated. Figure 53 shows four classes of bedform size and their corresponding symmetry skews. All demonstrate a slight median skew suggesting downstream (NW) migration but, as noted, also many values are in the opposite direction.

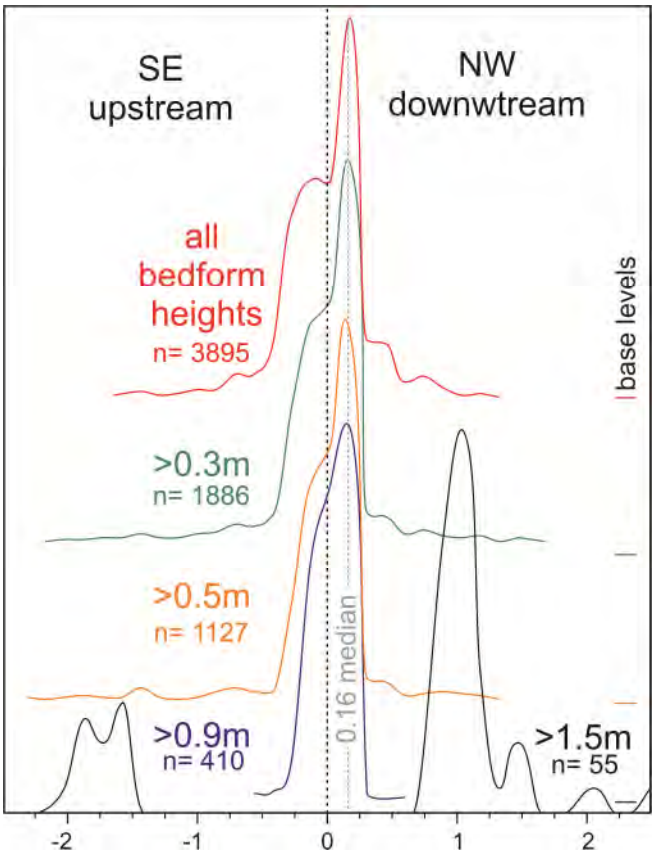

Figure 53. Symmetry distributions of N-1 field sandwaves. Median symmetry values are about 0.16 for all classes of bedform heights, suggesting overall northwestward (general downstream) migration, compatible with a NW-flowing contour current. The highest of bedforms (black curve, higher than 1.5 m) display the strongest asymmetry, most with northwestward skew but with a clearly separate population displaying southeastward skew. The distribution of progressively smaller height sandwaves includes increasingly greater numbers of southeastward (upstream) skews. Note the separate base levels (zero occurrences) are separated to minimize curve overlap.

However, distributions in Fig. 53 are nearly identical until bedforms are greater than 1.5 m high at which point two separate populations are revealed. These represent only a small portion of the total population (1.4%).

6.6 Bedform slope

While symmetry should provide an indication of sandwave migration directions, slope measurements should also provide a signal of bedform activity and direction. Steeper slopes, approaching the angle of repose should distinguish relatively active bedforms from more moribund forms and the ratio of lee and stoss slopes, it is reasoned, should provide an indication of migration direction.

6.6.1 Technique

The crest-trough auto-pick routine was modified to recognize the steepest slopes (stoss and lee, Fig. 29) and present their ratio. In this compilation the ratio of NW flank over SE flank was calculated, such that positive values represent an asymmetry suggesting an upstream (SE-directed) migration while negative values suggest downstream flow direction (toward NE). Fractional slope ratio values were assigned negative inverse values such that frequency distribution histograms would display normally distributed, just as for the symmetry ratios (eg. the mirror image of a slope ratio of 2 is 0.5; so -1/0.5=-2). Derived slopes and slope ratio values for both troughs and crests were then imported and displayed in GIS.

One advantage of the technique is simply to highlight slope values for display purposes; DEM-derived slope raster images alone are unsuitable for overviews because colour-coded lee and stoss flanks represent too little area to recognize at large map display scales. Also, the point derivations allow filtering and statistical calculations with the capability of differentiating bedforms both spatially and according to other attributes (e.g. location, size, backscatter etc.).

6.6.2 Results

6.6.2.1 Multibeam limitations

The video observations are not quantifiable in terms of heights, wavelengths or slope but the impression from derived photographs is that lee slopes are much greater than that measured from the multibeam. This may be true to the degree that the multibeam measurements are relatively meaningless. It is clear that crest to trough distances on lee slopes (in the video photographs) cover metres or less; this is considerably less than the binning resolution of the multibeam. A 20 degree slope on a 2 m high hypothetical sandwave, for example has a crest to trough distance close to the 5 m binning resolution, largely constrained by the limitations of acoustic spreading, in this case through 600 m of water column. This hypothetical sandwave as “seen” from multibeam under the best case scenario (acoustic “hits” at the top and base of lee slope) would recognize this slope magnitude but the worst case scenario would yield a slope measurement of only 7 degrees. This situation worsens with slopes greater than 20 degrees. Only 0.1% of measured slopes exceed 20 degrees in this compilation. This does not necessarily negate the slope ratio index, which is a relative measure, but it is clear that smoothing due to acoustic spreading sets serious limitations on small, angular seabed features such as observed in the video. Therefore the following maps must be viewed in the context that these are minimum slope values.

6.6.2.2 Slope maps

Figures 54 to 56 show the map distribution of flank slope values for the various sandwave fields. The illustrations contrast NW slopes with SE-facing counterparts. Expectedly, the clustering of higher values correlates with the larger bedforms, both lee and stoss sides. Given the assumptions of a simple contour current traveling to the NW the relatively even distribution of southerly versus northerly values is unexpected. Given the discussion in the preceding section and the very steep slope observations in some video transects, the most straightforward interpretation is that the values are not representative of the true forms. Alternatively, the sandwave forms deviate greatly from a gentle up-current and steep down-current face and may be recording a much more complex hydrologic regime.

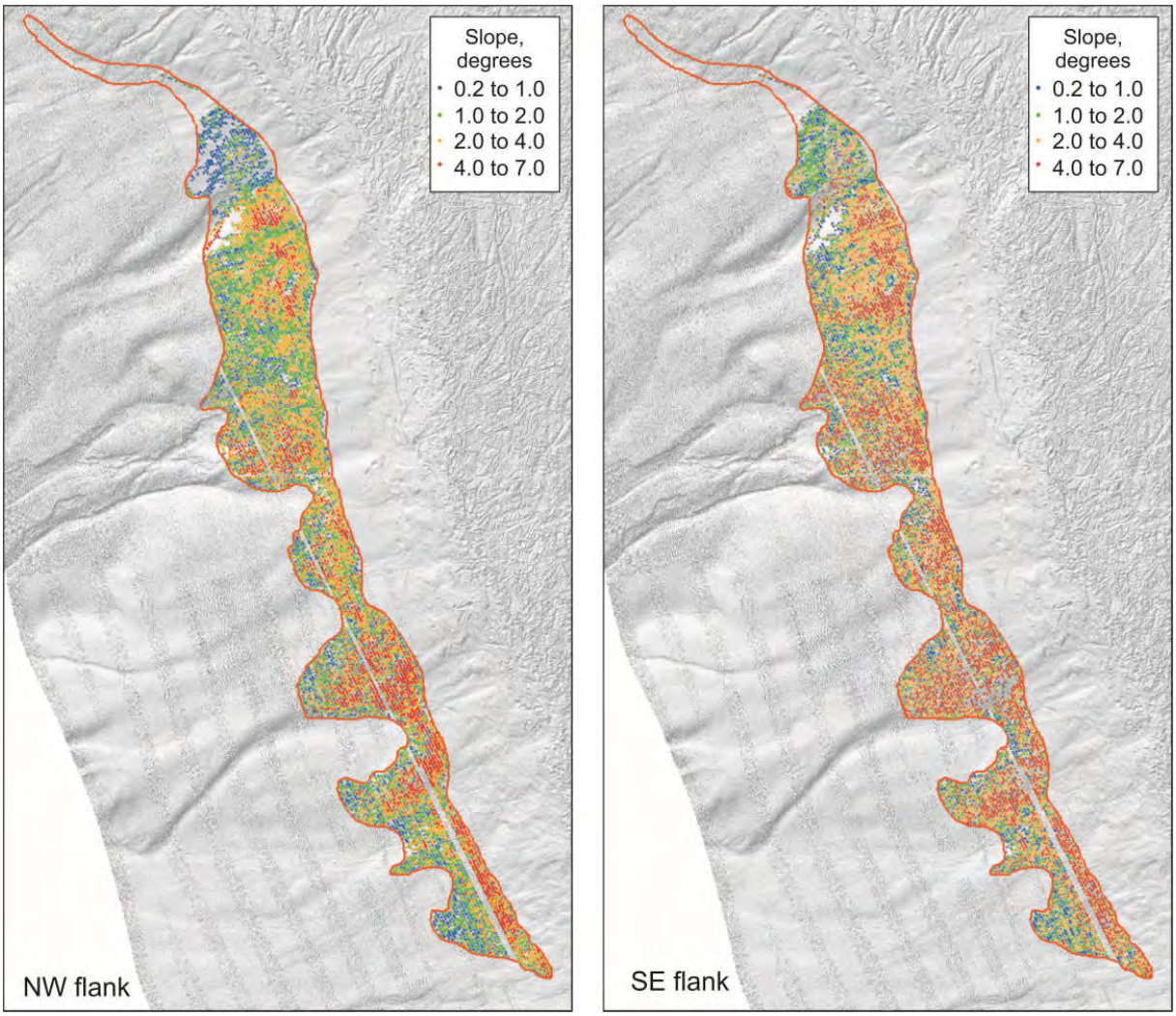

Figure 54. Highlighted slope values extracted from slope grids derived from the original DEMs (S-1 field). Maximum slopes for each bedform were derived for both the NW (or lee) and SE (or stoss) flanks. Higher NW flank values than SE flank should indicate a general NW (contour current downstream) migration direction. This applies for the following two illustrations. Surprisingly, high (red) SE slope values seem to have a greater distribution than for NW flanks.

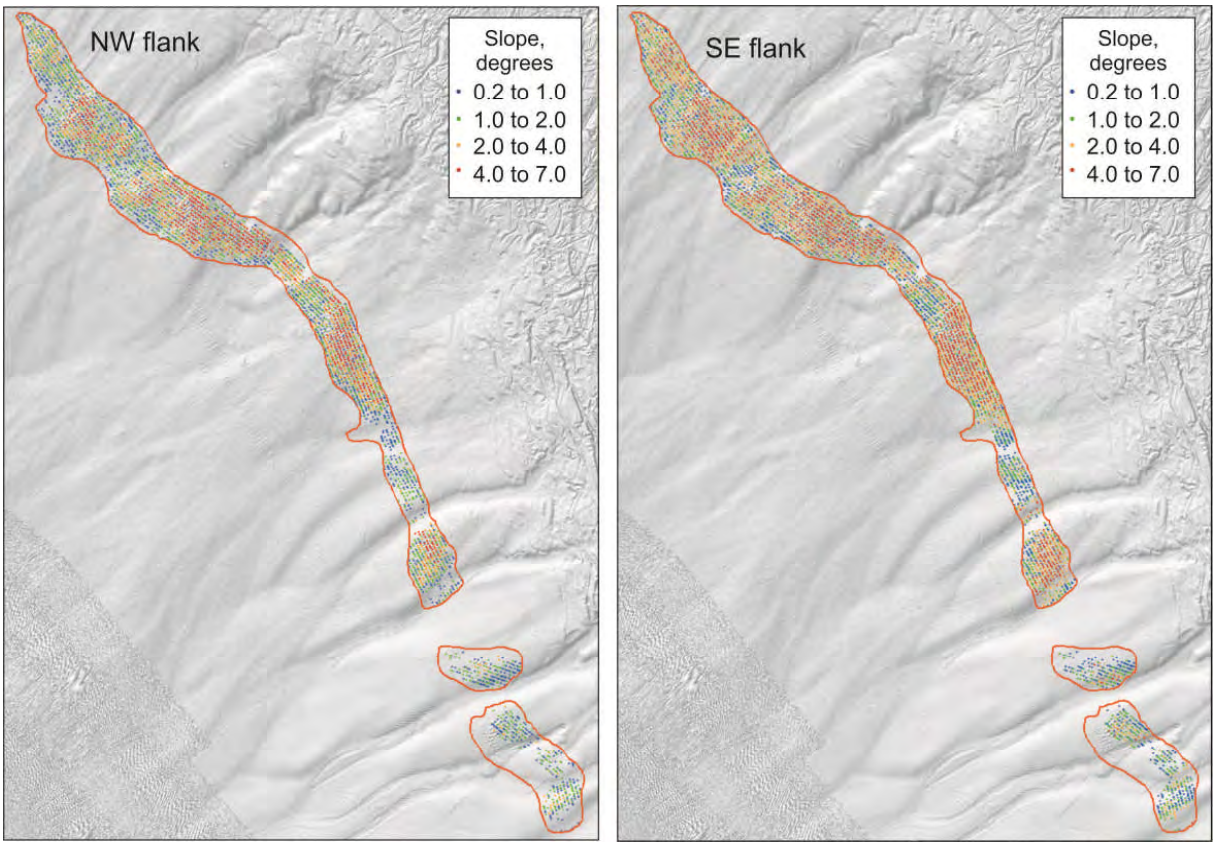

Figure 55. Highlighted slope values for the N-2 to N-4 fields. Slope values show some variation that is clustered, i.e. sub-fields of dominantly blue greens versus red-orange dominated. There may also be a coincided of these with the chute and interfluve topography.

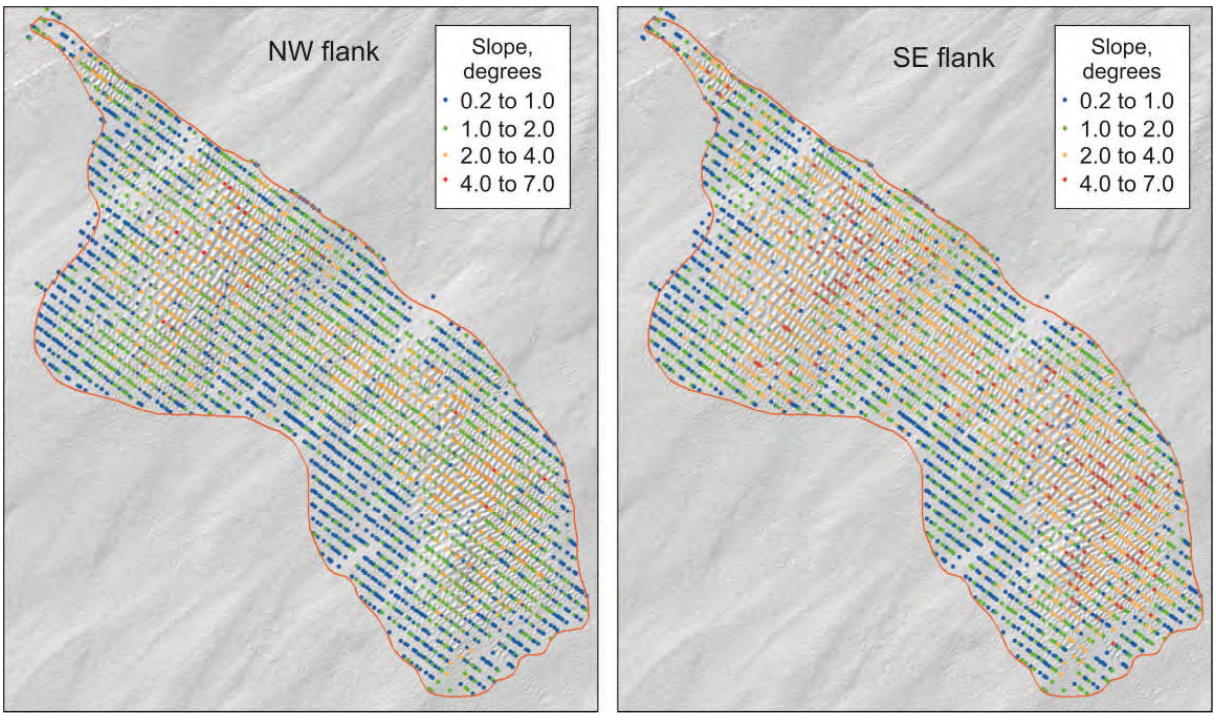

Figure 56. Highlighted slope values for the N-1 field. Slope values on both NW and SE flanks are generally greater than 2 degrees in the larger bedforms but a slightly greater extent and magnitude of SE slopes is observed.

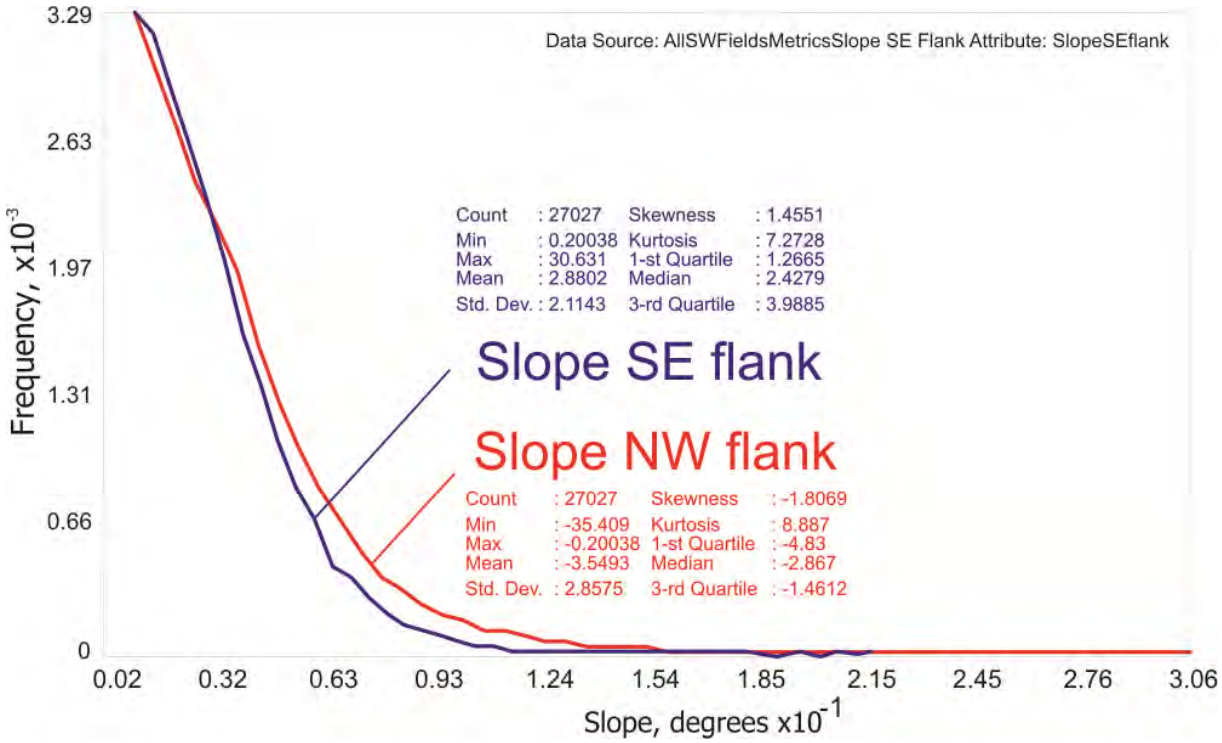

Figure 57. Comparison of the slope value distribution for NW (or lee) and SE (or stoss) flanks. Despite apparent spatial distributions suggesting a more common SE maximum slope in the previous illustration, the overall distributions favour (but only slightly) a greater NW slope value, especially in the steeper (5 to 10 degree) range. Thus, a downstream migration is suggested by the morphology.

Despite many locations with examples to the contrary, Figure 57 shows that NW-facing slopes are marginally steeper than SE, considering the entire dataset. This could be interpreted as a general northwesterly flux of sediment, or at least a preferred migration of bedforms with that trend.

6.6.2.3 Slope ratio maps

Figures 58 to 60 show maps of the ratio of the slope values (NW flanks compared to its companion SE slope). This is an alternative display of the maps in the previous section, with maps displaying a similar concept. Again, some clustering of dominantly green versus blue colours is present and this may have some tuning to the meso-scale topography, mainly the GDF chutes.

Figure 58. The slope ratio values for the S-1 field indicate a relatively even distribution of values suggesting northwesterly and for southeasterly sandwave migration directions. There is apparent clustering of sub-fields with dominant green (downstream migration) in the north and blue (upstream) just south of that.

Figure 59. The slope ratio values for the N-2 to N-4 fields. Some clustering of the colours suggest sub-field domains with tendencies to migration in one direction, despite much mixing of values.

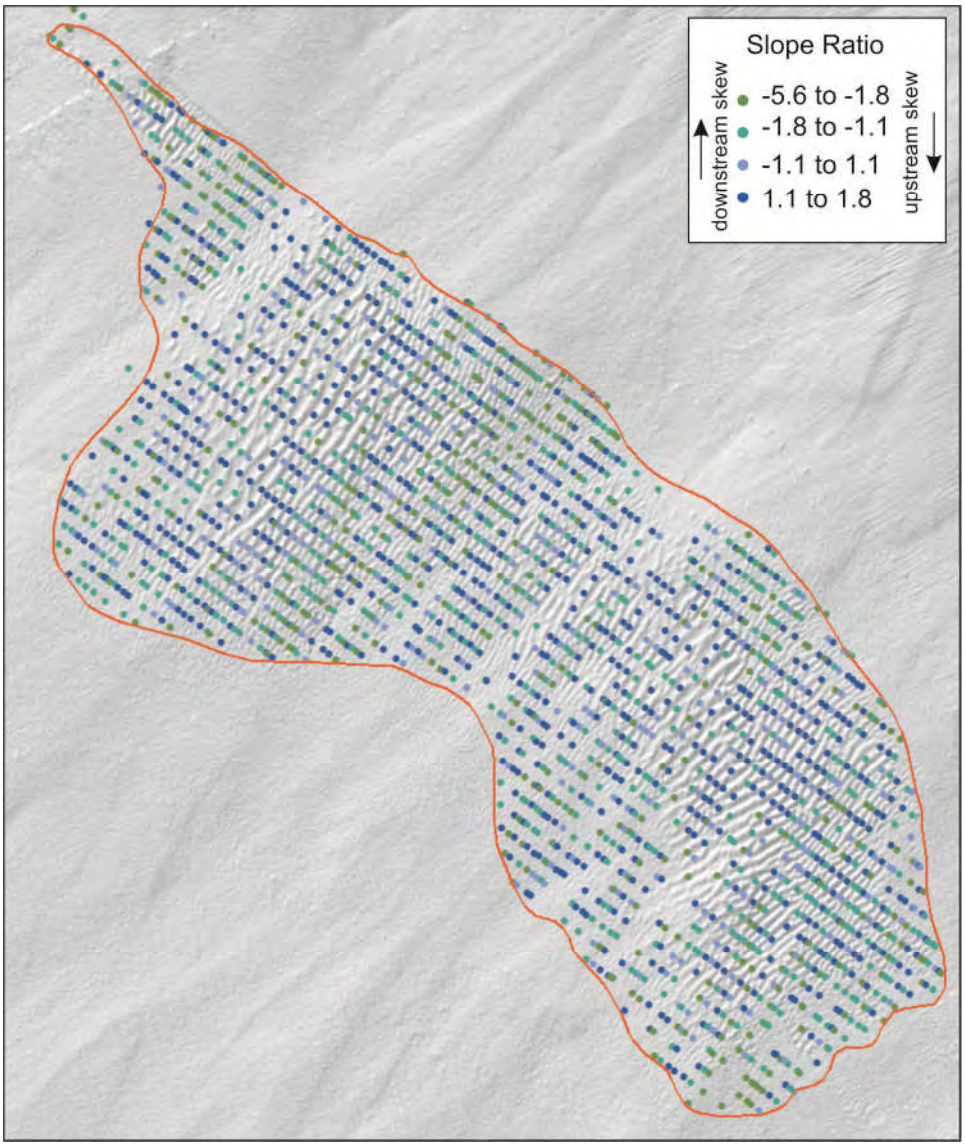

Figure 60. The slope ratio values for the N-1 field. Despite considerable mixing of values, there is a tendency for coloured bands across the field, possibly tuned to the meso-morphology of the glacigenic debris flow chutes as observed in the symmetry maps.

6.6.3 A slope-determined path of grain migration

Figure 61 shows the results of an ArcMap tool which traces the downhill path (gravity driven only) of any particle set in motion. Selected starting points on the stoss and lee flanks of a set of sandwaves demonstrate that the regional downhill slope (trough-parallel) is almost as great as the sandwave flank slope. This observation must be qualified with the recognition that while the multibeam smoothing has little affect on regional slopes, it can have significant effect on slopes occurring within the original binning distance (5 m).

As the video observations suggest much higher slopes than do the multibeam measurements, this flank-trough difference in slope is probably greater than that shown in the slope and slope ratio illustrations. Nevertheless, cumulative mobility of sand would soon migrate the grains

downhill and out of the field. This may be the case and if so, sand bypass would be a major process across the fields. Alternately, to maintain a dynamic equilibrium of the field, there must be an uphill hydrological force counteracting gravity. Perhaps the straight-crested ripples on the lee flanks and troughs as observed on the videos are evidence of this uphill flow. Note that without a compass orientation of the video instrument, uphill versus downhill direction is apparently indistinguishable.

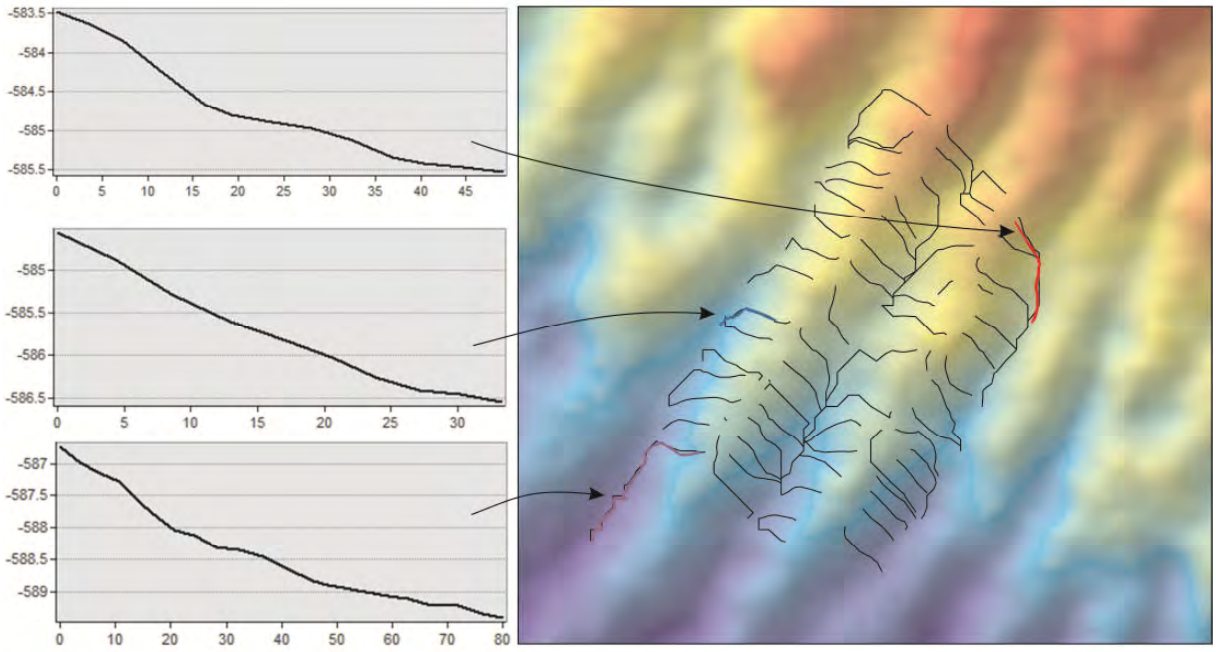

Figure 61. An GIS tool traces the path of maximum slope from a selected point. Several selected points on the upper flanks of several sandwaves show such paths. Most revealing is that the slopes on the bedform flanks are similar in magnitude to the general (along-trough) regional downhill slope. The implication is that gravitational forces alone would soon cause a cumulative downhill migration of mobile sand grains. The upslope forces here are counterbalancing this, presumably hydrological. Are these oblique components of the contour current or do periodic internal waves maintain this balance? The trough-parallel flow-generated ripples in video images (Figs. 7 to 11) are further evidence of a trough-parallel flow process.

As suggested in the proposal outline, perhaps intra-gravity (or internal) waves impacting the slope at this depth are responsible. Alternatively, some oblique or helical component of the contour current exists. The planned winter 2012 current instrument deployments might register either process. Placement of the HI current meters to optimize trough-parallel up-hill flow may be critical if it is a trough phenomenon. Furthermore it might be a process initiated by turbulence generated by the bedform itself and as such a seabed phenomenon only. Current meters placed several metres above the seabed may not be sensitive to this. This point is reiterated in the recommendations, Section 8.7.

6.7 Summary of morphometrics

Tables 1 and 2 show a summary of the morphometrics findings on a field by field basis.

Table 1. Summary of size, volume, depth, height and wavelength, and asymmetry index statistics for Eggakanten sandwave fields.

Field ID	Length	Width	Area	Water Depth			No. Measurments	Height			Wavelength (crests)				Height Wavelength ratio		Volume Estimate ($10^6 m^3$)	Symmetry (positive is downstream; NW)			
	metres	metres	sq. km	maxi-mum	mini-mum	mean	(measurments at 100 m spacing along crest)	maxi-mum	mean	SD	maxi-mum	mini-mum	mean	SD	H/W mean	SD	(using mean height)	maxi-mum	mini-mum	mean	SD
N-1	7000	2700	12	648	561	600	3840	2,5	0,4	0,3	205	15	58,6	23,8	0,019	0,011	3,9	14	-14	0,2	3,1
N-2	20100	1800	26	564	645	606	4831	5,5	0,9	0,8	205	15	65,3	26,1	0,018	0,011	15,7	14	-14	0,6	3,0
N-3	2300	1000	2	609	548	581	170	1,9	0,4	0,3	180	20	70,8	36,1	0,011	0,004	0,5	6	-12	-2,8	3,3
N-4	4100	1400	6	623	550	588	567	2,2	0,5	0,4	200	15	71,0	34,9	0,010	0,004	1,4	14	-14	-1,1	4,5
N-5	1600	170	0	582	553	574	47	1,9	0,7	0,5	150	25	65,3	31,3	0,020	0,015	0,1	3	-13	-2,2	4,1
N-6	2200	400	1	low amplitude and noisy data			0	-	-	-	-	-	-	-			-	-	-	-	-
S-1	36000	3500	82	753	487	594	19182	5,5	0,8	0,6	205	15	55,8	22,0	0,020	0,015	50,1	17	-14	0,0	2,6
All Fields	**73300**	**10970**	**130**	**754**	**487**	**597**	**28637**	**5,5**	**0,7**	**0,6**	**205**	**15**	**58,2**	**23,8**	**0,019**	**0,011**	**300,6**	**17**	**-14**	**0,1**	**2,8**

Table 2. Summary of slope metrics and backscatter statistics for Eggakanten sandwave fields.

Field ID	Slope, NW flank			Slope, SE flank			Slope Ratio (negative suggests flow toward NW)				Backscatter Strength, dB				Backscatter Strength, Crests only				Backscatter Strength, Troughs only			
	maxi mum	mean	SD	maxi-mum	mean	SD	mini-mum	maxi-mum	mean	SD	maxi-mum	mini-mum	mean	SD	maxi-mum	mini-mum	mean	SD	maxi-mum	mini-mum	mean	SD
N-1	9,6	2,0	1,4	6,3	1,8	1,2	-14	16	0,4	2,6	-3	-35	-17,7	4,9	-3	-35	-18,2	4,85	-4	-34	-17,37	4,8
N-2	24,3	3,4	3,1	30,6	2,9	2,1	-31	48	0,2	3,8	-3	-39	-17,4	5,0	-3	-39	-18,1	5,1	-3	-37	-16,56	4,9
N-3	5,5	2,0	1,0	5,9	1,4	1,0	-9	19	1,7	3,6	-6	-37	-19,2	5,2	-6	-33	-19,5	4,9	-3	-39	-18,1	5,1
N-4	6,7	1,9	1,2	5,5	1,4	1,0	-14	16	0,9	4,0	-2	-36	-16,8	5,7	-2	-34	-17,3	5,7	-3	-36	-16,2	5,5
N-5	12,1	2,9	1,9	20,7	4,1	5,1	-12	7	0,1	4,1	-2	-32	-15,0	7,3	-3	-29	-15,4	7,01	-2	-32	-14,5	7,5
N-6	low amplitude and noisy data			-	-	-	-	-	-	-	-	-	-	-	-	-	-	-	-	-	-	-
S-1	35,4	3,9	2,9	21,8	3,0	2,2	-54	77	0,7	3,7	2	-48	-17,8	6,2	2	-42	-17,7	5,97	1	-48	-17,8	6,5
All Fields	**35,0**	**3,5**	**2,8**	**30,0**	**2,8**	**2,1**	**-54**	**77**	**0,6**	**3,6**	**2**	**-48**	**-17,0**	**5,6**	**2,0**	**-42,0**	**-17,0**	**5,5**	**1,0**	**-48,0**	**-17,0**	**5,7**

The tabulated findings are also presented graphically in Figures 62 to 64. Figure 62 summarizes the general size and bedform sample numbers, the water depth and ranges, the height and wavelength statistics, and the profile asymmetry index. Figure 63 shows slope parameters graphically and Figure 64 summarizes backscatter values for the individual fields.

Apart from defining or cataloguing the bedforms precisely, the various indices were generated to identify if morphology from multibeam data could point toward sediment processes. Most indices have yielded a wide range in values whose interpretation is not straightforward. It may be questioned if the data have resolution limitations skewing the findings and this is difficult to assess. The straightforward interpretation of the various indices suggests that there is considerable intra-field clustering, or domains of forms, each domain having rather contrasting morphological properties such that on average the whole field shows a large spread of values and no strong trends. Earlier sections have shown the apparent tuning to

meso-scale topography and the thought experiment this induces is that the local topography strongly affects sediment processes, apparently through its effect on the currents.
The sandwave project, as a whole, is well poised to address this directly, together with its partners, largely through the planned observed and modeled hydrological conditions.

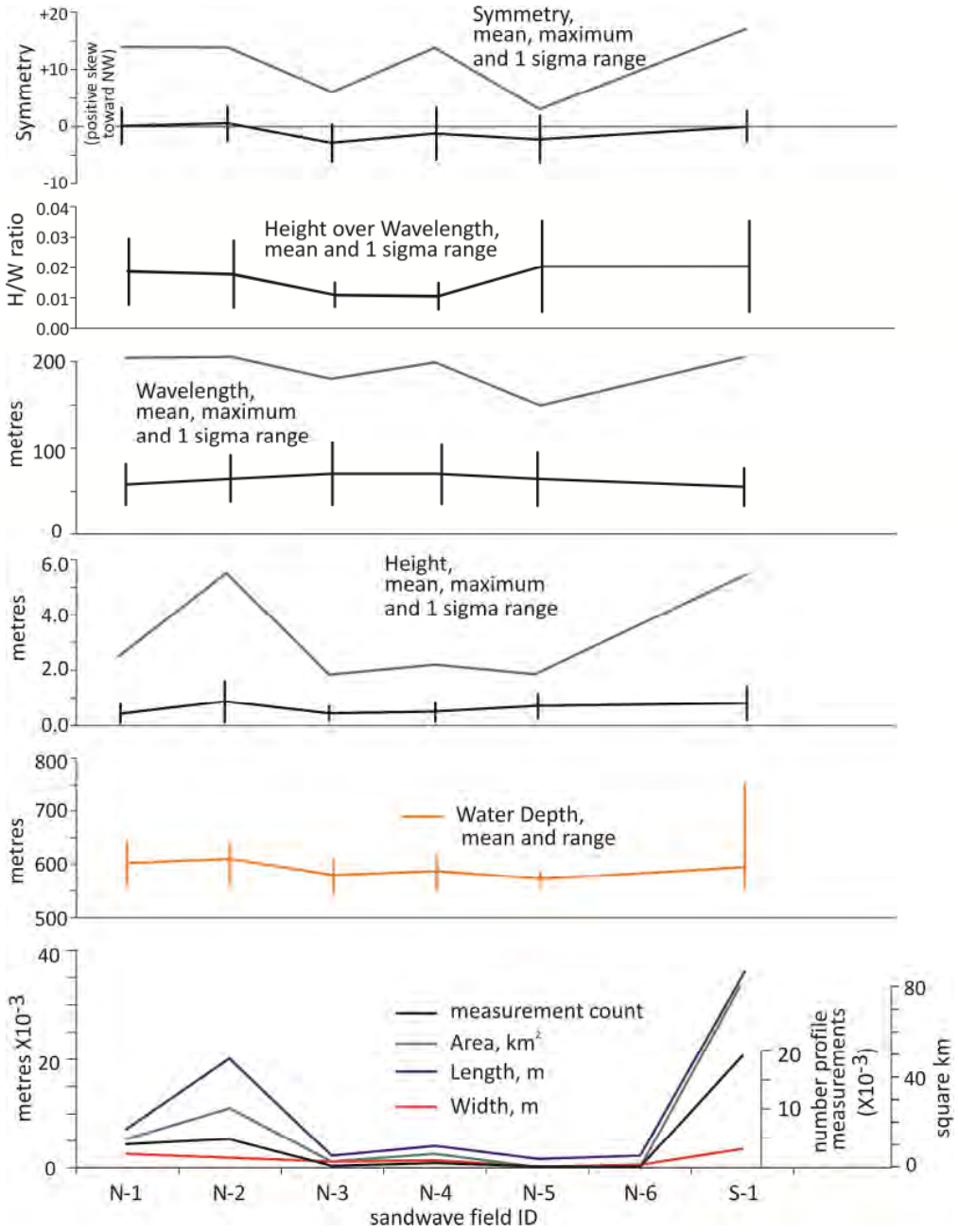

Figure 62. Summary of basic bedform metrics for individual fields. The N-2 and S-1 are the larger fields and have more outliers in terms of larger bedforms. H/W ratios suggest average to lower than average values for sandwaves in general. Symmetry values are spread across a fair range, centered just below null, suggesting many occurrences have a skewed profile indicating southeasterly migration, that is, contrary to expected given what is known of the general currents. The spread certainly arises from original multibeam resolution deficiencies but the trends may be correct.

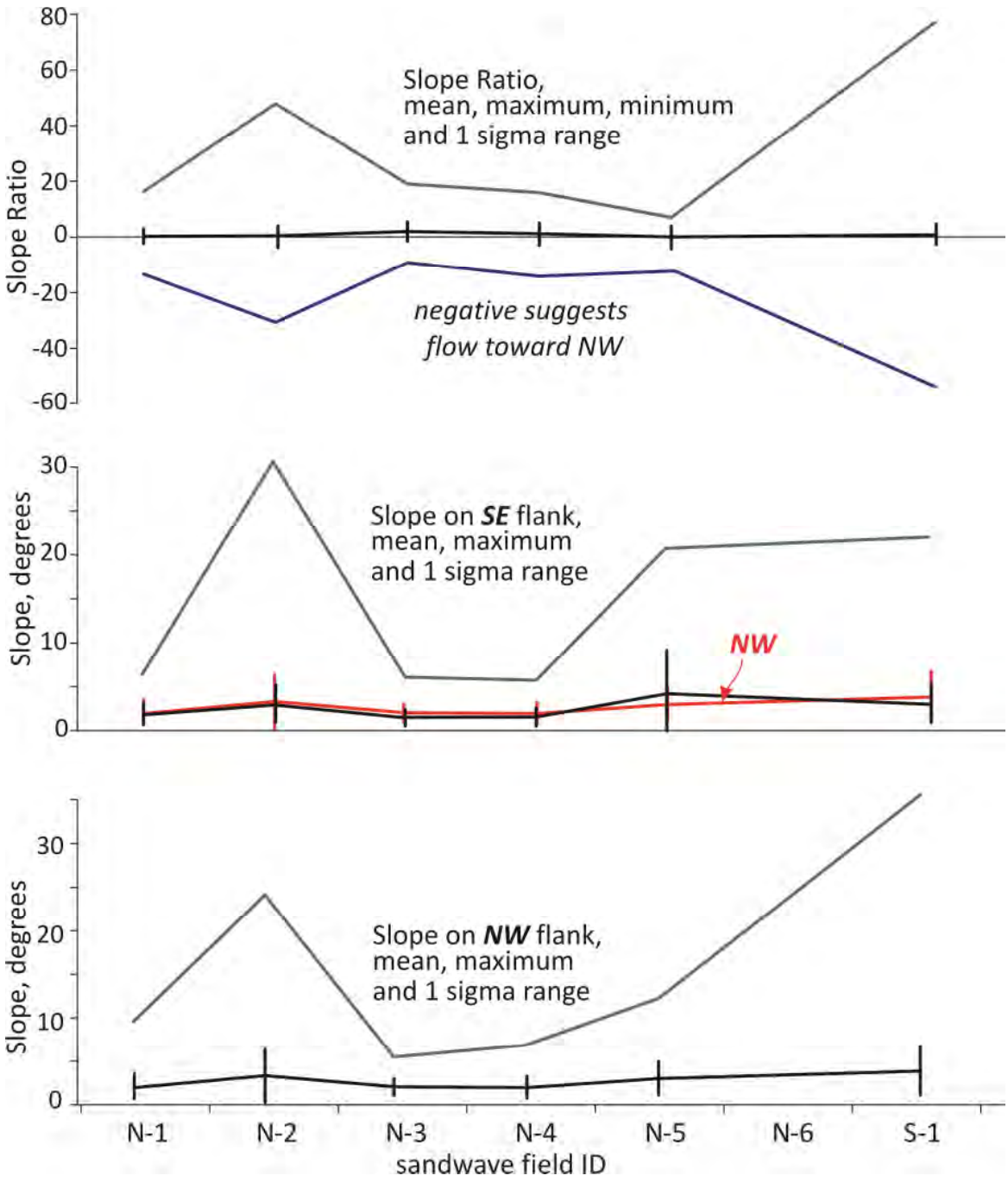

Figure 63. Summary of slope metrics for individual sandwave fields. While slope measurements are generally below 5°, the larger fields have slightly higher average and maximum values. The red slope average and SD in the middle panel is a duplicate of the NW values, for direct comparison. Slope ratios suggest little or no NW versus SE flank difference but this might be largely a limitation of the multibeam data resolution.

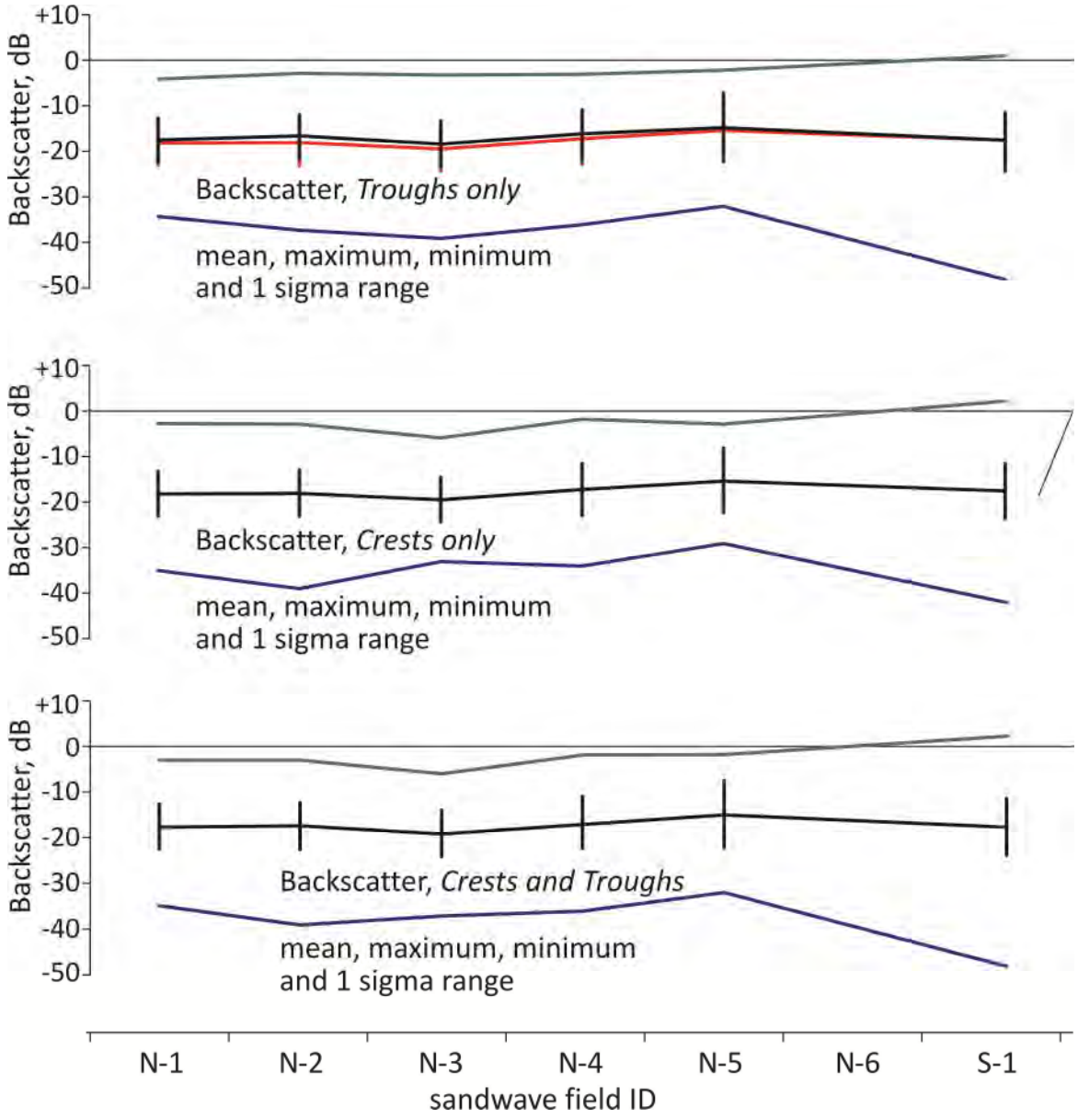

Figure 64. Summary of backscatter metrics for individual fields. There is little discernable difference between Crest and Trough backscatter values when all sandwaves are considered despite clearly coarser troughs, including glacial gravels, in some trough examples. The red in the upper panel is a duplicate of the crest values for direct comparison.

6.7.1 Discussion: Metrics and Bedform Activity

These bedform occurrences are mid-range in size within a global context, the larger falling in the mid to large range (Amos & King 1984). Sandwave heights and wavelengths have been shown to exhibit some water depth and slope dependency (Xu et. al. 2008) but these studies were in relatively shallow sites (20 to 60 m) and most studies suggest a water depth independence where bedform heights are less than 1/6 water depth (Rubin and McCulloch 1980). Generally, bedform size is positively related to current velocity (e.g. Ruben et.al. 1980)

and there is generally a grain size dependency, with coarser sands supporting higher forms, though the opposite has also been demonstrated in flume studies. These relationships apparently only hold for the smallest bedforms (Whitmeyer & FitzGerald 2006). Figure 65 shows the effect current strength and grain size variables have on bedform configuration. If the sediment is too fine or too coarse, sandwaves do not develop. There are several documented cases where bedform field boundaries are due to increased velocities, not decreased, where sand becomes suspended instead of in traction. The diagram (Fig. 65) suggests there should be some predictability of bedform dimensions but a comprehensive evaluation of numerous published predictive bedform equations (Whitmeyer & FitzGerald 2006) indicates their size is generally strongly under predicted, at least in fluvial/tidal examples. Other factors such as consolidation, lag deposits, and response time are also strong governers.

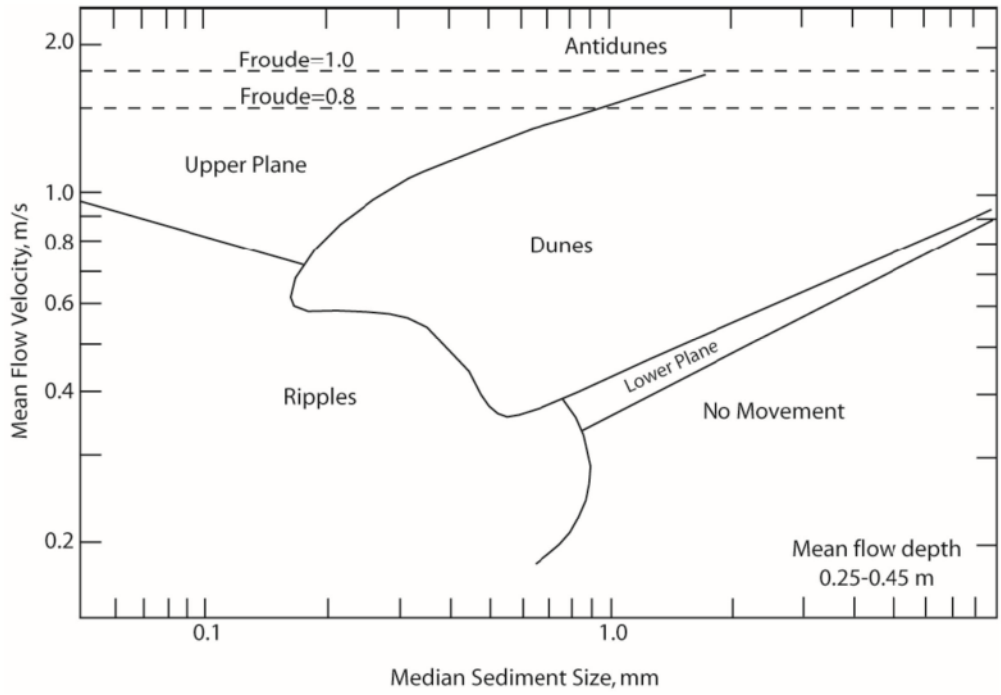

Figure 65. Current velocity and bed grain size have a relationship to bedform configuration. (after Ashley 1990). Dunes are termed sandwaves in this study. Note that this refers largely to fluvial forms.

If unsteady currents dominate (more common in tidal environments) then response time of the bedform can lag significantly, especially for large forms. Demonstration of any long term cyclicity of the current at this study site, if demonstrated in upcoming deployments, will be important to process understanding. These two factors (lag response time and unsteady currents) can contribute to a system which is never in full equilibrium.

The superimposed ripples can represent secondary, unsteady spatial variations in the general flow, caused by the local flow separation associated with the larger sandwave (cf. Allen and Collinson 1974; Allen 1978). Dalrymple and Rhodes (1995) found divergence of crestline

orientations for superimposed bedforms was up to 90° from the larger sandwave crestlines but that 30–60° is more common. Similar observations on eolian dunes (Sweet & Kocurek 1990) were limited to lee-side slopes less than 20°, below which flow separation did not occur. All attributed to topographic steering. The very abrupt orientation and form change (3-D on crest to 2-D on lee and trough) of the superimposed ripples observed from the video (e.g. Fig. 8) are difficult to envisage as topographic steering; possibly there is some additional time aspect such that lee forms cross-cut earlier ripples as the more trough-parallel forms evolve. The coincidence of the strong thermocline and its seasonal spatial variations is a strong alternative to topographic steering but this process is not well enough understood. The planned current deployments might provide the hydrologic setting which forms these ripples. There is some risk that this is only a boundary layer phenomenon and that the current meters, which are primarily designed to sense upwards, will not register the phenomenon. Other, bottom sensing landers would be better suited (e.g. RALPH; Li and Heffler, 2002) but these are generally prohibitively expensive or logistically difficult.

In terms of activity, the literature generally recognizes a height to wavelength ratio, the larger the more active. Small bedforms (less than about 30 m wavelength, often termed megaripples) tend to have a mean height/wavelength ratio of about 0.1 and that of sand waves is around 0.03 (Dyer 1986). Figure 62 shows that the higher (1 sigma) H/W ratios are typical of active sandwaves but significant portions of the population lie at a considerably lower 0.01. This suggests they are certainly not moribund. Sand availability is, of course, a constraining factor and may be significant at this study site because, apart from small scale washing and sorting of sand from underlying glacial sediments, the source is not obvious and may be a limiting factor.

Superimposed megaripples on top of sandwaves are generally a strong indicator of migration activity level. Megaripples vary considerably in size (5 to 40 m wavelength) and are best recognized in contrast to larger sandwaves on which they lie; they are the “workhorses” which actually transport the sand grains to the sandwave lee face. In the Eggakanten sandwave fields one might term many of the smaller examples megaripples but the continuum in scale with the sandwaves makes any terminology differentiation artificial. Here instead, the superimposed ripples are assumed to play the transport role. This interpretation is compatible with strongly asymmetric ripples whose form, where observed in relation to the sandwave crest, are migrating toward the lee face. Furthermore, they are generally of the 3-D form, generally associated with higher flow regimes than the 2-D (straight crested). In the author’s experience one major contrast with the Eggakanten forms is that active megaripples on top of sandwaves elsewhere are typically less than an order of magnitude smaller in wavelength than the forms on which they sit (cf. Amos & King, 1984 on Georges Bank, Barnard et. al. 2011 in San Francisco Bay). In contrast, the Eggakanten ripples are only 10s of cm in wavelength and cm high, and so typically at least three orders of magnitude smaller.

Given that the ripples are obviously active, at least periodically, this suggest an active or mobile layer of at least centimetres thickness but this is a minimum. The steep lee slopes from video observations would suggest that the whole bedform is in at least slow migration.

Lacking any explanation, it may be prudent to note that deep water contouritic sandwaves are not as studied as those in tide and tide-wave dominated environments and these different drivers may well typically produce different bedform suites.

6.7.2 Sand volume estimate

Sandwave distribution and height alone allow a minimum estimate of the sand now contained within the system of sandwave fields. Figure 66 shows some of the assumptions of such a volume estimate. In section 5.2 there is evidence for a considerable amount of sand (locally only) beneath the sandwave troughs (eg. configuration 3 in Figure 66). Accordingly volume estimates can be perhaps a maximum of ½ order of magnitude in error, considering that a thin sandwave unit is generally observed. Proposed further sonar surveying will help quantify this uncertainty. Total sand volume of the entire field is estimated at a minimum of 300 million ($3.0x10^8$) cubic metres.

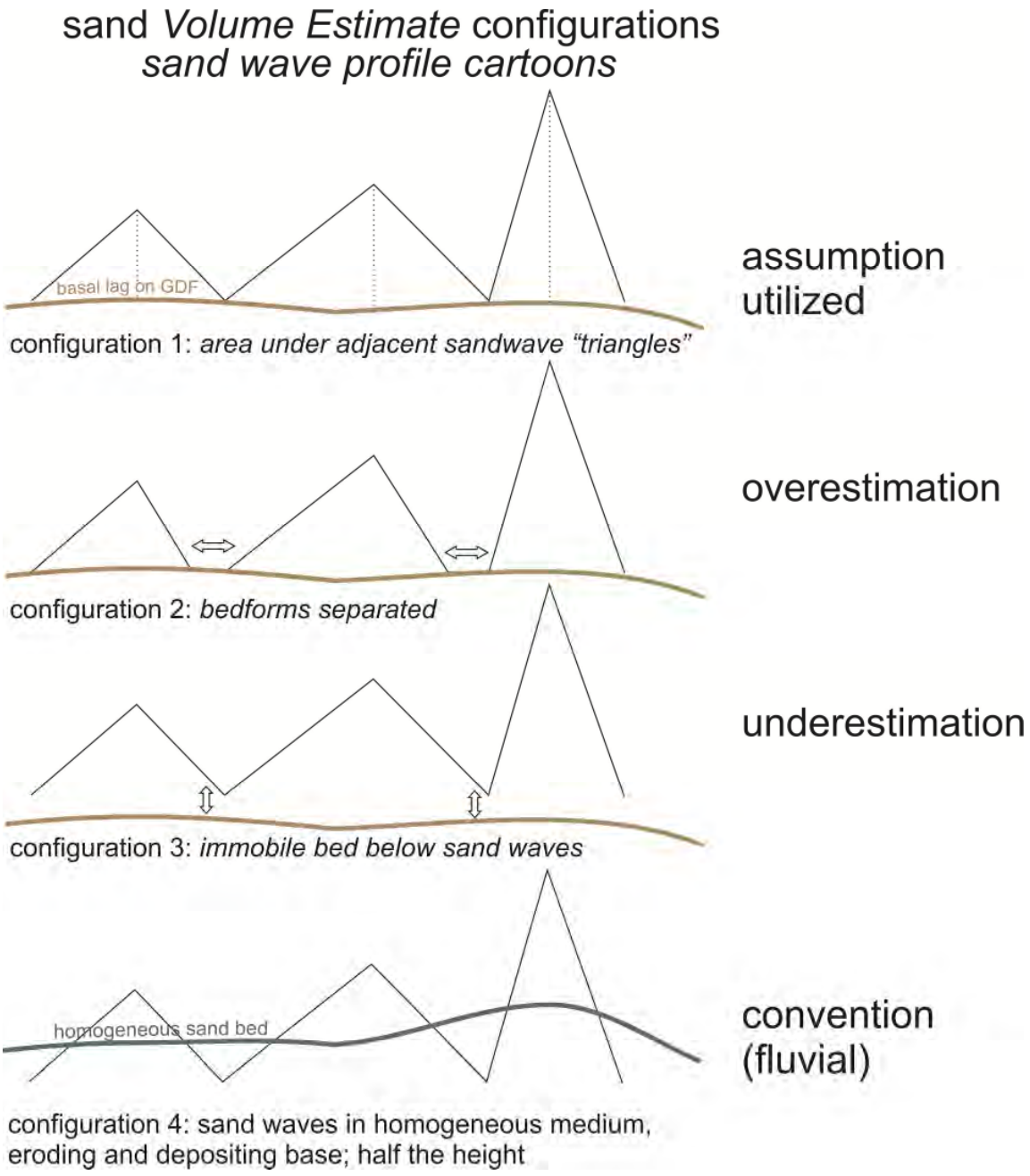

Figure 66. Cartoon of the technique for establishing a minimum sand volume for the sandwave fields. Average height and wavelength values for an assumed triangle form were utilized. The brown stratum represents the top of the glacial sediments, usually a lag below which the troughs are probably unable to cut. Compared to the configuration utilized for the calculation, over- and under-estimations would result for configurations 2 and 3 respectively. Configuration 4, though the convention in flume and most fluvial situations, was eliminated. The TOPAS data combined with the backscatter images suggest that configurations 1 to 3 all exist but that configuration 1 is most common.

7. Conclusions

The ultimate goal of the sandwave field study is to establish the extent, size, composition, and long and short term transport activity of the bedforms. One approach is to view them from a geological and stratigraphic viewpoint, to establish if there might be long term source or sink of sediment which provides clues as to the rates and duration of the processes. Such a framework has been established on a broad level. This provides broad temporal understanding for the sandwaves.

The sandwave fields overly glacigenic sediments both from times when the ice margin sat at the shelf break some kilometres up-slope (until ca. 15 000 years ago) and when it retreated to supply hempelagic muds and ice rafted material. A number of gravity mass failures occurred afterward, some within the sandwave fields and stratigraphic relations suggest that even these pre-date the sandwave field initiation. Parent material was likely the hemipelagic glacimarine sediments from de-glacial times. However, other than the sands, post-glacial sedimentation, which is generally soft clay on the continental shelf and slope, is so limited as to be not registered on the sonar and video transects. Thus there is little medium to record events of the last ca. 10 000 years apart from the sandwaves themselves.

Age and duration of sandwave activity is therefore only constrained by thousands of years. A sand source and sink need to be identified in order to better judge long term processes. The long term needs to be understood in order to evaluate any evidence of short-term processes; there must be a mass balance between sink, flux and source. Recommendations of sonar surveying will address this directly. Initial interpretation is that the sand source is local, from current washing of the uppermost glacial sediments and the sink may be within the sandwave fields themselves, preserved as immobile sand beneath more active forms.

Further age constraint may come from recommended fieldwork sampling and age dating of the small gravity slides (following section). Sampling of the shell material may also provide age constraints and source indications but these, too may be quite broadly constrained.

A robust technique and results for morphometric description and cataloguing of the bedforms has been established. Robust statistical presentations present several indices which suggest a clustering or domains of bedforms which are somewhat tuned to the meso-morphology of the terrain in which they lie, a terrain inherited from glacial processes. This gives rise to the hypothesis that there a much more complex hydrologic regime than a simple continuous northward contour current which drives the bedforms.

Local steering, current acceleration and perhaps induced turbulence are suggested. An upward driving hydrologic component must be able to balance mid-term tendencies of down-slope grain migration. Other components of the project are well poised to address the validity of this. The complexity suggested provides some support for the initial hypothesis that relatively unique and poorly understood oceanic conditions are at play, possibly including tidal-wave

driven internal waves channelled on the thermocline and tied to interaction with the slope near the shelf-break.

Visual observations based on existing data indicate that small ripples (10-15 cm wavelength and only centimetres high) are nearly ubiquitous, superimposed on the sandwaves which are metres to several metres in amplitude and 10s to 150 m wavelength. Orientations are largely unknown but starkly contrasting directions at the sharp transition from bedform stoss to lee slopes suggests local hydraulic regimes which are important to transport direction and magnitude and must be better understood. Most indications are that the sandwave crests are sharp and lee sides steep. All these indications suggest *active bedform mobility*, both in a mobile layer several centimetres thick and, at a much slower pace in the larger bedforms. The pace of mobility is *low* given initial comparisons of new multibeam data, not reported here. Pre-survey investigation of these new data will help optimize the planned fieldwork.

The setting and morphometrics provides a good framework for future fieldwork by providing concepts and constraints for further sonar surveying, sampling and analysis of the samples.

8. References

Allen, JRL 1978: Polymodal dune assemblages: an interpretation in terms of dune creation-destruction in periodic flows. Sedimentary Geology 20, 17-28.

Allen, JRL, & Collinson, JD 1974: The superimposition and classification of dunes formed by unidirectional aqueous flows. Sedimentary Geology 12, 169-178.

Allen, JRL 1980: Sand waves: a model of origin and internal structure. Sedimentary Geology 26, 281-328.

Amos, CL & King, EL 1984: Bedforms of the Canadian eastern seaboard: A comparison with global occurrences. Marine Geology 57 (1-4), 167-208.

Andreassen, K, Laberg, JS & Vorren, T 2008: Seafloor geomophology of the SW Barents Sea and its glaci-dynamic implications. Geomorphology 97, 157-177.

Ashley, GM 1990: Classification of large-scale subaqueous bedforms: a new look at an old problem. Journal of Sedimentary Research 60, 161-172.

Bellec, VK, Wilson, M, Bøe, R, Rise, L, Thorsnes, T, Buhl-Mortensen, L & Buhl-Mortensen, P 2008: Bottom currents interpreted from iceberg ploughmarks revealed by multibeam data at Tromsøflaket, Barents Sea. Marine Geology 249, 257-270.

Bellec, VK, Bøe, R, Rise, L, Slagstad, D, Longva, O & Dolan, MFJ 2010: Rippled scour depressions on continental shelf bank slopes off Nordland and Troms, Northern Norway. Continental Shelf Research 30, 1056-1069.

Baraza, J, Ercilla, G, & Nelson, CH 1999: Potential geological hazards on the eastern Gulf of Cadiz slope (SW Spain). Marine Geology 155, 191-215.

Barnard, PL, Erikson, LH & Kvitek, RG 2011: Small-scale sediment transport patterns and bedform morphodynamics: new insights from high-resolution multibeam bathymetry. Geo-Marine Letters 31, 227-236.

Belderson, RH, Johnson, MA & Kenyon, NH 1982: Bedforms, *In:* Stride, A.H. (Ed.), *Offshore Tidal Sands: Processes and Deposits*. Chapman & Hall, London, pp. 27-57.

Buhl-Mortensen PB, Buhl-Mortensen, L, Dolan, M, Dannheim, J & Kröger, K 2009: Megafaunal diversity associated with marine landscapes of northern Norway: a preliminary assessment. Norwegian Journal of Geology 89, 163-171.

Buhl-Mortensen, L, Hodnesdal, H, Thorsnes, T. (Eds.) 2010. *Til bunns i Barentshavet og havområdene utenfor Lofoten - ny kunnskap fra MAREANO for økosystembasert forvaltning*. Norges geologiske undersøkelse, Trondheim, 128 pp. (English summary).

Bøe, R., Bellec, VK, Dolan, MFJ, Buhl-Mortensen, PB, Buhl-Mortensen, L & Rise, L 2009: Giant sand waves in the Hola glacial trough off Vesterålen, North Norway. Marine Geology 267, 36-54.

Caston, VND 1972: Linear sand banks in the southern North Sea. Sedimentology 18, 63-78.

Caston, GF 1981: Potential gain and loss of sand by some sandbanks in the Southern Bight of the North Sea. Marine Geology 41, 239-250.

Courtney, R 2007: Storage and Dissemination of SEGY Data in JPEG2000 Format. American Geophysical Union, Fall Meeting abstract #IN51B-0402.

Dalrymple, RW, LeGresley, EM, Fader, GBJ & Petrie, BD 1992: The western Grand Banks of Newfoundland: transgressive Holocene sedimentation under the combined influence of waves and currents. Marine Geology 105, 95-118.

Dalrymple, RW & Rhodes, RN. 1995: Estuarine dunes and bars. *In:* GME Perillo, Editor *Geomorphology and sedimentology of estuaries*. Elsevier, Amsterdam, 359–422.

Deleu, S, Van Lancher, V, Van den Eynde, D & Moekerke, G 2004: Morphodynamic evolution of the kink of an offshore tidal sandbank: the Westhinder Bank (Southern North Sea). Continental Shelf Research 24, 1587-1610.

Dolan, M, Mortensen, PB, Thorsnes, T, Buhl-Mortensen, L, Bellec, VK & Bøe, R 2009: Developing seabed nature-type maps offshore Norway: initial results from the MAREANO programme. Norwegian Journal of Geology 89, 17-28.

Dyer, KR, 1986: *Coastal and estuarine sediment dynamics*. Wiley & Sons, Chichester, England, 342 pp.

Elliott, GM, Shannon, PM, Haughton, PDW, Praeg, D & O'Reilly, B 2006: Mid- to Late Cenozoic canyon development on the eastern margin of the Rockall Trough, offshore Ireland. Marine Geology 229, 113-132.

Faugères, JC, Stow, DAV, Imbert, P & Viana, A 1999: Seismic features diagnostic of contourite drifts. Marine Geology 162, 1-38.

Flemming, BW 1978: Underwater sand dunes along the southeastern African continental margin - observations and implications. Marine Geology 26, 177-198.

Flemming, BW 1980: Sand transport and bedform patterns on the continental shelf between Durban and Port Elizabeth (southeast African continental margin). Sedimentary Geology 26, 179-205.

Gabrielsen, RH, Færseth, RB, Jensen, .N, Kalheim, JE & Riis, F 1990: Structural elements of the Norwegian continental shelf. Part I: The Barents Sea Region. NPD-Bulletin No 6, 33 p.

Habgood, EL, Kenyon, NH, Masson, DG, Akhmetzhanov, A, Weaver, PPE, Gardner, J & Mulder, T 2003: Deep-water sediment wave fields, bottom current sand channels and gravity flow channel-lobe systems: Gulf of Cadiz, NE Atlantic. Sedimentology 50, 483-510.

Hald, M, Vorren, TO 1984: Modern and Holocene foraminifera and sediments on the continental shelf off Troms, North Norway. Boreas 13, 133-154.

Hulscher, SJMH & van den Brink, GM 2001: Comparison between predicted and observed sand waves and sand banks in the North Sea. Journal of Geophysical Research, 106 (C5), 9327-9338.

Kenyon, NH 1970:. Sand ribbons of European tidal seas. Marine Geology 9, 25-39.

Kenyon, NH, Belderson, RH 1973: Bedforms of the Mediterranean undercurrent observed with sidescan sonar. Sedimentary Geology 9, 77-99.

King, EL, Sejrup, HP, Haflidason, H, Elverhøi, A, & Aarseth, I. 1996: Quaternary Seismic Stratigraphy of the North Sea Fan: Glacially-fed Gravity Flow Aprons, Hemipelagic Sediments, and Large Submarine Slides. Marine Geology 130, 293-315.

Knies, J., Vogt, C, Matthiessen, J, Seung-Il Nam, Ottesen, D, Rise, L, Bargel, T & Eilertsen, R 2007: Re-advance of the Fennoscandian Ice Sheet during Heinrich Event 1. Marine Geology 240, 1-18.

Laberg, JS & Vorren, T 1993: A Late Pleistocene submarine slide on the Bear Island Trough Mouth Fan. Geo-Marine Letters 13, 227-234.

Laberg, JS & Vorren, T 1995: Late Weichselian submarine debris flow deposits on the Bear Island Trough Mouth Fan. Marine Geology 127, 45-72.

Laberg, JS, Vorren, TO & Knutsen, S-M 1999: The Lofoten contourite drift off Norway. Marine Geology 159, 1-6.

Laberg, JS & Vorren, TO 2004: Weichselian and Holocene growth of the northern high-latitude Lofoten Contourite Drift on the continental slope of Norway. Sedimentary Geology 164, 1-17.

Laberg, JS, Andreassen, K, Knies, J, Vorren, TO & Winsborrow, M 2010: Late Pliocene-Pleistocene development of the Barents Sea Ice Sheet. Geology 38/2, 107-110.

Le Bot, S, Trentesaux, A 2004: Types of internal structure and external morphology of submarine dunes under the influence of tide- and wind-driven processes (Dover Strait, northern France). Marine Geology 211, 143-168.

Li, MZ & King, EL 2007: Multibeam bathymetric investigations of the morphology of sand ridges and associated bedforms and their relation to storm processes, Sable Island Bank, Scotian Shelf, Marine Geology 243 (1-4), 200-228.

Li, MZ & Heffler, DE 2002: Continental shelf sediment transport studies in Canada: Basic theories and recent technology advances. Environmental Marine Geoscience 3. Geosci. Can., 29, 35–48.

Oljedirektoratet 2010: Geofaglig vurdering av petroleumsressursene i havområdene uenfor Lofoten, Vesterålen og Senja. 93 pp.

Orvik, KA, Skagseth, Ø & Mork, M 2001: Atlantic Inflow to the Nordic Seas. Current structure and volume fluxes from moored current meters, VM-ADCP and SeaSoar-CTD observations, 1995-1999. Deep-Sea Res. 48, 937-957.

Ottesen, D, Dowdeswell, JA, Rise, L, 2005: Submarine landforms and the reconstruction of fast-flowing ice streams within a large Quaternary ice sheet: the 2,500 km-long Norwegian–Svalbard margin (57°-80° N). Geological Society of America Bulletin 117, 1033–1050.

Ramsay, PJ 1994: Marine geology of the Sodwana Bay shelf, southeast Africa. Marine Geology 120, 225-247.

Reynaud, J-Y, Tessier, B, Berné, S, Chamley, H & Debatist, M, 1999: Tide and wave dynamics on a sand bank from the deep shelf of the Western Channel approaches. Marine Geology 161, 339-259.

Rise, L, Olsen, HA, Bøe, R., Ottesen, D 1996: Thickness, distribution and depositional environment of Holocene sediments in the Norwegian part of the Skagerrak. Norges geologiske undersøkelse Bulletin 430, 5-16.

Rise, L, Bellec, V, Bøe, R &. Thorsnes, T. 2009: The Lofoten – Vesterålen continental margin, North Norway: Canyons and Mass-movement activity. International Conference on

Seafloor Mapping for Geohazard Assessment, 11-13 May 2009, Ischia, Italy. In Chiocci, F.L. et al. (eds.): Rendiconti Online, Societa Geologica Italiana, Extended Abstracts, Vol. 7, 79-82.

Rise, L., Chand, S., Haflidason, H., L'Heureux, J.S., Hjelstuen, B.O., Bellec, V., Longva, O., Brendryen, J., Vanneste, M. and Bøe, R. 2012: Chapter 15 Investigations of Slides at the Upper Continental Slope off Vesterålen, North Norway. In: Y. Yamada et al. (eds.), Submarine Mass Movements and Their Consequences. Advances in Natural and Technological Hazards Research 31, 167-176. DOI 10.1007/978-94-007-2162-3_15, © Springer Science+Business Media B.V. 2012.

Rubin, D M, & McCulloch, DS. 1980: Single and superimposed bedforms: A synthesis of San Francisco Bay and flume observations. Sedimentary Geology, 29, 207-231.

Skagseth, Ø. & Orvik, KA. 2002: Identifying fluctuations in the Norwegian Atlantic Slope Current by means of Empirical Orthogonal Functions. Cont. Shelf Res. 22, 547-563.

Skagseth, Ø. & Orvik, K.A., Furevik, T. 2004: Coherent variability of the Norwegian Atlantic Slope Current derived from TOPEX/ERS altimeter data, Geophysical Research Letter 31, L14304, doi:10.1029/2004GL020057, 2004.

Sweet, ML & Kocurek, G. 1990: An empirical model of aeolian dune lee-face airflow. Sedimentology, 37, 1023–1038.

Viana, A.R., Faugères, J.-C., Stow, D.A.W., 1998a: Bottom-current-controlled sand deposits - a review of modern shallow- to deep-water environments. Sedimentary Geology 115, 53-80.

Viana, A.R., Faugères, J.-C., Kowsmann, R.O., Lima, R.O., Caddah, J.A.M., Rizzo, J.G., 1998b: Hydrology, morphology and sedimentology of the Campos continental margin, offshore Brazil, in: Stow, D.A.W., Faugères, J.-C. (Eds.), Contourites, Turbidites and Process Interaction. Sedimentary Geology 115, 133-157.

Vorren, T.O., Lebesbye, E., Andreassen, K., Larsen, K.B., 1989: Glacigenic sediments on a passive continental margin as exemplified by the Barents Sea. Marine Geology 85, 251–272.

Vorren, T.O., Laberg, J.S., Blaume, F., Dowdeswell, J.A., Kenyon, N.H., Mienert, J., Rumohr, J. and Werner, F. 1998: The Norwegian-Greenland Sea continental margins: morphology and late Quaternary sedimentary processes and environment. Quaternary Science Reviews 17, 273-302.

Whitmeyer, S J, & FitzGerald, D. 2006: Sand waves that impede navigation of inlet navigation channels. ERDC/CHLCHETN IV-68, Vicksburg, MS: U.S. Army Engineer Research and Development Center.

Xu, JP, Wong, FL, Kvitek, R, Smith, DP, & Paull, CK. 2008: Sandwave migration in Monterey Submarine Canyon, Central California, Marine Geology, 248 (3-4),193-212.

Ådlandsvik, B. and Ostrowski, M. 2010: Fysiske forhold utenfor kysten av Nord-Norge. I: Buhl-Mortensen, L. et al. (eds.) Til bunns I Barentshavet og havorådene utenfor Lofoten, 77-81, Norges geologiske undersøkelse, Trondheim.

Norges geologiske undersøkelse
Postboks 6315, Sluppen
7491 Trondheim, Norge

Besøksadresse
Leiv Eirikssons vei 39, 7040 Trondheim

Telefon 73 90 40 00
Telefax 73 92 16 20
E-post ngu@ngu.no
Nettside www.ngu.no

Geological Survey of Norway
PO Box 6315, Sluppen
7491 Trondheim, Norway

Visitor address
Leiv Eirikssons vei 39, 7040 Trondheim

Tel (+ 47) 73 90 40 00
Fax (+ 47) 73 92 16 20
E-mail ngu@ngu.no
Web www.ngu.no/en-gb/